BLEACHING KINETICS OF VISUAL PIGMENTS

by
Judith Arlene Resnik

Dissertation submitted to the Faculty of the Graduate School
of the University of Maryland in partial fulfillment
of the requirements for the degree of
Doctor of Philosophy
1977

APPROVAL SHEET

Title of Dissertation: Bleaching Kinetics of Visual Pigments

Name of Candidate: Judith Arlene Resnik
Doctor of Philosophy, 1977

Dissertation and Abstract Approved:

Felix E. Zajac III
Associate Professor
Department of Electrical Engineering

Date Approved: April 13, 1977

ABSTRACT

Title of Dissertation: Bleaching Kinetics of Visual Pigments

Judith Arlene Resnik, Doctor of Philosophy, 1977

Dissertation directed by: Felix E. Zajac III, Associate Professor, Department of Electrical Engineering

A rapid scanning microspectrophotometer (RMSP) has been developed and utilized to study the photoproducts resulting from the bleaching of rhodopsin in the isolated retina of the frog. The RMSP is capable of measuring absorption spectra at multiple wavelengths within the milliseconds and longer time domain. The unusual characteristic of the instrument is the use of a special cathode ray tube as a measuring light source. Spectral scanning is accomplished electronically, with a sampling interval of 600 microseconds for each waveband. A lock-in amplifier system enables the RMSP to be utilized as either a single or dual beam instrument.

The results discussed in this dissertation have shown that hydrogen ion availability is a primary cofactor in determining the relative concentration of the metarhodopsin III photoproduct, with less appearing, in lieu of greater free retinal formation, at low pH levels. Metabolic factors have also been shown to influence the pathways of photoproduct decay. The most significant effect has been observed in non-acidic intracellular environments, with deficiencies in metabolic energy production also favoring the direct formation of free retinal from metarhodopsin II.

The half-times of formation and decay of metarhodopsin III have also been observed to vary, depending on the extracellular environment of photoreceptor cells. In general, both half-times tend to be greater when proportionately more metarhodopsin III is formed. The ratio of the two half-times, however, remains relatively constant, except in anoxic conditions, in which the decay half-time is significantly prolonged with respect to the formation half-time.

Several problems associated with the control of experimental conditions have been discussed as they relate to photoproduct sequence and kinetics. The elimination of as many metabolic, ionic, and other insufficiently controlled conditions as possible has been pointed out as a necessary requirement for obtaining meaningful quantitative results.

In addition, the baseline magnitude of the optical density of the retina, which is, in part, a quantification of light scattering, has been shown to be significantly larger in conditions of low intracellular pH or insufficient substrate supply. The utilization of this parameter as an indirect indicator of the probably sequence of photoproducts has been discussed.

In conclusion, this research has provided a greater insight into the mechanisms affecting the later, slow photoproduct processes in isolated retinas. In particular, the interaction of hydrogen ions and metabolic factors influences the pathways of photoproduct decay in isolated retinas, subsequent to metarhodopsin II. The results and methods described

here should be useful in establishing a context in which to study the faster mechanisms involved in photochemical and electrical transduction in photoreceptor cells. In addition, these results may become important in understanding the normal and pathological functionings of the eye.

DEDICATION

To my father.

ACKNOWLEDGMENTS

I would like to acknowledge Drs. G. C. Murray, T. G. Smith, Jr., T. R. Colburn, and F. E. Malerba, who jointly conceived the rapid scanning microspectrophotometer. I am also grateful to Drs. D. Bertrand and G. E. Loeb and to Mr. W. Vaughn for their continued interest and suggestions during the course of this research. I thank Drs. H. Shichi, R. A. Normann, J. L. Barker, and W. A. Hagins for reading the manuscript and offering their comments and criticisms. Mrs. G. Hall and Mrs. M. L. Adams assisted in the preparation of the manuscript.

Finally, I am indebted to Drs. T. G. Smith, Jr., and F. E. Zajac III, whose dedication to physiology and biomedical engineering have encouraged me throughout the duration of this project.

This work was supported in part by a grant from the American Association of University Women; by the RCA Corporation, Cherry Hill, New Jersey; and by the Laboratory of Neurophysiology, National Institute of Neurological and Communicative Disorders and Stroke, National Institutes of Health, Bethesda, Maryland.

TABLE OF CONTENTS

LIST OF FIGURES

LIST OF TABLES

INTRODUCTION

Photochemical Processes in Vision

Visual photoreceptor cells are capable of responding to visible light over a considerable range of intensities and of transmitting this information to the rest of the visual nervous system. One of the main gaps in our knowledge of the physiology of visual sensation is an understanding of the biophysical and biochemical mechanisms underlying the transduction processes which occur in photoreceptors. That is, how does the absorption of photons by visual pigments in photoreceptor cells result in electrical events in those cells?

The first observations on photochemical processes in the retina occurred as early as 1876, when Boll observed that the pink color of a freshly removed frog retina faded slowly in the light (Boll, 1876). Kühne (1878) extracted a pink substance from the frog retina with bile salts, confirming that this pigment "rhodopsin" was indeed "bleached" upon exposure to light.

Reasonably purified solutions of frog rhodopsin were first prepared by Lythgoe (1937) and Lythgoe and Quilliam (1938). The peak sensitivity of this rhodopsin to visible light was found to be 500 nanometers. Formation of a well-defined pigment intermediate, "transient orange," was observed after the solutions had been exposed to bright light. Transient orange decomposed spontaneously to "indicator

yellow," which was pale yellow in alkaline solution and deep yellow in acid. The photochemical reaction in the retina was postulated to consist of a "primary process," unaffected by temperature, in which a pigment molecule became activated after absorption of a quantum of light, and a "secondary process" of further "chain-reaction" decompositions, which were definitely influenced by temperature (Dartnall, Goodeve, and Lythgoe, 1938). Broda and Goodeve (1941) utilized a non-freezing, glycerol-water solvent for frog rhodopsin to isolate transient orange at -73°C. They found transient orange to be thermally stable in the light or dark at this temperature and attributed it to be the photoproduct of the "primary process."

Wald, Durell, and St. George (1950) studied solutions of cattle rhodopsin at temperatures as low as -100°C and measured the absorption spectra of the observed photoproducts. The first product possessed an absorption maximum at 497 nanometers and spontaneously formed a second intermediate at 478 nanometers when the solution was warmed to above -20°C in the dark. These products were named "lumirhodopsin" and "metarhodopsin," respectively, and the production of lumirhodopsin was proposed to be the "primary process" in photic excitation of rhodopsin.

Subsequently, rhodopsin was found to consist of a protein (opsin) united with a prosthetic group, based on the aldehyde of vitamin A, 11-cis retinal (Wald, Brown, and Smith, 1955). Dartnall (1957) suggested qualitatively that the "primary

process" altered the structural integrity of the visual pigment, thereby initiating the thermal changes which followed. Hubbard and Kropf (1958) then established that the absorption of light caused isomerization of the chromophore from 11-cis to all-trans retinal and proposed that this isomerization was the nature of the "primary process."

About the same time, Yoshizawa and Kito (1958) identified a new intermediate that preceded the production of lumirhodopsin and which was stable at liquid-air temperature (-186°C). The absorption maximum of this "prelumirhodopsin" was found to be 543 nanometers (Yoshizawa and Wald, 1963). Yoshizawa and Horiuchi (1973) later developed a technique for liquid-helium temperature (-268°C) spectrophotometry, with which they detected an even earlier possible photoproduct, "hypsorhodopsin," appearing when cattle rhodopsin was illuminated with long-wavelength light. At this time, they renamed prelumirhodopsin "bathorhodopsin." This change of name may have contributed further to an already confusing nomenclature. The change did, however, have the redeeming virtue of removing the paradox of a photoproduct that appeared "before the light," which is the literal translation of "prelumi-rhodopsin."

While speculation as to the identity of the "primary" visual pigment photoproduct has continued, a picture of the probable sequences of the subsequent thermal photoproducts has emerged. Various photoproduct schemes, illustrated in Figure 1, were gradually compiled from results obtained in several laboratories. The characteristics of these thermal

photoproducts will be considered in the next section of this thesis, which deals with photoproduct kinetics. The photoproducts of rhodopsin have historically been "identified" on the basis of their spectral absorptance characteristics and their thermal stabilities. Recently, however, the kinetic properties have become important in characterizing rhodopsin photoproducts.

Since the nomenclature assigned to each photoproduct by various investigators has been inconsistent and often confusing, current commonly-used nomenclature, along with former identifications, have been summarized below for clarity, as an introduction to the discussion of photoproduct kinetics:

1. Rhodopsin, also known as "visual purple" (Kühne, 1878).

2. Hypsorhodopsin (Yoshizawa and Horiuchi, 1973).

3. Bathorhodopsin (Yoshizawa and Horiuchi, 1973), also known as "prelumirhodopsin" (Yoshizawa and Wald, 1963) and "liquid-air illuminated rhodopsin" (Yoshizawa and Kito, 1958).

4. Lumirhodopsin (Wald, Durell, and St. George, 1950), also known as "transient orange" (Lythgoe, 1937).

5. Metarhodopsin I (Matthews, Hubbard, Brown, and Wald, 1963), also known as "metarhodopsin" (Wald, Durell, and St. George, 1950) and "intermediate A" (Hagins, 1956).

6. Metarhodopsin II (Matthews, Hubbard, Brown and Wald, 1963), also known as "intermediate B" (Hagins, 1956).

7. Metarhodopsin III (Matthews, Hubbard, Brown, and Wald, 1963), also known as "pararhodopsin" (Wald, 1968) and "intermediate C" (Hagins, 1956).

8. N-retinylidene opsin (Morton and Pitt, 1955), also known as "indicator yellow" (Lythgoe, 1937).

9. Retinal, also known as "retinene" (Wald, 1933) and "stabilized metarhodopsin II" (Donner and Reuter, 1969).

10. Retinol (Bliss, 1949).*

Photoproduct Kinetics

The kinetics of formation and decay of certain intermediate rhodopsin photoproduct species have been studied by numerous investigators. A review of the experimental observations related to such kinetics is presented below, in the order of appearance of the various intermediates, based upon the sequences outlined in Figure 1. These studies have been undertaken on a diverse set of specimens, including solutions of extracted rhodopsin, suspensions of detached photoreceptor outer segments, isolated intact retinas, and intact, in vivo eyes.

The general procedure has been to irradiate or "bleach" the preparation, in order to initiate the series of transitional chemical changes. By observing shifts in the wavelengths of light where light absorption by the pigment is maximum, the kinetics of the photoproduct transitions have

---

*Retinol (vitamin A) is only formed in intact photoreceptor cells and is not found in solubilized extracted rhodopsin.

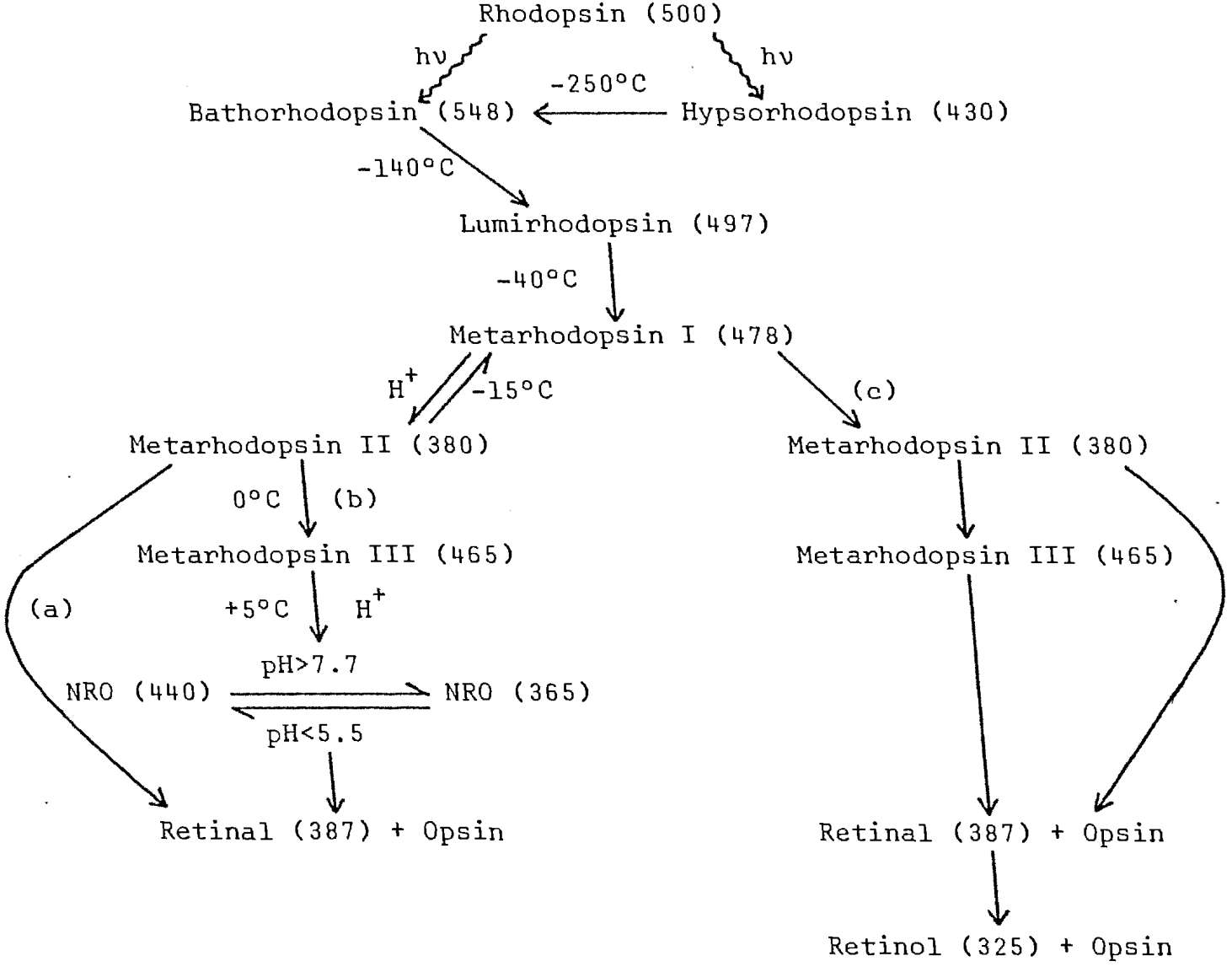
Rhodopsin (500)
hν
hν
-250°C
Bathorhodopsin (548)
Hypsorhodopsin (430)
-140°C
Lumirhodopsin (497)
-40°C
Metarhodopsin I (478)
H+
-15°C
(c)
Metarhodopsin II (380)
Metarhodopsin II (380)
0°C
(b)
Metarhodopsin III (465)
Metarhodopsin III (465)
(a)
+5°C
H+
pH>7.7
NRO (440)
NRO (365)
pH<5.5
Retinal (387) + Opsin
Retinal (387) + Opsin
Retinol (325) + Opsin

Figure 1

Figure 1. Proposed sequences of photolysis of rhodopsin. Wavelength of maximum absorption is indicated in parentheses for frog rhodopsin. (a) Route according to Matthews, et al., in solutions of cattle rhodopsin (1963). (b) Route according to Ostroy, et al., in solutions of cattle rhodopsin (1966). (c) Route according to Baumann (1972) in the perfused, isolated retina of the frog.

been identified spectrally as a function of time. The tacit assumption which has been invoked in specifying the kinetics in this manner is that optical density changes, which are measured at the wavelength of maximum absorption for a given photoproduct, are proportional to concentration changes in the photoproduct. When the reaction rates are rapid, the procedure requires the delivery to the preparation of a high intensity light for a very brief period. This procedure is called "flash photolysis."

A frequent goal of the kinetic studies of rhodopsin photoproducts is a determination of which photoproduct(s) or photoproduct change(s) generate(s) the "signal" that results in the electrical events in photoreceptors (see section on Transduction Processes). Instrumental limitations often prevent measurement of the early photochemical events at physiological temperatures. It is a common practice, therefore, to determine the photoproduct kinetics at low temperatures, where the necessary measurements are feasible, and to extrapolate these measurements to physiological temperatures.

Such extrapolations require certain assumptions about the nature of the chemical reactions of the photoproducts. The most common assumption is that the reactions are linear and first-order, such that the concentration, C(t), of a particular photoproduct is specified by the equation,

$$\frac{dC(t)}{dt} = -k\ C(t) \quad . \qquad (1)$$

The rate constant, k, is related to the half-time of a process, the time required for the concentration to decrease to one-half of its initial value, by the relationship,

$$t_{\frac{1}{2}} = \frac{\log 2}{k} \quad . \qquad (2)$$

Based upon Arrhenius' theory, the rate constant is related to the absolute temperature, T, as follows:

$$\log k = a_1 \left(\frac{1}{T}\right) + a_2 \quad ; \qquad (3)$$

where a_1 and a_2 are constants. A graphical plot of the logarithm of the rate constant versus the reciprocal of absolute temperature yields a straight line, from which the influence of temperature upon the reaction kinetics is easily determined. Thus, photoproduct kinetics at physiological temperatures can be extrapolated from low-temperature observations if the assumption of first-order, linear processes is valid.

The earliest photoproduct transition for which kinetic information currently exists involves the decay of bathorhodopsin to lumirhodopsin in solutions of extracted cattle rhodopsin. Bathorhodopsin was observed less than 20 picoseconds following laser flash photolysis at 21°C (Busch, Applebury, Lamola, and Rentzepis, 1972). The decay of bathorhodopsin to lumirhodopsin, expressed as a single first-order process, was extrapolated to a half-time of 10 nanoseconds at 38°C.

In contrast, earlier investigations of bathorhodopsin

decay, in solutions of cattle rhodopsin at -67°C and -50°C, had been resolved into three, simultaneous first-order processes with half-times of decay of 15 nanoseconds, 86 nanoseconds, and 38 microseconds, respectively, when extrapolated to 38°C (Grellman, Livingston, and Pratt, 1962). Similar results were obtained by the same laboratory from cattle rod outer segment particles, whose extrapolated half-times were 13 nanoseconds, 78 nanoseconds, and 280 nanoseconds (Pratt, Livingston, and Grellman, 1964). Treatment of the rate data as three simultaneous processes suggested the existence of three forms of bathorhodopsin (see Wulff, Adams, Linschitz, and Abrahamson, 1958).

Cone (1964) observed that the action spectrum of an early receptor potential (ERP), recorded extracellularly from photoreceptor cells, matched the absorption spectrum of the pigment contained within the cells, with the amplitude of the ERP being proportional to the amount of pigment present. This observation was utilized to study the kinetics of formation and decay of several photoproducts in dark-adapted intact retinas, beginning with the formation of lumirhodopsin. ERP measurements indicated that lumirhodopsin appears in less than 1 microsecond (Cone, 1972).

The conversion of lumirhodopsin to metarhodopsin I was difficult to study spectrophotometrically because of the similarity of the absorption spectra of the two species. In solubilized cattle rhodopsin, lumirhodopsin decay was characterized to be one (Matthews and Wald in Hubbard, Bownds,

and Yoshizawa, 1965), two (Rapp, 1970), or three (Erhardt, Ostroy, and Abrahamson, 1966) simultaneous first-order processes with substantially different rate constants, which varied by up to two orders of magnitude.

An attempt has also been made to account for the decay of lumirhodopsin, measured in solutions and in outer segment suspensions, in terms of a bi-molecular, second-order process (Rapp, Weisenfeld, and Abrahamson, 1970). This hypothesis was formulated to account for binding-site studies, which suggested that lumirhodopsin was mobile in the photoreceptor membrane and could presumably collide with proteins or other molecules in the membrane. This hypothesis required the additional postulation of a second, unknown substrate, in addition to the lumirhodopsin molecule.

Studies of lumirhodopsin decay in intact retinas have failed to confirm the complicated behavior of the kinetics apparently found in solution or in outer segment suspensions. ERP measurements in intact retinas determined a single decay half-time of lumirhodopsin to be 50 microseconds (Cone, 1972). Baumann (1976) found similar lumirhodopsin kinetics using single-wavelength spectrophotometry on whole, isolated frog retinas.

The decay of metarhodopsin I was the first intermediate process whose kinetics were studied in aqueous, digitonin solution (Wulff, Adams, Linschitz, and Abrahamson, 1958). It was in these studies that the postulate of multiple forms of photoproduct existing simultaneously in solution was first

suggested. Half-times of decay, extrapolated to 37.6°C were calculated to be 14 microseconds, 110 microseconds, and 1.5 milliseconds, respectively. Pratt, Livingston, and Grellman (1964) also obtained results indicating two or three simultaneous first-order processes for metarhodopsin I in solution, depending on the temperature of study. At 37°C, they reported characteristic half-times of 600 microseconds and 3 milliseconds. However, Applebury, Zuckerman, Lamola, and Jovin (1974) reported that metarhodopsin I, formed from rhodopsin which had been purified and reassociated with phospholipid, decayed with a single time constant.

Matthews, Hubbard, Brown, and Wald (1963) observed a quasi-equilibrium between metarhodopsins I and II in solution at temperatures above -17°C. The relative proportions of the two metarhodopsins was found to depend on the pH of the solution, with acid conditions decreasing metarhodopsin I and increasing metarhodopsin II. This important observation led to the hypothesis that the transition of metarhodopsin I to metarhodopsin II was associated with the uptake of a hydrogen ion. Extrapolation of their data to 25°C indicated a first-order process of equilibration between the two pigments with half-time of 1 millisecond. Subsequently, Falk and Fatt (1966) produced electrochemical evidence which supported this hydrogen-uptake hypothesis and closely agreed with the time course proposed by Matthews, et al. This initial observation that a microenvironment factor, the hydrogen ion concentration, could significantly

affect the chemical course of events of the rhodopsin photoproducts, is particularly relevant to the results to be reported in this dissertation.

Williams and Breil (1968) measured the formation of metarhodopsin II in rhodopsin solutions, utilizing different solubilizing agents. In digitonin extracts, all of the detected metarhodopsin II was present within approximately 10 milliseconds following flash photolysis. By comparison, complete formation of metarhodopsin II was observed in less than 200 microseconds in rhodopsin solubilized in hexadecyl trimethylammonium bromide.

Von Sengbusch and Stieve (1971) detected a first-order decay of metarhodopsin I in rod outer segment suspensions, with half-time of 600 microseconds at 37°C. A study of sonicated, cattle rod outer segments similarly indicated a half-life of metarhodopsin I decay of 500 microseconds (Rapp, Wiesenfeld, and Abrahamson, 1970).

The conversion of metarhodopsins I to II has also been studied in intact retinas. ERP measurements determined the half-time of conversion of metarhodopsins I to II to be 40 microseconds at 37°C in the excised eye of the rat (Ebrey, 1968). Similar ERP measurements by Cone and Cobbs (1969) indicated a different half-time of decay time of 250 microseconds. Baumann (1976) recorded a half-time of formation of metarhodopsin II of approximately 700 microseconds in the isolated retina of the frog, which was significantly faster than the reported time of 3 milliseconds in a similar preparation (Liebman, Jagger, Kaplan, and Bargoot, 1974).

Hagins (1956, 1957) studied living and excised intact eyes of rats and rabbits, utilizing flash photolysis, by performing measurements on light reflected from the fundus of the eye. He detected the appearance of "intermediate A," identical in retrospect with metarhodopsin I, within one millisecond at 8°C. Extrapolation of Hagins' observations to 37°C resulted in a half-time of transition from intermediate A to "intermediate B" (metarhodopsin II) of 120 microseconds.

The thermal decay of photoproducts beginning with metarhodopsin II has been relatively easier to study, owing to the slower time course of these events. However, a number of alternate physiological pathways of decay have been postulated by different investigators, based upon differences in the various results (Figure 1). Ostroy, Erhardt, and Abrahamson (1966) suggested that cattle metarhodopsin II in solution decayed quantitatively to metarhodopsin III, followed by an acid-catalyzed decay to N-retinylidene opsin (NRO) and a subsequent hydrolysis to free retinal plus opsin. Matthews, Hubbard, Brown, and Wald (1963), however, claimed that metarhodopsin II decayed directly to free retinal plus opsin in solution, with metarhodopsin III and NRO being merely side products, out of the main sequence of events.

In a perfused, isolated frog retina, evidence also suggested the existence of two pathways to free retinal, which were, nevertheless, different from the two pathways in rhodopsin solutions (Baumann, 1972). Metarhodopsin II

proceeded to retinal either directly or by way of metarhodopsin III, without passing through the NRO state. Additional evidence suggested that the route through metarhodopsin III was by-passed when only a few percent of the rhodopsin was bleached (Donner and Hemila, 1975). In the intact eye, Hagins (1957) observed that only part of intermediate B decayed via "intermediate C" (metarhodopsin III).

ERP measurements in the rat eye indicated a half-time of decay of metarhodopsin II of 140 seconds at 37°C (Ebrey, 1968), versus 63 seconds reported at the same temperature by Cone and Cobbs (1969). Slow spectrophotometric measurements made on isolated frog retinas could not distinguish between metarhodopsin II and free retinal, since their absorption maxima were virtually identical, so that direct measurement of metarhodopsin II decay was unobtainable (Frank, 1969; Baumann, 1972; Gyllenberg, Reuter, and Sippel, 1974).

However, metarhodopsin III decay could be followed to completion in the isolated frog retina. A peak in the amount of metarhodopsin III present was found to occur between 120 and 140 seconds at 21°C, according to Hagins (1957), Donner and Reuter (1967), and Baumann (1972), with complete disappearance reported after 50 minutes (Frank, 1969). ERP measurements in the rat eye illustrated a half-time of metarhodopsin III decay of 18 minutes at 37°C (Ebrey, 1968) when compared with Frank's result of 11 minutes at 22°C in the frog (Frank, 1969).

Conflicts in the Literature

The historical background described above demonstrates the lack of a well-established, incontrovertible, and consistent body of knowledge which could uniquely characterize either the existence or the formation and decay kinetics of the various rhodopsin photoproducts. At best, photoproduct and kinetics data available to date are confusing and might even be misleading, in view of the variety of experimental conditions under which the results were obtained.

It is not known, for example, whether it is valid to compare kinetics among intact eyes, isolated retinas, detached photoreceptor cell suspensions, and extracted rhodopsin in solution. A systematic study of visual pigment photoreceptors in all types of preparations, obtained from the same type of animal, has not been accomplished to date. One indication of the problems associated with such comparisons is the observation of possibly up to three different forms of several particular photoproduct species, which apparently exist simultaneously in solubilized rhodopsin and in photoreceptor cell suspensions. To date, similar indications of multiple forms of photoproduct species have not been confirmed in intact retinas, although Bowmaker and Loew (1976) have suggested the possibility of three forms of the parent rhodopsin pigment in isolated frog retinas, which show different stability toward hydroxylamine.

The study of visual pigment bleaching kinetics in the

past has been complicated by the rapidity of the intermediate chemical transformations and the inherent instability of certain photoproducts near physiological temperatures. A question can be raised concerning the validity of extrapolating rate data, obtained at very low temperatures, to the physiological temperature range. Such extrapolations not only employ assumptions about the organization of visual pigment molecules and the relationship of such molecules to their environment that may not be justified, but also imply that only a single, linear, first-order process is involved. These assumptions are questionable, in light of the observation of multiple simultaneous photoproduct forms. The studies of photoproduct kinetics which are reported in this document have been restricted to within the physiological temperature range of the experimental animal, in order to eliminate such extrapolations.

Still another problem arises when one attempts to compare results, even among studies using the same type of preparation. Investigators studying photoproduct kinetics in solubilized rhodopsin preparations, for example, have used a variety of different detergent agents to extract the rhodopsin from the tissue. In studies of isolated retinas, as a second example, the external bathing media has contained concentrations, volumes, and types of buffering agents and electrolytes that have varied from investigator to investigator.

In addition, certain investigators have included some

sort of energy source, such as glucose, in the solution surrounding the preparation, while others have chosen to omit such additions. Recent evidence of reversible phosphorylation of rhodopsin at even low levels of illumination suggests that metabolism probably plays an important role in photoproduct physiology (Bownds, Dawes, Miller, and Stahlman, 1972; Miller and Paulsen, 1975). Results to be reported in this thesis are in agreement with the importance of metabolic activity in influencing photoproduct behavior.

It would appear reasonable to inquire whether some of the inconsistencies in the reported data are attributable to such variable environmental and metabolic conditions. The experimental protocol of this dissertation research has been designed, therefore, to vary systematically the external pH and metabolic state of the preparation, in the presence of constant ionic concentrations, in an attempt to elucidate their role in determining photoproduct kinetics.

Transduction Process

It is well-known that vertebrate photoreceptors exhibit a late receptor potential following a light stimulus, which can be measured extracellularly, with a latency as small as 1.5 milliseconds (Brown, Watanabe, and Murakami, 1965). Intracellular recordings show a hyperpolarization of the cell membrane to light (Tomita, 1970), which is attributable to conductance changes in the photoreceptor plasma membrane

(Baylor and Fuortes, 1970; Brown and Pinto, 1974; Lasansky and Marchiafava, 1974). These conductance changes reflect alteration of the ionic permeability of the membrane, particularly to sodium ions. In addition, local illumination of vertebrate photoreceptor outer segments produces membrane current changes which are mainly confined to the region where the photons are absorbed (Hagins, Penn, and Yoshikami, 1970).

Thus, it would appear that visual pigment molecules somehow control the membrane permeability at nearby sites in the photoreceptor surface or plasma membrane. This is consistent with the observation that the visual pigments are membrane-bound. Evidence that visual pigments are membrane components comes, in part, from ERP experiments (Brown and Murakami, 1964; Cone, 1964). Since the early receptor potential is observed to change sign when the measuring electrode is moved from the intracellular region to the extracellular space, some of the pigment molecules are therefore concluded to lie within the membrane (Smith and Brown, 1966). The fact that photoreceptor outer segments exhibit altered dichroism, after exposure to light, additionally supports the concept of photopigment as a membrane component (Hárosi, 1972). Structural studies on photoreceptors have been reviewed by Worthington (1974). Recent neutron diffraction analyses have indicated that most of the rhodopsin molecule is embedded in the hydrophobic core of the photoreceptor membrane (Saibil, Chabre, and Worcester, 1976).

Evidence has been presented that the activation of a rhodopsin molecule by light cannot itself produce the conductance changes observed, without some amplifying system intervening between the visual pigment and the surface membrane (Baylor and Fuortes, 1970; Cone, 1972). Thus, it has been suggested that visual pigment molecules excite the photoreceptor cell by releasing an intracellular transmitter substance, which modulates membrane conductance (Fuortes and Hodgkin, 1964). Calcium ion has been proposed as the transmitter (see Hagins, 1972).

Rationale

It is commonly held that one or more of the rhodopsin photoproducts or photoproduct changes initiates some process which eventually results in excitation of the photoreceptor cell membrane. As yet, it is unknown which of these photoproducts or photoproduct changes are most directly related or coupled to the electrical events in the photoreceptor. The fact that some of the thermal reactions are faster than the latency of the electrical response of the photoreceptor implicates that these reactions could play an important part in initiating such events. Most specifically, metarhodopsin I is of special interest, since it is probably the last intermediate species to disappear before the late receptor potential occurs.

A knowledge of the kinetics of formation and decay of metarhodopsin I in intact retinas would be useful in trying

to understand better its potential role in the transduction process in photoreceptor cells. However, inconsistencies in the literature, discussed previously, prevent one from developing specific conclusions as to the behavior of metarhodopsin I, or any other photoproduct. A new set of experiments, in which closer study of the effects of ionic and metabolic alterations on photoproduct kinetics, in the physiological temperature range, was attempted, would perhaps be helpful in clarifying some of the reported disparities.

An investigation of such factors on the kinetics of slower photoproducts would be a logical starting point for such experiments. Results obtained for these later photoproducts would establish a context for evaluating eventual studies on metarhodopsin I itself. Such a study of the kinetics of the slower photoproducts, subsequent to metarhodopsin II, has been the main objective of the research described here. The results of this research will hopefully contribute to a better understanding of the role of bleaching in the excitation mechanisms of photoreceptors.

Microspectrophotometry

The technique of microspectrophotometry was first conceptualized by Caspersson (1940), who devised the optics and electronics necessary to record absorption spectra of cellular systems. Several years passed before its application to *in situ* identification of visual pigments (Hanaoka and Fujimoto, 1957). Since then, the technique

has been used increasingly in the study of visual pigments and their photoproducts.

Microspectrophotometry can be summarized as the projection of a microbeam of monochromatic radiation through photoreceptor cells that contain light-sensitive pigment and recording the subsequent photon loss due to absorption by that pigment (Carlson, 1972). A microspectrophotometer consists, in general, of an illumination source in series with a monochromator, which separates the light spatially, either stepwise or continuously, into a selected range of its spectral components. The exit radiation of the monochromator is directed along an optical path, where the light is stopped down with an aperture and the image of the monochromator exit slit is demagnified by a condenser lens.

This beam is normally partitioned or chopped into two parts. One portion passes through the specimen to be measured, while the other "reference" beam is directed either to a clear area within the microscopic field (Liebman, 1962; Marks, 1965) or through a completely separate light path (Brown, 1961). The relative intensities of the fluxes of the sample and reference beams are then measured by a photomultiplier tube, whose photocurrent is proportional to the transmitted flux of the illuminated part of the specimen.

Microspectrophotometers have increased in sophistication since Caspersson's time. His original method measured transmittance values at individual wavelengths, using electrometers as the indicating instruments (Caspersson, 1940).

Caspersson obtained reasonably accurate measurements of the absorption spectra of nucleic acids in cellular nuclei as small as 1 micron in diameter.

Increased speed, improved accuracy, and automatic recording were features incorporated into an instrument used to study kinetics of respiratory enzymes in solution (Chance, 1951; Yang and Legallais, 1954). A later version of this apparatus (Chance, Perry, Akerman, and Thorell, 1969) improved noise control, electronic stability, and response time to obtain more sensitivity to small variations in absorption as well as automatic wavelength scanning of 50 nanometers per minute.

Brown (1961) modified a commercially available spectrophotometer to study photopigments in man and monkey (Brown and Wald, 1963). By field masking, retinal patches as small as 4 microns in diameter could be measured. A modification of Chance's instrument yielded a microspectrophotometer with scanning rates of 40 nanometers per second, to permit a detailed study of the visual pigments in the frog and tadpole (Liebman, 1962; Liebman and Entine, 1968). The reference beam of this instrument was used in a feedback mode to control the gain of the photomultiplier, so that its output remained consistent with variations in light source intensity.

Marks (1965), reversing the trend, developed an instrument with a slower scan rate of only 2.3 nanometers per second but with higher photon flux. This choice of instrument parameters was based on Marks' analysis of the best

means of optimizing the signal-to-noise ratio. He then modified his results by developing a computerized correction factor, which effectively eliminated the resultant distortion caused by bleaching photopigment during the measured scan. He also introduced additional photodiode feedback to the light source of his instrument to maintain constant flux out of the monochromator over the entire spectrum.

Several investigators have modified the fundamental designs of these established instruments to study invertebrate photopigments as well. Langer and Thorell (1966) improved Chance's design to examine insect rhabdoms, while Goldsmith, Dizon, and Fernandez (1968) and Waterman, Fernandez, and Goldsmith (1969) adapted Liebman's design by adding a superior photomultiplier tube to study rhabdoms of prawns and crayfish.

More recently, Hárosi and MacNichol (1974) developed a single-beam, polarized light, microspectrophotometer to study visual pigments. That instrument scans the spectrum at the rate of 500 nanometers per second and resolves cell absorption into two orthogonal components to determine orientational characteristics of the visual pigment chromophore in single photoreceptor cells. Alignment problems, common to most microspectrophotometers, were reduced because of the use of a single beam. Multiple scanning and computer averaging reduced spectral distortions produced by bleaching with the measuring light.

A primary consideration in the design and use of a microspectrophotometer for the study of visual pigments is the necessary compromise in the intensity of the measuring light source. The light intensity must be high enough to obtain a good signal-to-noise ratio, yet low enough to insure that the pigment being studied is not significantly bleached by the measuring scan (Marks, 1963, 1965; Liebman and Entine, 1964). Coupled with this is the necessary requirement of efficient photon detection and the desirable requirement of illuminating the specimen only during the measuring scan. These standards, which were not so critical in Caspersson's or Chance's experiments on non-photolabile substances, were first acknowledged by Hanaoka and Fujimoto (1957), who detected bleachable pigments in carp cones but were unable to obtain accurate estimates of the absorption spectra with their instrument.

An additional microspectrophotometer design requirement involves the minimization of light lost due to scattering by the specimen. A judicious selection of the numerical apertures of the demagnifying, microscope condenser and the collecting, microscope objective, such that the objective has the larger numerical aperture and thus possesses a wider collection angle, is useful in decreasing the amount of scattered light which is undetected (Hárosi and MacNichol, 1974).

The aforementioned considerations are applicable to all microspectrophotometers, whether they be used for "steady-state" or kinetic measurements. Additional factors must be considered in the design of instruments employed for kinetic studies with flash photolysis. For example, one of the major limitations of existing instruments used for such kinetic studies has been their inability to initiate the bleaching process rapidly, to initiate spectral measurements with a short latency after the bleach, and to scan the spectrum to be measured at high speed. So far, the microspectrophotometers reported to date which have been capable of measuring multiple photoproduct transitions sequentially, in the same preparation, have not been able to detect products earlier than metarhodopsin III formation at physiological temperatures (Frank, 1969; Hárosi, 1972; Gyllenberg, Reuter, and Sippel, 1974). Moreover, instruments which have been rapid enough to detect some of the earlier photoproducts have been incapable of scanning the spectrum in order to observe subsequent photoproducts with different absorption maxima (Liebman, Jagger, Kaplan, and Bargoot, 1974; Baumann, 1976).

The rapid scanning microspectrophotometer (RMSP) at the Laboratory of Neurophysiology, NIH, operates at a rate of 600 microseconds per waveband and with a measuring latency of only milliseconds. This instrument, therefore, can be utilized to detect millisecond-latency photoproducts, not only following their kinetics to completion but also recording all subsequent photoproduct species kinetics in sequence.

Thus, within the milliseconds and longer time domain, a complete, composite picture of the photoproduct sequence and kinetics can be obtained.

The RMSP is capable of measuring absorption spectra from selected 400 micron diameter patches of isolated retina with intact photoreceptor cells. Since the instrument incorporates a perfusion system into the chamber of the preparation, the effects of any desired extracellular ionic and metabolic conditions upon the kinetic rates can be determined easily by a change in composition of the perfusate. The RMSP is thus a flexible instrument for studying photoproduct kinetics in the retina under a variety of experimental conditions. A detailed description of the instrument is given in Appendix A.

Specific Aims of Results To Be Reported

In view of the inconsistent and incomplete previously reported data, both on the sequence of the photoproducts of rhodopsin as well as on the kinetics of formation and decay of those photoproducts, it is readily apparent that additional experiments are required to resolve the difficulties in interpreting past results. In addition, it would appear necessary to resolve those difficulties in the later, slow photoproducts before a rational effort can be made to understand the chemical pathways and kinetics of the earlier,

faster photoproducts that are involved in the phototransduction process.

The objective of the research reported here, therefore, has been to study the kinetics of formation and decay of visual pigment photoproducts, beginning with the decay of metarhodopsin II. The bulk of the data presented and analyzed in detail, however, will concentrate on the kinetic properties of metarhodopsin III. The isolated, dark-adapted, and perfused retina of the frog, Rana pipiens, has been selected as the experimental specimen. Since much of the recent research has been performed on this animal, the use of this species allows an easy comparison of results. The RMSP has been utilized to measure absorption spectra of the preparation as a function of post-bleach time, in order to identify the active pigment species and their kinetics.

Moreover, since a review of the existing literature suggests that the milieu of visual pigments may affect their sequence and their kinetics, a series of experiments attempting to determine the effects of systematic alteration of environmental factors on the photoproduct sequence and their kinetics has been devised. In order to establish the context in which experimental metabolic alterations have been performed, a summary of the pathways of cellular energy transfer in the retina is briefly reviewed at this time.

There is considerable evidence that the transformation of energy into a usable form in the retina follows the same sequential pathways which are present in most living cells (Cohen and Noell, 1960; Lowry, 1964; Klethi, Urban, and Mandel, 1970). This scheme is diagrammed schematically in Figure 2 (Lehninger, 1975), in which glucose is indicated to be the basic substrate for cell metabolism.

Glycolysis, which is the anaerobic degradation of glucose to yield lactic acid, operates in the cell cytoplasm under conditions when a supply of molecular oxygen is inadequate. Eleven enzymes act sequentially as catalysts in the glycolytic pathway. All of the intermediates of glycolysis between glucose and pyruvate are phosphorylated compounds, with the primary function of the phosphate group being the conservation of energy. Two molecules of adenosine triphosphate (ATP), which is a store of chemical potential energy, are required to prime the glycolytic process, while four molecules of ATP are produced. The net yield of ATP is thus two molecules for each molecule of glucose that is degraded to lactate.

The pyridine nucleotide, nicotinamide adenine dinucleotide (NAD), functions as the coenzyme during the oxidation step which leads to the formation of pyruvate. In the last step of glycolysis, pyruvate is reduced to lactate via the reduced form of the coenzyme (NADH). Lactate, the end product of anaerobic glycolysis, diffuses at a slow rate through the cell membrane as waste.

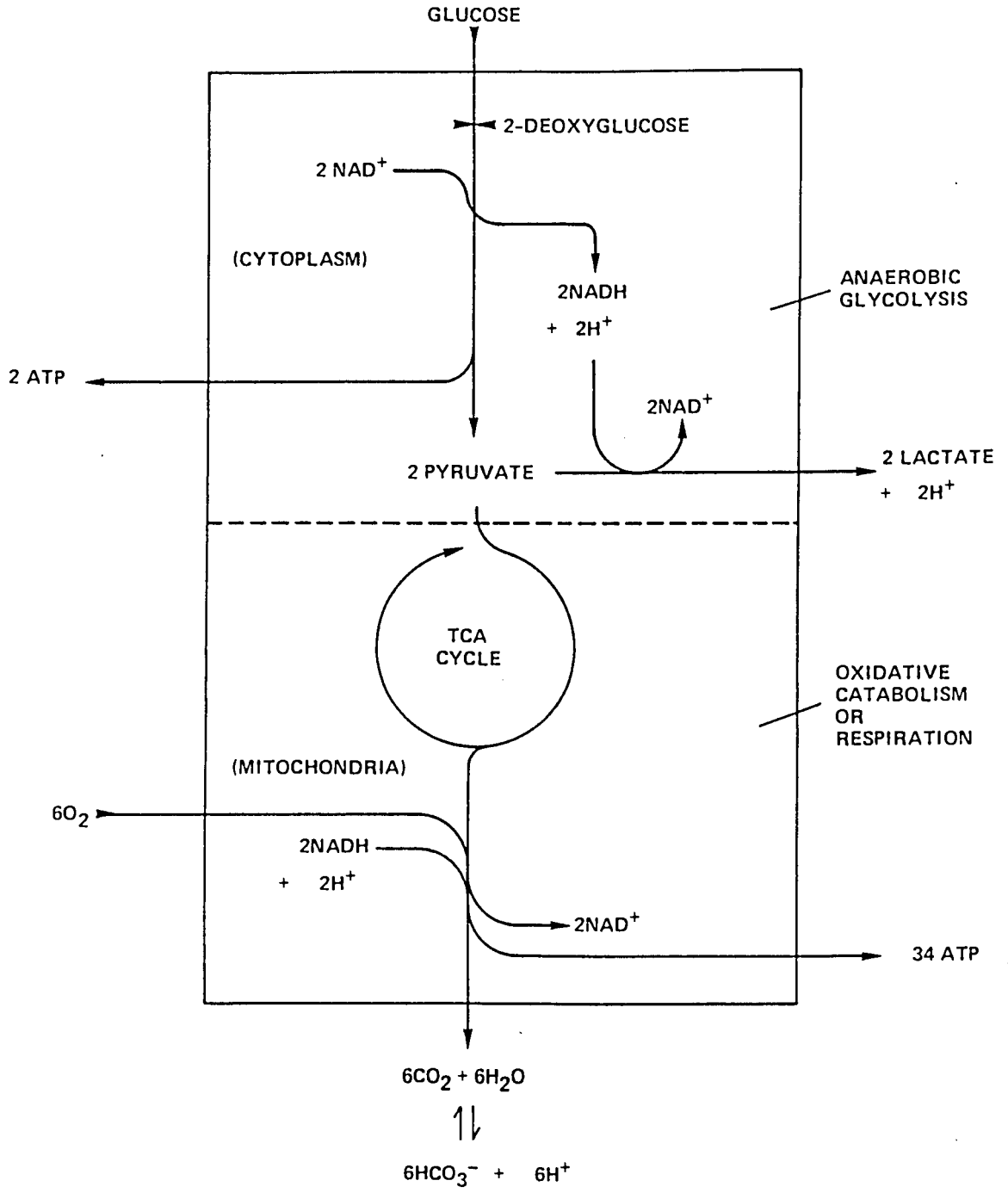
GLUCOSE
2-DEOXYGLUCOSE
2 NAD+
(CYTOPLASM)
2NADH
+ 2H+
ANAEROBIC
GLYCOLYSIS
2 ATP
2NAD+
2 PYRUVATE
2 LACTATE
+ 2H+
TCA
CYCLE
OXIDATIVE
CATABOLISM
OR
RESPIRATION
(MITOCHONDRIA)
6O2
2NADH
+ 2H+
2NAD+
34 ATP
6CO2 + 6H2O
6HCO3− + 6H+

Figure 2

Figure 2. Schematic diagram of cellular metabolism. Only fundamental reactions are shown. See text for explanation.

In addition to the glycolytic pathway as an energy producer, aerobic cells, such as those in the retina, also obtain energy from the oxidation of fuel molecules by molecular oxygen. The process of aerobic respiration releases considerably more energy, by oxidizing glucose to carbon dioxide and water, than that produced during anaerobic glycolysis.

Pyruvate, instead of being reduced to lactate, becomes the primary substrate in the respiratory pathway. The oxidation of pyruvate to acetyl-Co-A makes the molecule accessible for the series of enzymatic reactions known as the tricarboxylic acid (TCA) cycle, in which two-carbon residues are degraded to carbon dioxide. During the reaction, NAD is reduced to NADH, which in turn donates electrons to molecular oxygen via an electron transport chain in the mitochondrion. The free-energy decrease which accompanies the transfer of electrons along the respiratory chain is coupled to the formation of 34 molecules of ATP. Thus, the complete, aerobic oxidation of a single molecule of glucose nets a total yield of 36 ATP molecules. Carbon dioxide, which is formed during the TCA cycle, is released by the cell as waste and can cross the cell membrane rapidly.

Under normal physiological conditions, the isolated retina utilizes oxygen and glucose at a very rapid rate (Lolley and Schmidt, 1974). The effects of metabolic variables on the rhodopsin photoproduct sequence and kinetic parameters have therefore been selected as a topic of study

in the experiments reported here. A perfusion system has been devised, in which the composition of the perfusate has been varied in a systematic way from the normal retinal conditions of ample glucose and oxygen. The metabolic modifier, 2-deoxyglucose, which blocks the action of the first enzymatic steps required in the catabolism of glucose (Wick, Dury, Nakada, and Wolfe, 1957), has been used to deprive the retina of an energy substrate. The perfusate has also been saturated with nitrogen gas instead of oxygen, in order to provide an anoxic condition to the retina.

In addition, since the concentrations of lactate and carbon dioxide waste products may affect the intracellular acidity of the retina, the pH of the extracellular perfusate has been altered by suitable selection of buffers to study the effects of hydrogen ion concentration variation. All experiments have been performed at 21°C, which is within the physiological temperature range of the active frog.

The remaining chapters of this dissertation outline experimental methods, present results, and discuss the implication of these results. In addition, supplemental appendices have been prepared to summarize the design of the RMSP and data analysis schemes and computational procedures.

METHODS

Introduction

A rapid scanning microspectrophotometer (RMSP) (see APPENDIX A) was utilized to measure absorption spectra from dark-adapted, isolated frog retinas. A perfusion system was incorporated into the experimental chamber, which was used to bathe the specimen extracellularly with solutions of selected composition.

Surgical Preparation

Common laboratory stock of male and female leopard frogs (Rana pipiens), obtained throughout the year (Lake Champlaign Frog Farm, Vermont), were used in all experiments. Animals were stored in the refrigerator at 4°C. Before use, the frogs were kept in the dark for at least 16 hours at 4°C.

The dark-adapted experimental animal was sacrificed in the dark by pithing the brain and spinal cord. The frog was then decapitated, and the eyes were excised under a dim, deep red light (Tungsen light source; Kodak, Series 2). Each eye was opened by cutting it sagitally with a razor blade, approximately at the ora terminalis. The anterior half of the eye and vitreous humor were removed and discarded. The posterior half, to be used in the experiment, was transferred to a Petri dish containing a small volume of the desired Ringer solution (see below).

The retina was gently separated from the pigment epithelium with a forceps under a dissecting microscope (5X) equipped with an infrared image converter (FJW Industries, Inc.). The retina was removed from the dish, by suction, into an eyedropper, along with a small quantity of the surrounding Ringer, and was transferred to a perfusion chamber.

Perfusion System

The experimental perfusion chamber, illustrated in Figure 3, consisted of three machined pieces of clear lucite: a base, an insert, and a lock. The base and insert had matching internal dimensions, so that two circular glass slides, one attached to each piece, formed a sandwich in the center of the perfusion chamber. The glass slides, 2.5 centimeters in diameter, were held in place and made water-tight by a small amount of transparent stopcock grease spread on the rims of the two respective lucite pieces.

Two semicircular pieces of rubber, 0.25 millimeter thick, were epoxied to each glass slide in such a way as to leave a clear, unobstructed strip, 2.5 millimeters wide, along the diameter of the glass slide. The glass slide affixed to the lucite base was aligned so that the clear, diametric strip was colinear with inflow and outflow ports in the base, as illustrated in Figure 4.

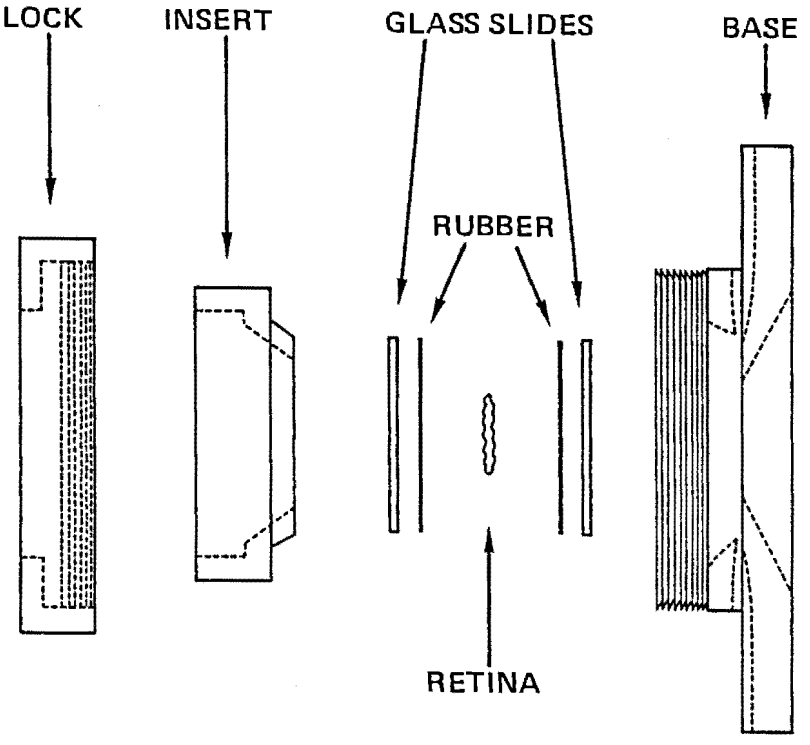

Figure 3

Figure 3. Perfusion chamber assembly. Exploded side view. See text for explanation.

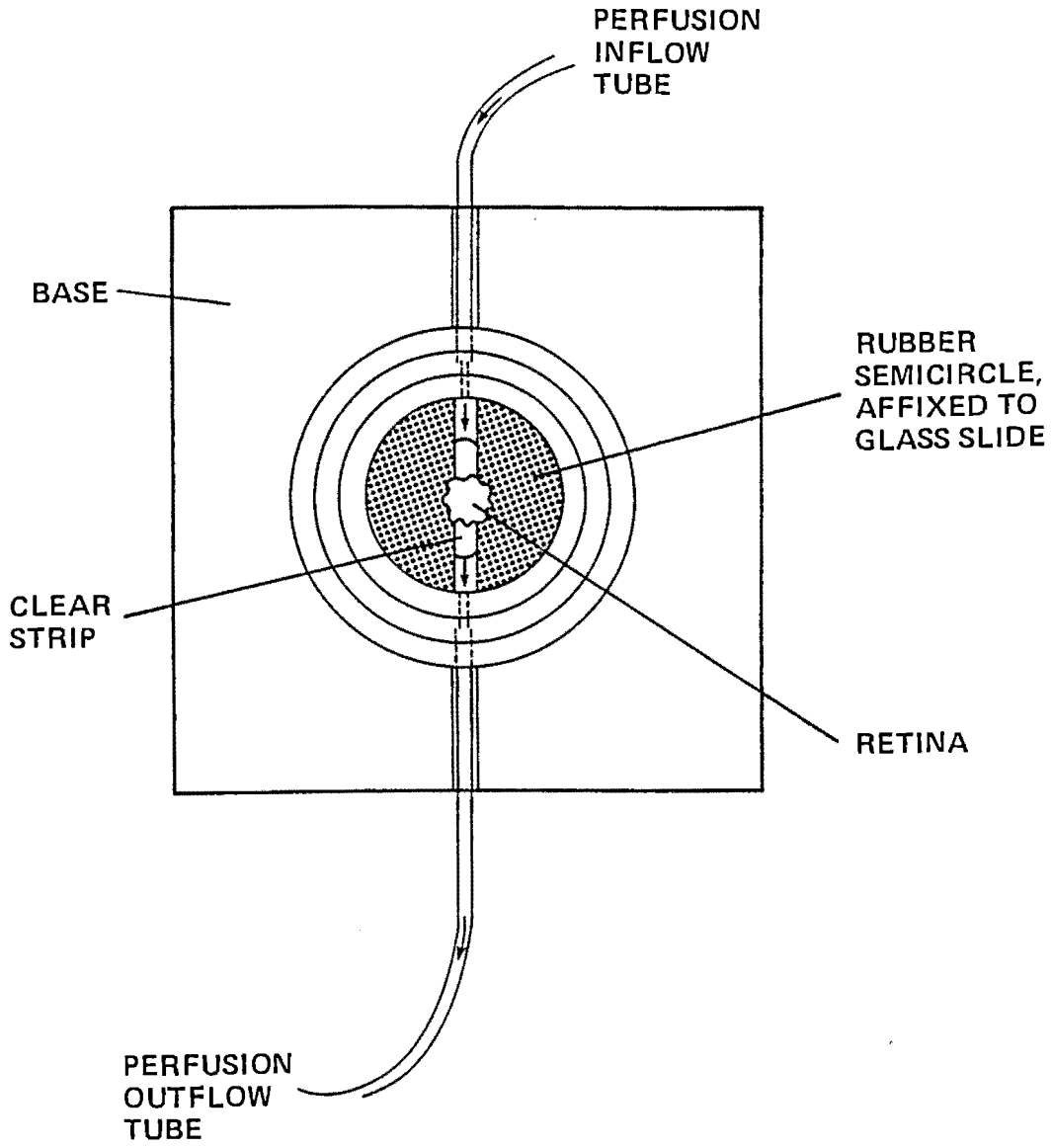
PERFUSION
INFLOW
TUBE
BASE
RUBBER
SEMICIRCLE,
AFFIXED TO
GLASS SLIDE
CLEAR
STRIP
RETINA
PERFUSION
OUTFLOW
TUBE

Figure 4

Figure 4. Pathway of perfusion. Perfusion medium, with gravity-controlled flow rate of approximately 2 milliliters/minute, entered inflow port of base via polyethylene tube. Perfusate flowed past the secured retina and exited through the outflow port via second polyethylene tube, as indicated by arrows. Insert and lock not pictured.

The rubber thus served the multiple purposes of delineating the path of the perfusion flow, securing the retina, and preventing its deformation and movement.

The retina was spread out in the center of the glass slide attached to the base, so that the edges of the retina barely overlapped the margins of the rubber semicircles. The insert was fitted into the base so that the boundaries of the two glass slide rubber edges were parallel and overlapped to hold the retina in place. The lock was screwed onto the base-insert combination to hold the pieces together in an air-tight seal.

Polyethylene tubes (.047 inches inside diameter) were inserted into the inflow and outflow ports of the perfusion chamber. The inflow tube was attached through a valve to a bottle containing the perfusate. Flow rate was gravity-controlled by the height of a bottle containing the perfusate with respect to the perfusion chamber and usually averaged approximately 2 milliliters/minute. The outflow effluate was allowed to drip freely into a large collecting beaker.

The foundation solution of all perfusate media (115 mM NaCl, 2.5 mM KCl, 2.0 mM $CaCl_2$, 0.5 mM $MgCl_2$) was a basic frog Ringer solution (Korenbrot and Cone, 1972), with the addition of Mg^{++} (Maker and Lehrer, 1972), which is required as a substrate by certain glycolytic enzymes (Lehninger, 1975). Studies were made at three different pH values: 5.5, 7.3, and 8.2. Table I summarizes the ionic concentrations of the perfusate components at each pH. The

	5.5	7.3	8.2	
Na^+ (sodium)	115.0	115.0	115.0	mM
K^+ (potassium)	2.5	2.5	2.5	mM
Ca^{++} (calcium)	2.0	2.0	2.0	mM
Mg^{++} (magnesium)	0.5	0.5	0.5	mM
Cl^- (chloride)	105.0	105.0	115.0	mM
CH_3COO^- (acetate)	10.0	--	--	mM
HEPES*	--	10.0	--	mM
Tris**	--	--	10.0	mM

*N-2-hydroxyethylpiperazine-N'-2-ethanesulfonic acid

**Tris (hydroxymethyl) aminomethane

Table I

Table I. Ionic composition of perfusate solutions. Concentrations (millimolar) of ions and buffering agents are given at each pH of study.

choice of the buffers was based on two considerations: first, that the buffering capacity of the buffer was high at the pH of interest; and second, that the buffers produced little or no effects on measurable physiological properties of photoreceptors or other excitable cells (T. G. Smith, personal communication).

In order to study the effects of metabolic substrates on photopigment kinetics, certain modifications in the perfusate composition were made. Under "ambient" conditions, the Ringer utilized had no added metabolic substrate. Alternatively, either D-glucose (20 mM) was added to promote metabolism or 2-deoxy-D-glucose (10 mM) was added to inhibit glucose catabolism (Wick, Dury, Nakada, and Wolfe, 1957). In addition, respiration of the tissue was controlled by continuously bubbling the perfusate with either oxygen or nitrogen gas (flow rate 1 liter/minute) for the duration of the experiment.

In summary, a total of 18 different perfusate compositions were utilized in this study. These were selected to include all of the combinations of the following three parameters, such that (a) the pH was buffered at either 5.5, 7.3, or 8.2; (b) the metabolic substrate consisted of either added glucose, no addition of substrate, or added 2-deoxyglucose; and (c) the respiratory state was either oxygen-saturated or nitrogen-saturated. In each case, the experiments were performed at 21°C.

Focusing

Once the retina had been placed in the chamber and the perfusion flow had begun, the chamber was mounted vertically in the RMSP. Thus, the chamber served as the stage of the microscope. The retina was then equilibrated for approximately five minutes in the perfusion medium prior to focusing.

In order to insure that the greatest amounts of light flux were both incident upon and collected from the cellular region of interest, two conditions were achieved. First, the microscope stage was positioned so that the boundary of the photoreceptor cells facing the incident light flux lay in the front focal plane of the condenser. Second, the objective was positioned so that the boundary of the cells facing the objective lay in the front focal plane of the objective. Except for the microscope stage and microscope objective, all of the other components of the RMSP were fixed. Thus, optimal focusing was achieved by appropriate positioning of the two adjustable components.

The sequence of steps required to accomplish optimal focusing began with the placement of an auxiliary lamp between the movable mirror and the condenser in order to permit dim, deep red background light to illuminate the specimen (see Figure A1, APPENDIX A). The objective was coarsely focused upon individual patches of photoreceptor cells located in the field of view, and the auxiliary lamp was temporarily extinguished and removed.

A deep red interference filter and several neutral density filters were placed in the path of the xenon bleaching lamp (see Figure A1: "FILTERS"). The shutter controlling the xenon light source was then opened to allow the heavily filtered, deep red light to illuminate the specimen. The stage and the objective lens were alternately moved along the optical axis, in incremental steps, during which time the objective kept the cells in focus by progressively following the stage. When both the border of the rods facing the light source and the image of the xenon arc came into the focus of the objective simultaneously, the process was stopped.

The bleaching shutter was closed and the auxiliary lamp was replaced and relit, after which the objective alone was moved away from the preparation in order to focus upon the surface of the rods facing the objective. The stage was moved in any direction perpendicular to the optical axis until a suitable test area of cells was located. The auxiliary lamp was then extinguished and removed from the instrument.

Measurements

After a test area had been selected and focused upon, a steady-state, pre-bleach measurement was recorded while

the visual pigment was in its original form.* The test area was then bleached for 300 milliseconds by the xenon light. A sequence of post-bleach measurements was begun 100 milliseconds after completion of the bleach (400 milliseconds after onset of the bleach). Measurements were recorded every 10 seconds for 3 minutes and then every 30 seconds for an additional 7.5 minutes.

Analysis of preliminary experiments, in agreement with common practice in the literature, indicated that the kinetics of the photoproducts being measured could be characterized by first-order, exponential processes. Thus, it was not necessary to follow the processes to completion, since data reduction techniques could extract all the required information (half-times and coefficients) from the kinetics of the partial measurements (see APPENDIX B). The 10.5-minute duration of an experiment was deemed sufficient for data analysis.

A measurement consisted of three consecutive spectral scans of 34 wavebands, from 370 to 640 nanometers. Each scan lasted 20.4 milliseconds. The average of the three scans was calculated during data reduction to improve signal-to-noise ratio. All measurements were either recorded on a

---

*The cathode ray tube measuring light bleached an insignificant amount of pigment.

Honeywell 5600C FM analog tape recorder or entered directly into a PDP-11/10 digital computer via an on-line connection.

Two additional measurements were recorded for computational purposes (see APPENDIX B). These measurements were a baseline measurement, with the CRT unlit, and a measurement through a clear area of the chamber, beyond the boundary of the retina. At the conclusion of each experiment, a series of three measurements was performed with the chamber removed and replaced, respectively, by 400, 500, and 600 nanometer interference filters for wavelength calibration.

The duration of an experiment was commonly two to three hours following surgery. During each experiment, six or more spots from each retina were routinely studied, in the manner described above. Data reduction was conducted on the PDP-11/10 computer, as described in APPENDIX B. Calculation of absorption spectra from a typical experiment of six retinal spots required approximately one hour of computer time.

RESULTS

Introduction

The primary purpose of the experiments presented in this section is to report on the effects of pH, metabolism, and respiration on the magnitude and kinetics of metarhodopsin III formation and decay in intact, isolated retinas of frogs by use of a rapid scanning microspectrophotometer (RMSP). The variables were changed by superfusing the retinas with different solutions of controlled composition, described in detail in the METHODS section. A total of 12 different controlled perfusate compositions were utilized. These consisted of all possible combinations of the three variables such that the perfusate had (a) a buffer, which set the pH at 5.5, 7.3, or 8.2; (b) a metabolic substrate, either glucose, which provided a source of energy, or 2-deoxyglucose, which blocked the energy-generating metabolic pathways; and (c) a respiratory regulator, such that the solutions were saturated with either oxygen or nitrogen.

Preliminary data reduction consisted of the calculation and graphical display of absorption and difference spectra, as described in APPENDIX B. The locations of the wavelengths where the greatest optical density changes occurred were determined by examining sequential difference spectra. These wavelengths were then isolated graphically as a function of time, in order to examine the kinetic changes taking place.

Figure 5 illustrates a typical example of such isolated-wavelength kinetics. The identification of the photoproducts whose kinetics were displayed in graphs such as Figure 5 was determined by referring to the schemes described in Figure 1. Since a rapid decay phase was observed at 380 nanometers, which was concurrent with a formation of pigment at 470 nanometers, the two pigments were identified to be metarhodopsins II and III, respectively, based upon their sequence, characteristic wavelengths, and timing. In a like manner, the slower decay at 380 nanometers, which occurred after the decay of metarhodopsin III had begun at 470 nanometers, was attributed to the retinal photoproduct.

For the remainder of this thesis, the results displayed at the wavelengths illustrated in Figure 5 will be referred to by the nomenclature described above, in accordance with the sequences of photoproducts previously reported in the literature.

Model for Metarhodopsin III Kinetics

In order to provide a means by which quantitative comparisons could be made between many experiments, a mathematical model was employed to describe metarhodopsin III kinetics. The model which was selected is based upon the assumption that metarhodopsin III formation and decay can best be described by unidirectional, linear, first-order processes. This assumption implies that the rate of change of pigment concentration is proportional to the amount of

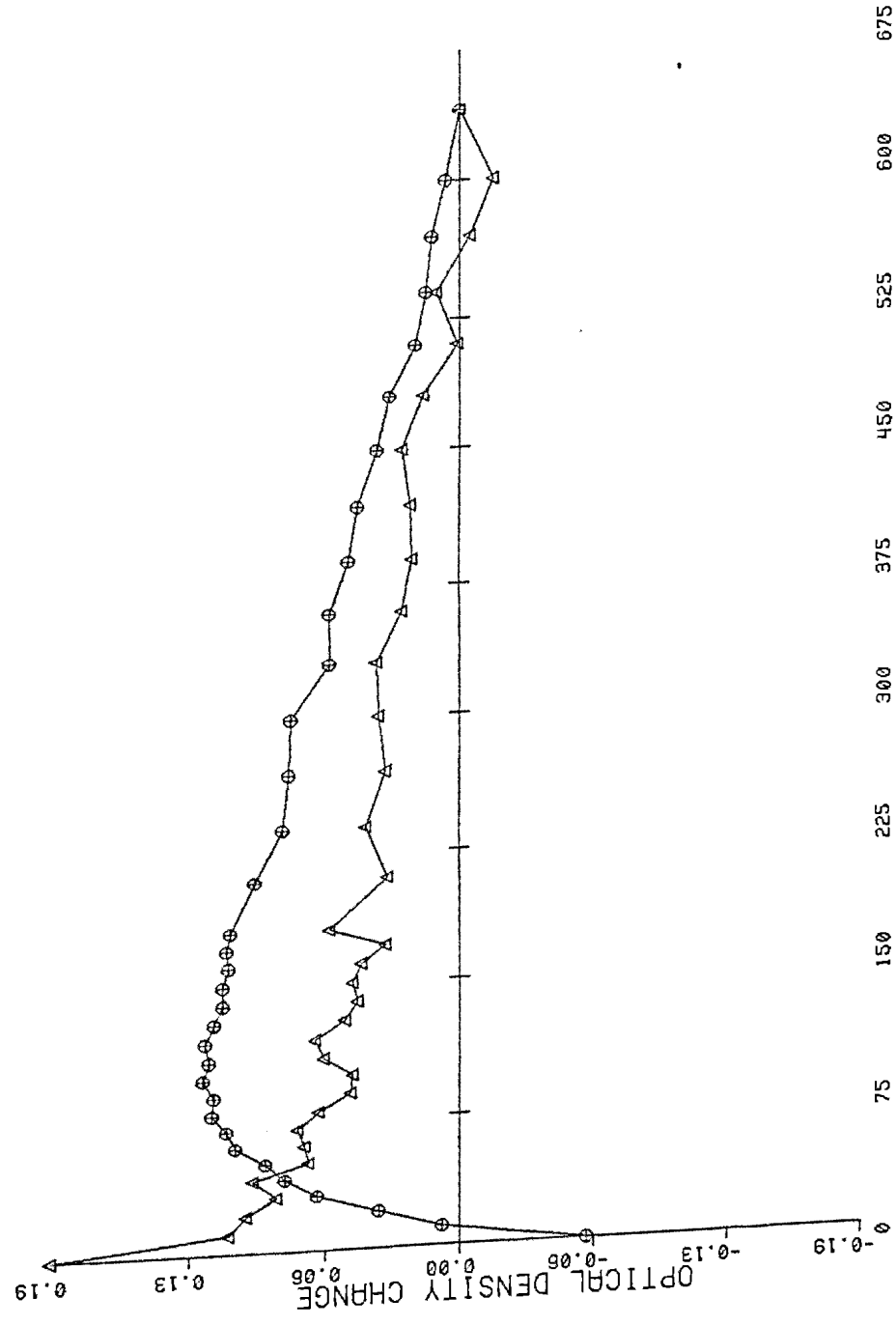
OPTICAL DENSITY CHANGE
0.19
0.13
0.06
0.00
-0.06
-0.13
-0.19
0
75
150
225
300
375
450
525
600
675
POST-BLEACH TIME (SECONDS)

Figure 5

Figure 5. Typical example of isolated-wavelength kinetics. Optical density differences are displayed as function of post-bleach time at wavelengths of maximum change. See APPENDIX B for complete description of derivation of records. Triangles: 380 nanometers. Circles: 470 nanometers.

pigment present at any given time, t.

If it is postulated that metarhodopsin III is characterized by half-times of formation, T_f, and decay, T_d, then its concentration, C(t), normalized with respect to the concentration of rhodopsin bleached, is quantitated by the equation,

$$C(t) = \frac{P'}{1-\frac{T_f}{T_d}} \left(e^{-t(\ln 2)/T_d} - e^{-t(\ln 2)/T_f}\right) \qquad (4)$$

A complete mathematical derivation of this model is described in APPENDIX B. P' is a measure of normalized metarhodopsin II concentration that is transformed into metarhodopsin III.

The scheme illustrated in Figure 6 describes the relationship of P' and metarhodopsin III more clearly. If, for example, all of the metarhodopsin II is transformed into metarhodopsin III, then $P'=1$. This relationship is valid if photoproduct concentrations are expressed in units normalized to the amount of rhodopsin bleached. If, however, only part of the metarhodopsin II is transformed into metarhodopsin III, then P' represents this fraction, and $(1-P')$ represents the remainder of the metarhodopsin II which decays via some alternate pathway (see DISCUSSION).

The model utilized for curve-fitting operations (see APPENDIX B) was characterized by the equation,

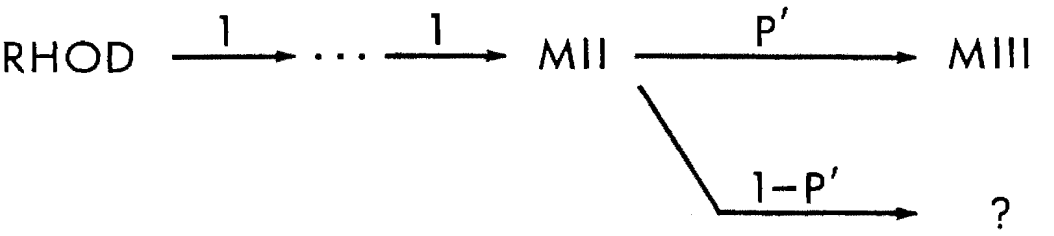

Figure 6

Figure 6. Model of alternate pathways of metarhodopsin II decay. Metarhodopsin II decay is shown schematically. If concentration of metarhodopsin II is normalized with respect to amount of rhodopsin bleached, then fraction P' decays into metarhodopsin III, and remainder $(1 - P')$ decays via alternate pathway(s).

$$C(t) = C_d\, e^{-t(\ln 2)/T_d'} - C_f\, e^{-t(\ln 2)/T_f'} . \qquad (5)$$

A single-coefficient model, to correspond with Equation (4), is more realistic physiologically than a two-coefficient model when independent processes are assumed. Thus, the average value,

$$\bar{C} = 1/2\ (C_d + C_f) \quad ; \qquad (6)$$

was employed when it could be determined that there was no statistically significant difference between the mean values of the populations of C_d and C_f (see APPENDIX B for details).

In order to calculate the metarhodopsin II concentration fraction, P', from the value of $\bar{C}$, one additional consideration was necessary. Although Equations (1) through (4) can be utilized as a model for the concentrations of metarhodopsin II and III, the magnitudes of the coefficients obtained via spectrophotometry are direct measures of absorptances, not concentrations. A proportionality between concentration changes of a photoproduct and optical density changes, measured at its characteristic wavelength, is a generally accepted assumption. However, the proportionality constant need not be identical for two different photoproducts.

Such an inconsistency is the case when metarhodopsins II and III are compared since it has been observed that metarhodopsin III absorbs light approximately ten percent less efficiently than metarhodopsin II (Abrahamson and Ostroy, 1967). This correction factor must be accounted for in any

equations which express the concentration changes between the two pigments in terms of optical density changes. Thus, by combining Equations (4), (5), and (6) in this manner,

$$P' = 1.1\bar{C}\left(1 - \frac{T_f'}{T_d'}\right) \quad ; \quad (7)$$

and magnitudes of the three parameters, P', T_f', and T_d', completely described the model of metarhodopsin III kinetics.

Acceptance Criteria

Thirty frog retinas, superfused with different solutions of controlled composition, were used to obtain the experimental results described in this section. A total of 151 individual retinal patches were studied from this population of retinas, so that the average number of observations obtained from each retina was approximately five.

Out of the 151 experiments, 48 were deemed to be suitable for quantitative data reduction and analysis. In general, there were three criteria which the accepted experiments were required to fulfill. First, it was necessary for there to be a significant amount of remaining rhodopsin available to be bleached before the experiment began. Since previously bleached rhodopsin is not spontaneously regenerated to any significant extent in an isolated, perfused retina preparation (Weinstein, Hobson, and Dowling, 1967), this requirement can be evaluated by a comparison between the optical densities of rhodopsin and of its late-occurring photoproducts.

As illustrated in Figure 7, if the pre-bleach absorption

spectrum has a relatively large, distinctive peak in optical density near 500 nanometers, where rhodopsin absorbs maximally, then this criterion is satisfied. If, however, the pre-bleach absorption spectrum is somewhat flattened around 500 nanometers, but shows a large optical density near 380 nanometers and below, where the later-forming retinal and retinol photoproducts absorb, then this area of the retina was likely to have been previously bleached and was, therefore, rejected for further analysis.

A second criterion for evaluating an experiment was that a significant amount of rhodopsin was removed as a result of the bleach. This requirement was necessary to insure sufficient signal-to-noise ratio, in order that the subsequent kinetic measurements would be meaningful. As illustrated in Figure 8, an experiment was evaluated by calculating a difference spectrum between the two measurements just prior to and immediately after the bleach. The optical density change at 500 nanometers, which is a measure of the amount of rhodopsin bleached, was required to be at least 0.20 logarithmic units for the experiment to be accepted. This lower limit was found to result in adequate signal levels for detecting optical density changes of the rhodopsin photoproducts.

Observations on the Baseline

Once an experiment had been determined to satisfy the two criteria described above, the sequence of measurements

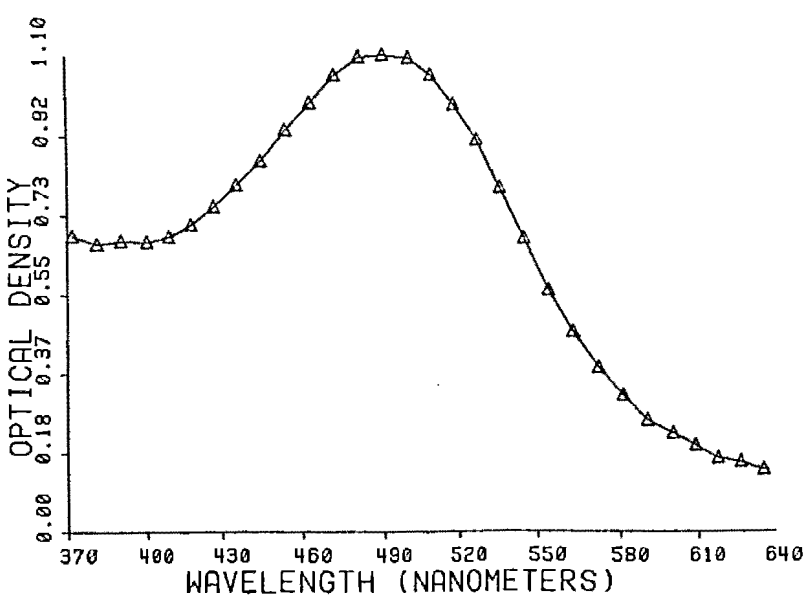
OPTICAL DENSITY
0.00
0.18
0.37
0.55
0.73
0.92
1.10
370
400
430
460
490
520
550
580
610
640
WAVELENGTH (NANOMETERS)

(a)

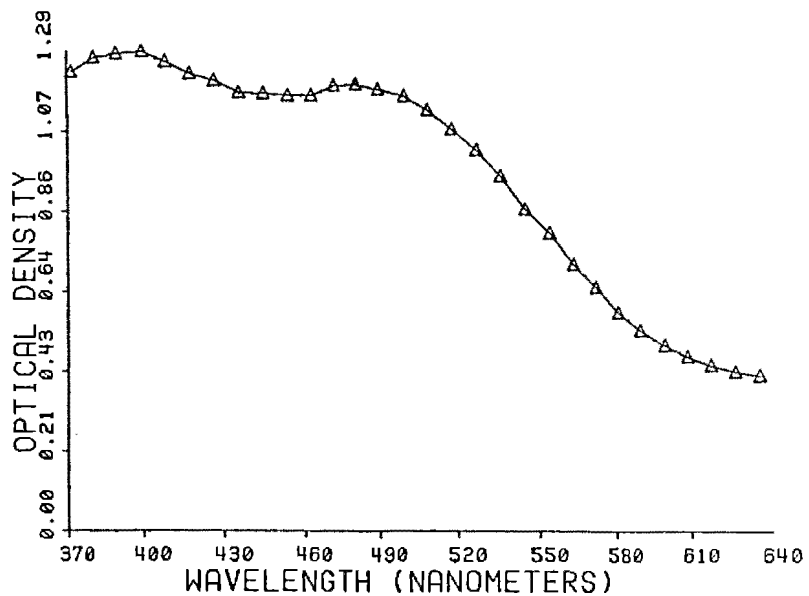
OPTICAL DENSITY
0.00
0.21
0.43
0.64
0.86
1.07
1.29
370
400
430
460
490
520
550
580
610
640
WAVELENGTH (NANOMETERS)

(b)

Figure 7

Figure 7. Example of pre-bleach acceptance criterion. Absorption spectra measured from two different experiments prior to bleaching. (a) Previously unbleached retina exhibits distinctive peak around 500 nanometers, indicating availability of significant concentration of rhodopsin to be bleached. (b) Previously bleached retina exhibits flattening of spectrum around 500 nanometers, with corresponding increase in optical density around 380 nanometers, indicating presence of considerable retinal. (See APPENDIX B for derivation of absorption spectra).

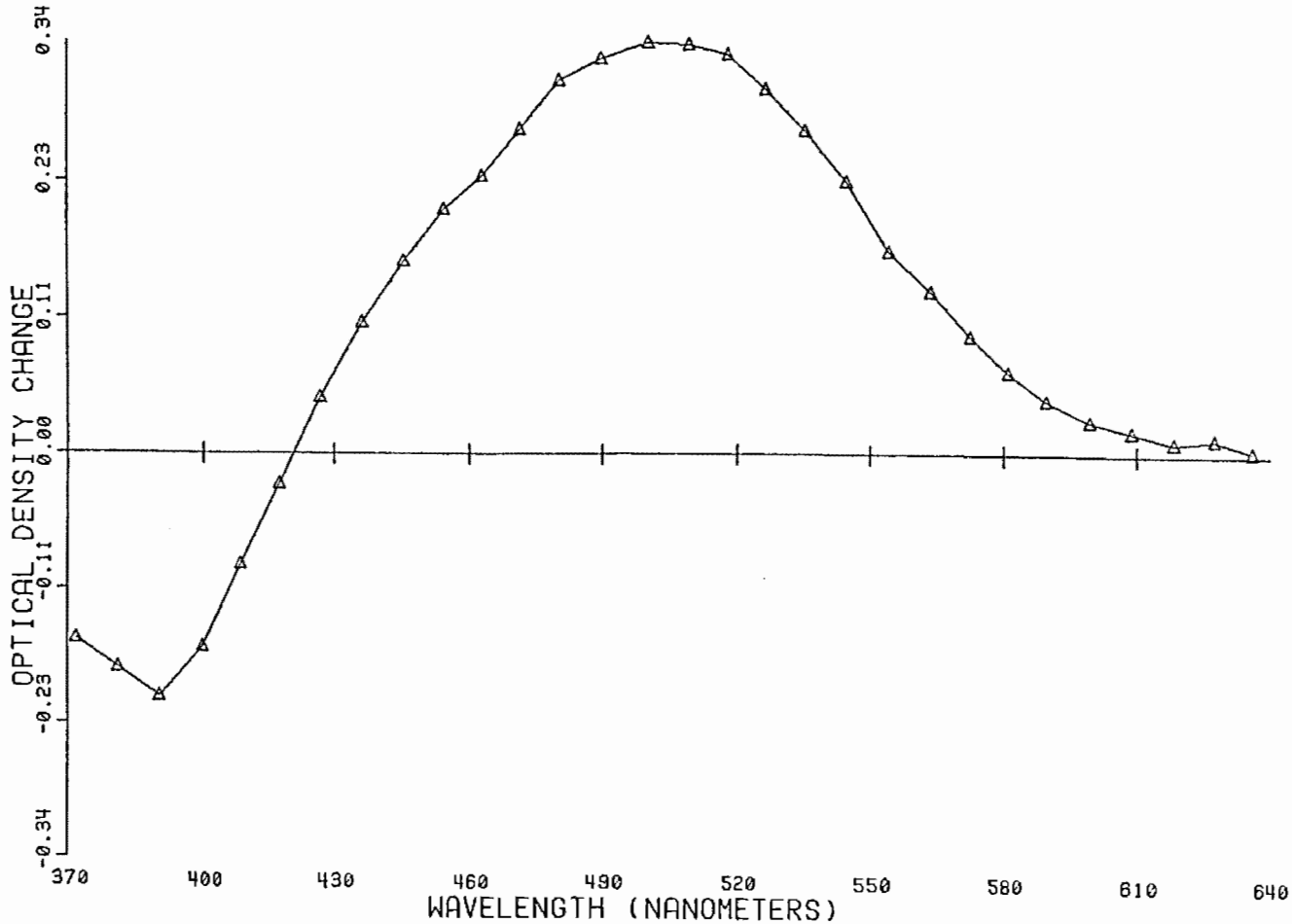
OPTICAL DENSITY CHANGE
0.34
0.23
0.11
0.00
-0.11
-0.23
-0.34
370
400
430
460
490
520
550
580
610
640
WAVELENGTH (NANOMETERS)

Figure 8

Figure 8. Example of adequate-bleach acceptance criterion. Difference spectrum between unbleached retina and first post-bleach measurement (400 milliseconds after onset of bleach). Magnitude of optical density change at 500 nanometers indicates measure of amount of rhodopsin bleached. (See APPENDIX B for derivation of difference spectrum).

was subjected to a third and final test which examined their stability. Since neither rhodopsin nor any of its photoproducts exhibit significant absorption toward the red end of the spectrum (Collins, Love, and Morton, 1952), it was strictly required that the absorption spectra, for every measurement of an experiment, should be coincident at 640 nanometers, the longest wavelength studied. An example of experiments which met this criterion is illustrated in Figure 9(a).

Since the electronics of the RMSP had been previously determined to be constant for the duration of an experiment, any changes in the "baseline" optical density, measured at 640 nanometers, were assumed to be the result of optical changes in the preparation. Thus, any experiment which did not exhibit a steady baseline for the duration of the measurements was excluded from the analysis.

Virtually all of the excluded experiments demonstrated a slow, gradual increase in optical density at 640 nanometers over the ten minutes of measurement (Figure 9(b)). Approximately ten percent of these were attributable to mechanical movement of the retina within the chamber, as confirmed by visual inspection through the eyepieces of the microscope. The remainder exhibited an increase in scattering, which usually was observed as a loss of transparency and a cloudy, milky appearance of the retina. Since the RMSP cannot distinguish scattered light from absorbed light, the resulting loss in transmission was manifested as increased optical

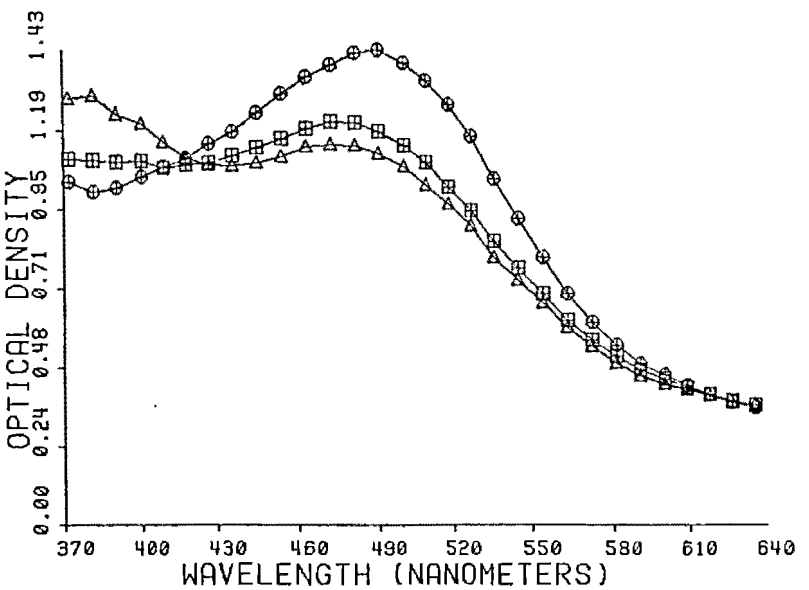
OPTICAL DENSITY
0.00 0.24 0.48 0.71 0.95 1.19 1.43
370 400 430 460 490 520 550 580 610 640
WAVELENGTH (NANOMETERS)

(a)

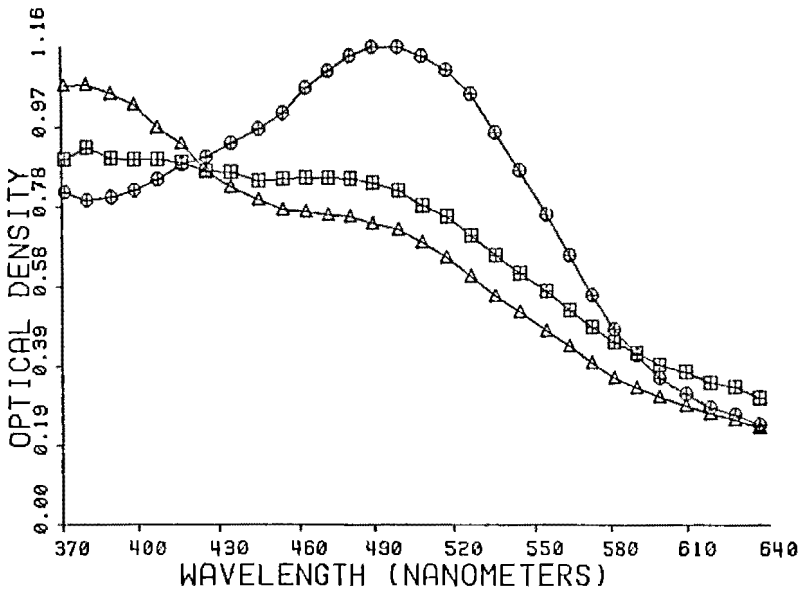
OPTICAL DENSITY
0.00 0.19 0.39 0.58 0.78 0.97 1.16
370 400 430 460 490 520 550 580 610 640
WAVELENGTH (NANOMETERS)

(b)

Figure 9

Figure 9. Example of baseline acceptance criterion. (a) Superposition of absorption spectra measured at different times from typical retinal patch. Circles: pre-bleach measurement. Triangles: measurement 400 milliseconds post-bleach. Squares: measurement 10 minutes post-bleach. Only three curves are illustrated for clarity. Optical density at 640 nanometers coincides for all curves. (b) Same as (a), except from rejected experiment. Optical density at 640 nanometers shows increase over measurement interval.

density which was observable at the 640 nanometer baseline (see APPENDIX B).

Table II illustrates the optical density value of the baseline, measured at 640 nanometers prior to bleaching, for the total population of experiments. The values have been categorized separately as a function of pH, substrate availability, and respiratory state, which are determined by the composition of the perfusate. In addition to the 151 experiments described previously, this table also includes 58 experiments which were performed with "ambient" glucose substrate; that is, without the addition of either glucose or 2-deoxyglucose to the perfusate. These additional experiments are described in detail in the DISCUSSION.

As indicated in Table II, the baseline magnitude tended, in general, to be larger in acidic media or in a state of deprived metabolic substrate, but was apparently not affected by the respiratory state of the retina. These observations suggest that a pH less than the physiological value, or the lack of sufficient metabolic substrate, contributes to increased opacity and scattering in the retina.

Table II also illustrates the proportion of experiments in each category that were discarded because of a shift in the baseline during the 10-minute measurement interval. The most noticeable trend is observed in the choice of categorization by pH value. A considerably greater percentage of the experiments were rejected from the population of acidic environments than from non-acidic perfusates. This

	(a) Optical Density at 640 nm	(b) Total # Experiments	(c) # Rejected Experiments	(d) % Rejected Experiments
pH: 5.5	.47±.13	56	50	89%
7.3	.40±.12	66	36	55%
8.2	.37±.14	87	42	48%
Metabolic substrate:				
Glucose	.37±.14	67	43	64%
Ambient	.39±.12	58	25	43%
2-deoxyglucose	.45±.13	84	60	71%
Respiration:				
Oxygen	.41±.14	112	70	62%
Nitrogen	.41±.14	97	58	60%
Totals		209	128	61%

Table II

Table II. Summary of baseline observations. Column (a): tabulation of optical density of absorption spectra baselines measured at 640 nanometers, immediately prior to bleach, as described in APPENDIX B. Mean value ± standard deviation is indicated separately as functions of extracellular pH, substrate availability, and respiratory state. (Note: categories include results from 58 experiments with ambient substrate only, in which neither glucose nor 2-deoxyglucose was component of perfusate. See DISCUSSION for further details). Column (b): total experiments performed for each category. Columns (c) and (d): number and percentage of experiments discarded because of baseline shift (see Figure 9).

was consistent with the observation made above, in that a gradual increase in scattering was more likely to occur in an acidic environment.

It has been a common practice among microspectrophotometrists to "re-zero" all absorption spectra, obtained from isolated retinas, with respect to the baseline optical density measured in deep red light (Frank, 1969; Donner and Reuter, 1969; Gyllenberg, Reuter, and Sippel, 1974). This procedure was usually undertaken due to the difficulty of maintaining sufficient stability of the preparation during prolonged recording from the tissue. In view of the observations described above, it can be seen how such a practice might lead to erroneous conclusions. This is especially true when difference spectra and kinetics are calculated, since it is known that scattering is not uniform at all wavelengths but is greater for short wavelengths than for long. Re-zeroing the baseline would thus lead to errors both in magnitude and in characteristic wavelengths of pigments being studied. Furthermore, the absolute magnitude of the baseline optical density might be an important indicator of the state of the preparation, suggested by the statistics tabulated in Table II.

For these reasons, the results described in this dissertation are presented without any re-zeroing of the baseline. As a consequence of the stringent acceptance criteria, a considerable proportion of the experiments have been discarded, as indicated in Table II. However, this practice was

deemed necessary in order to insure a high level of confidence in the quantitative and statistical analyses which are described in subsequent sections of this dissertation.

Typical Kinetic Results

Temporal optical density changes were observed for the metarhodopsin III pigment in 40 of the 48 experiments which were suitable for quantitative analysis. As illustrated in Figure 10, metarhodopsin III typically exhibited a rapid formation, which was followed by a slower decay. The remaining 8 experiments showed no evidence of metarhodopsin III formation or decay.

Pigment changes were also observed around 380 nanometers for all 48 of the experiments. Based upon a qualitative examination of the population of experiments, three distinct patterns were observed over the 10-minute measurement interval and are illustrated in Figure 11. On the basis of their spectral and temporal characteristics (see Figure 1), optical density changes showed either a single, rapid decay (Figure 11(a)), a single, slow decay (Figure 11(c), or a combination of the two (Figure 11(b)). These three categories were attributed to metarhodopsin II decay, retinal decay, or a combination of both, respectively. In none of the three categories was a distinct formation phase ever observed from the time of the first measurement.

A great deal of variability of metarhodopsin III kinetics was observed with respect to the metarhodopsin II/retinal kinetics. Most noticeable was the relationship between their

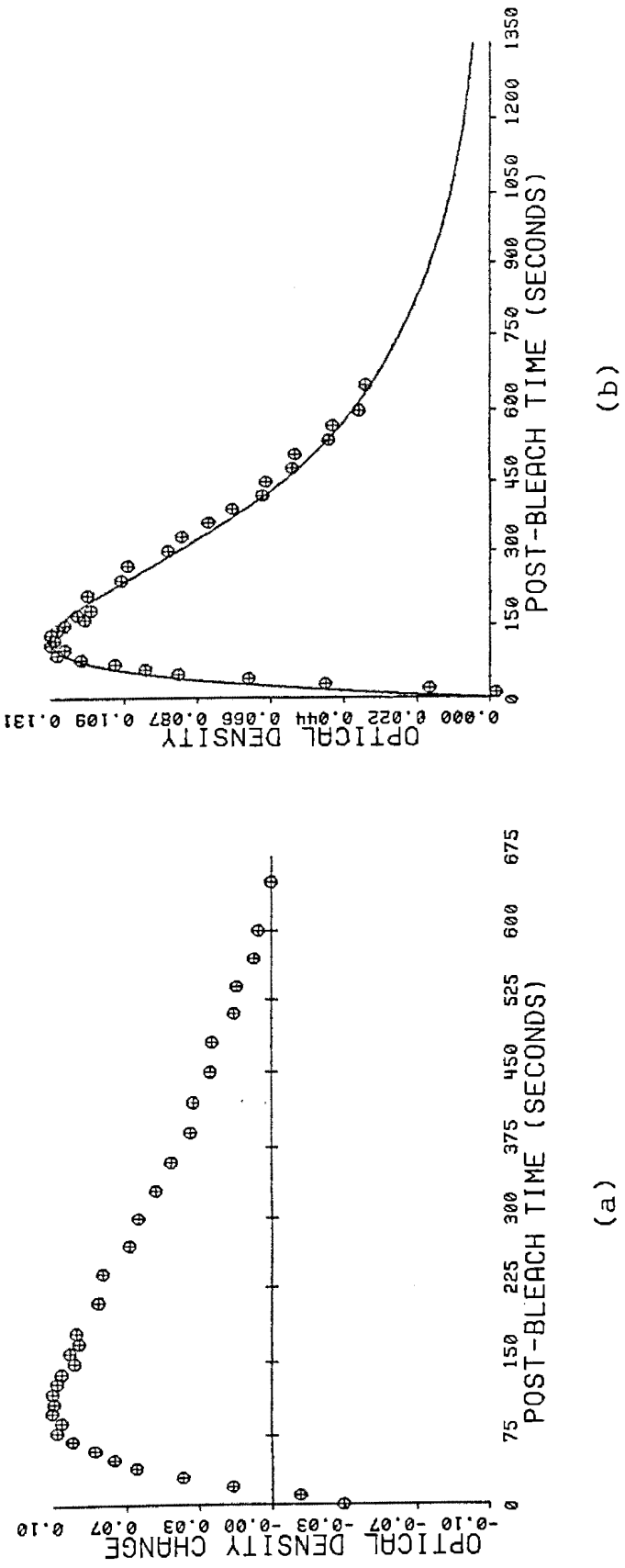
OPTICAL DENSITY CHANGE
-0.10 -0.07 -0.03 -0.00 0.03 0.07 0.10
0 75 150 225 300 375 450 525 600 675
POST-BLEACH TIME (SECONDS)
(a)
OPTICAL DENSITY
0.000 0.022 0.044 0.065 0.087 0.109 0.131
0 150 300 450 600 750 900 1050 1200 1350
POST-BLEACH TIME (SECONDS)
(b)

Figure 10

Figure 10. Typical example of metarhodopsin III kinetics. (a) Typical optical density changes measured at 470 nanometers are illustrated as a function of post-bleach time, with measurement at 650 seconds subtracted as reference. Note: negative intercept on ordinate axis is with respect to reference measurement (see APPENDIX B). (b) Solid line represents simulation of the best fit of data to model described in text. Data of (a) are shown as circles.

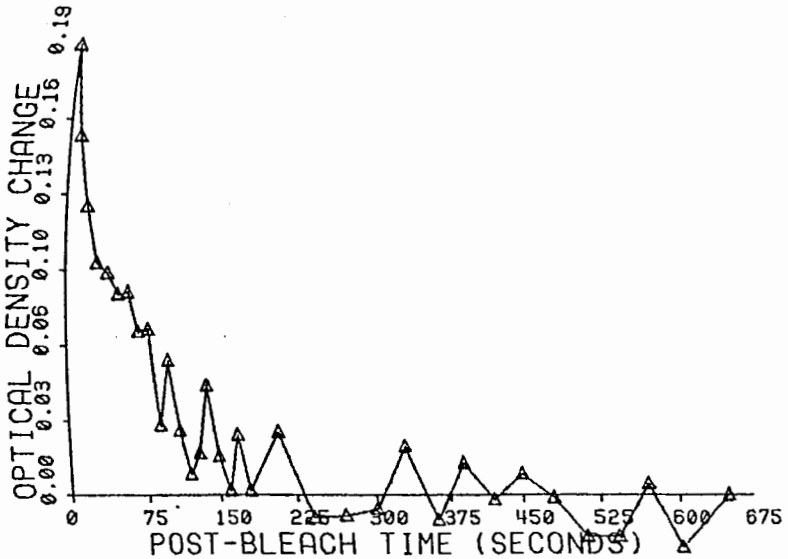

(a)

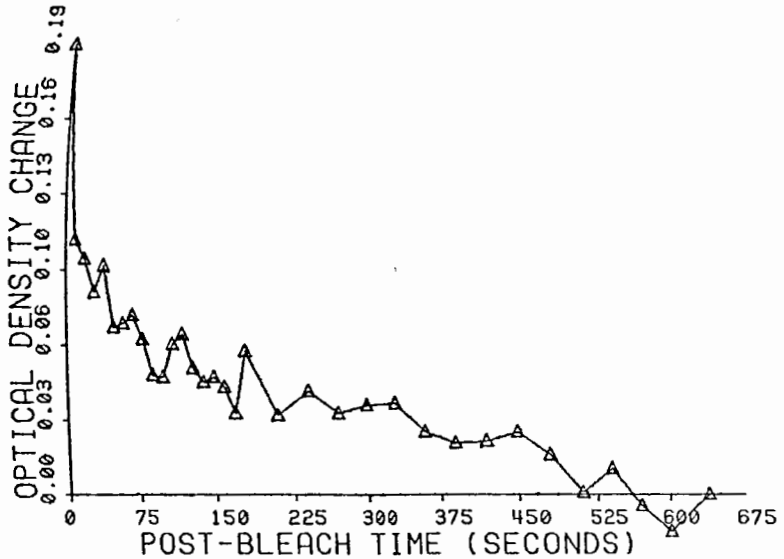

(b)

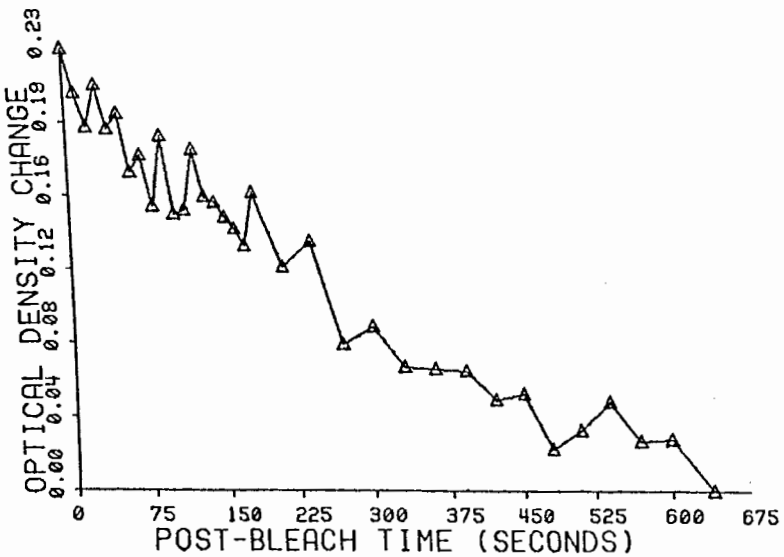

(c)

Figure 11

Figure 11. Typical examples of metarhodopsin II and/or retinal kinetics. Optical density changes measured at 380 nanometers are illustrated as function of post-bleach time, with measurement at 650 seconds subtracted as reference. (a) Single, rapid decay only, identified to be metarhodopsin II. (b) Two-phase decay, beginning with rapid metarhodopsin II phase, followed by slower retinal decay. (c) Single, slow decay only, identified to be predominantly retinal.

respective magnitudes. This relationship was generally correlated with the type of decay process observed at 380 nanometers. Five relative categories are illustrated in Figure 12, although virtually a continuum of comparative magnitude relationships was observed over the population of experiments. In general, as the amount of measured metarhodopsin III decreased, the decay observed at 380 nanometers progressed from primarily that of combined metarhodopsin II/retinal to a predominantly retinal phase.

Results of Curve-Fitting

Table III summarizes the values of metarhodopsin III parameters which were obtained by computer-simulated curve-fitting of data observations to the model described by Equation (4). The mean values and standard deviations of the parameters are tabulated for each of the 12 different controlled perfusate compositions studied.* Several observations about the influence of the environmental components on metarhodopsin III behavior can be made by examining its formation and decay half-times, T_f and T_d, along with the fraction of metarhodopsin II, P', which decays into metarhodopsin III.

Of the 40 controlled experiments performed at pH 5.5, only four were not discarded because of a shift in the base-

*The exception for which $\bar{C}$ was not calculated, because of statistically significant differences between C_f and C_d, is described in greater detail in the DISCUSSION.

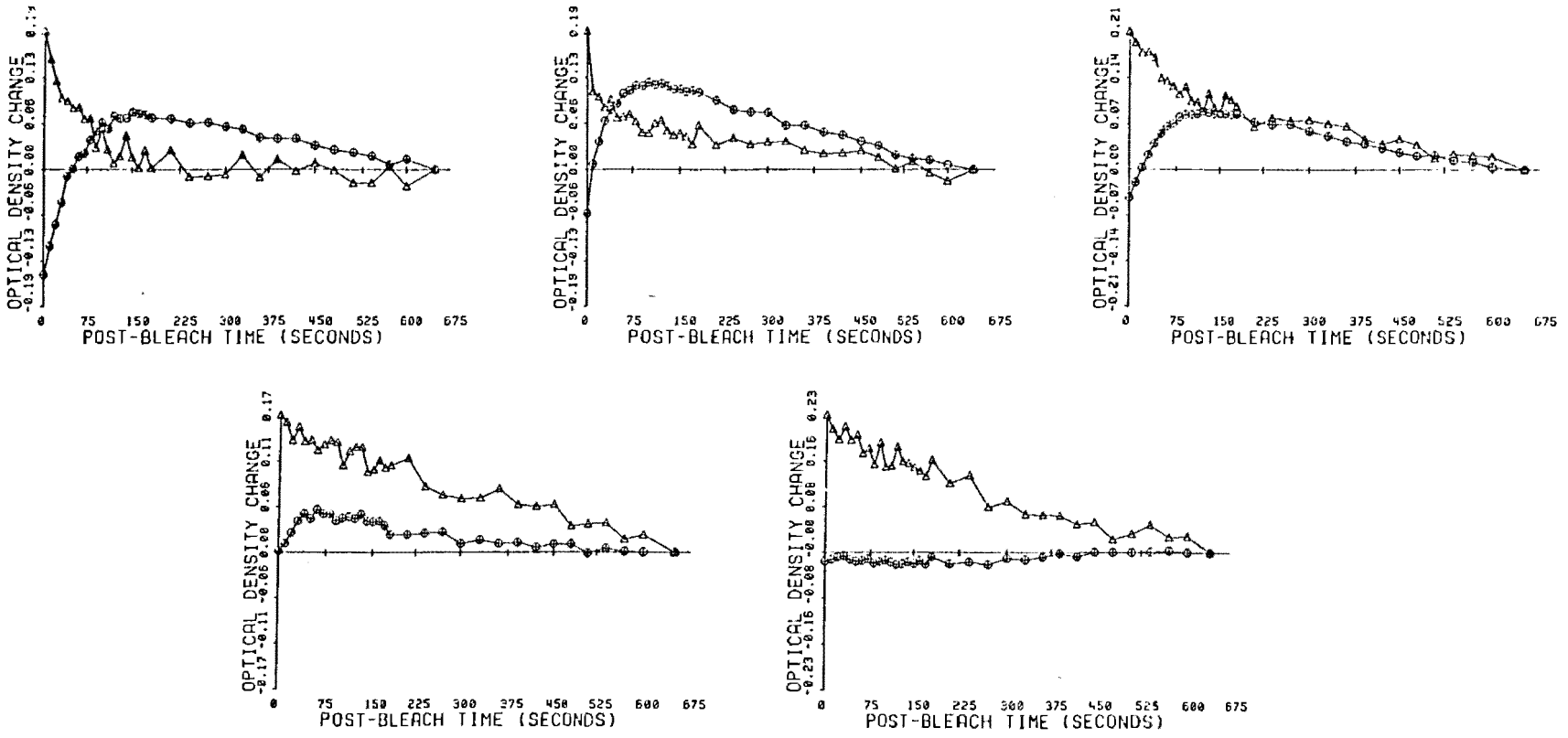
OPTICAL DENSITY CHANGE
POST-BLEACH TIME (SECONDS)
0
75
150
225
300
375
450
525
600
675

Figure 12

Figure 12. Representative relationships between metarhodopsins II and III and retinal kinetics. Optical density changes measured at 380 nanometers (triangles) and 470 nanometers (circles) are illustrated as function of post-bleach time, with measurement at 650 seconds subtracted as reference. Rapid phase of 380 nanometer decay in (a) is attributed to metarhodopsin II; slow phases in (d) and (e) are attributed to retinal; (b) and (c) illustrate combined decay of both pigments. Metarhodopsin III is present in decreasing concentrations in (a) through (d); no evidence of metarhodopsin III in (e).

	(1)	(2)	(3)	C_f	C_d	$\bar{C}$	P'	T_f	T_d	$\frac{T_f}{T_d}$
8.2-O_2-glu	14	3	3	.70±.14	.73±.15	.71±.11	.66±.13	41±3	329±123	.16±.09
8.2-O_2-2DG	13	6	6	.48±.21	.43±.24	.45±.21	.44±.21	27±6	250±128	.13±.04
8.2-N_2-glu	11	7	4	.63±.04	.91±.05	--	.66±.03*	28±3	600± 83	.05±.01
8.2-N_2-2DG	27	13	10	.78±.11	.76±.14	.77±.08	.72±.09	41±5	299± 88	.15±.05
7.3-O_2-glu	11	8	8	.51±.18	.54±.12	.53±.15	.45±.09	43±9	231± 46	.20±.08
7.3-O_2-2DG	13	2	2	.16±.11	.19±.10	.17±.11	.15±.09	19±8	122± 4	.15±.06
7.3-N_2-glu	9	3	3	.10±.01	.18±.08	.14±.04	.14±.04	18±7	162± 48	.11±.01
7.3-N_2-2DG	13	2	2	.54±.11	.53±.06	.54±.09	.38±.06	35±2	166± 96	.33±.21
5.5-O_2-glu	17	2	0	0	0	0	0	--	--	--
5.5-O_2-2DG	7	1	1	.05	.08	.07	.06	20	147	.14
5.5-N_2-glu	5	0	0	0	0	0	0	--	--	--
5.5-N_2-2DG	11	1	1	.13	.11	.12	.11	17	223	.08
Totals	151	48	40							

Table III

Table III. Summary of metarhodopsin III parameter magnitudes for first-order model. Mean value ± standard deviation of parameters is indicated for perfusate compositions shown. pH 5.5, 7.3, and 8.2: buffer concentration, 10 mM. Perfusate saturated with respiration gas, O_2 or N_2. Substrate concentrations: glucose, 20 mM; 2-deoxyglucose, 10 mM. Number of experiments accepted (Column (2)) out of total performed (Column (1)) is determined by acceptance criteria, described in text and illustrated in Figures 7, 8, and 9. Number of experiments fit to model (Column (3)) includes only those which showed measurable optical density changes at 470 nanometers. Parameters C_f, C_d, T_f, and T_d were calculated directly by curve-fitting algorithm (see APPENDIX B). $\bar{C}$ and P' were computed from Equations (6) and (7) for all populations of experiments except those in which there was statistically significant difference between mean values of C_f and C_d (see DISCUSSION). Asterisked (*) value of P' was calculated from value of C_f only. C_f, C_d, $\bar{C}$, and P' are expressed as fraction, normalized with respect to amount of rhodopsin bleached. Half-times T_f and T_d are expressed in seconds. P' is measure of fraction of metarhodopsin II which is transformed into metarhodopsin III.

line during the measurements. None of these four experiments showed large amounts of metarhodopsin III. In two of the experiments, there was no evidence of any metarhodopsin III formation. In the remaining two experiments, only approximately ten percent of the metarhodopsin II was transformed into metarhodopsin III.

In fact, even those experiments at pH 5.5 which were discarded showed either little or no optical density changes at 470 nanometers, independent of substrate or respiration. Furthermore, the entire population of experiments performed at pH 5.5 were associated with the exclusively slow phase of decay measured at 380 nanometers (Figure 12(d) and (e)). Thus, it would seem that more retinal was present when metarhodopsin III was scant. This observation suggests that metarhodopsin II decays directly into retinal when the formation of metarhodopsin III is hindered in an acidic environment.

When the experiments performed at pH 7.3 and 8.2 are examined, it can be seen that there is considerable variability between the parameters as a function of the composition of the perfusate environment. For example, in the presence of glucose substrate, the formation half-time of metarhodopsin III is greater in the presence of oxygen than in the presence of nitrogen. Also, the fraction of metarhodopsin II which decays into metarhodopsin III, for any combination of substrate availability and respiratory state, tends to increase as the medium becomes less acidic.

It is also interesting to note that the metarhodopsin III half-times of formation and decay often tend to change in the same direction, so that their ratio remains virtually unchanged. For example, an approximate doubling of both T_f and T_d is observed, in the presence of oxygen, between the extreme states of supplied and deprived substrates. This observation suggests that, although the time required for metarhodopsin III to form and decay might each be affected by environmental conditions, they are often both affected in the same way.

As an additional means of understanding the metarhodopsin II-metarhodopsin III-retinal transformation process, the metarhodopsin III parameters calculated from the model were also tabulated on the basis of the relative kinetics illustrated in Figure 12. This alternate categorization, which is summarized in Table IV, was performed without regard to the composition of the perfusate solution.

There was consistent agreement between the values calculated for P' and the general shape of the decay kinetics measured at 380 nanometers. Thus, as mentioned previously with respect to the experiments performed at pH 5.5, as the fraction of metarhodopsin II which was transformed into metarhodopsin III decreased, a greater amount of retinal was observed.

It can also be seen from Table IV that the half-time of metarhodopsin III formation was comparatively short when only the slow, retinal decay was observed, when compared with the other categories which exhibited the more rapid, metarhodopsin

Pigment Category	# Exper	C_f	C_d	$\overline{C}$	P'	T_f	T_d	$\frac{T_f}{T_d}$
A	8	.79±.14	.69±.14	.74±.09	.69±.08	38± 6	313±139	.15±.06
B	13	.64±.13	.74±.19	.69±.14	.66±.16	38± 6	348±124	.13±.07
C	12	.48±.21	.55±.21	.52±.19	.45±.18	35±11	258±161	.19±.13
D	7	.13±.07	.12±.03	.12±.05	.12±.05	17± 5	149± 46	.12±.03
E	8	0	0	0	0	--	--	--
Total	48							

Table IV

Table IV. Summary of metarhodopsin III parameter magnitudes as function of relative kinetics. Mean ± standard deviation of parameters is indicated for categories, based on illustrations in Figure 12. A: Large metarhodopsin III, measured at 470 nanometers; rapid metarhodopsin II decay only, measured at 380 nanometers. B: Large metarhodopsin III; combined rapid metarhodopsin II and slow retinal decay. C: Medium metarhodopsin III; combined metarhodopsin II and retinal decay. D: Small metarhodopsin III; slow retinal decay only. E: No metarhodopsin III; slow retinal decay only. Categorization is performed without regard to perfusate composition. See legend of Table III for description of parameters.

II phase. In contrast, the half-time of decay exhibited a more gradual, less abrupt decrease, which was generally correlated to the decreasing proportion of metarhodopsin II which was transformed into metarhodopsin III. Again, however, it is noted that the ratio of the half-times remained approximately the same for the four categories in which metarhodopsin III pigment was observed.

Even more information can be obtained by sub-classifying these five pigment categories as a function of the various components of the perfusate. This is illustrated in Table V. Once again, it is seen that experiments performed at pH 5.5 exhibited neither a relatively large proportion of metarhodopsin III nor a distinct decay phase of metarhodopsin II. Experiments in which the pH of the perfusate was 7.3 and within the physiological range more often exhibited medium levels of metarhodopsin III. This was coupled with detectable phases of both metarhodopsin II and retinal decay, measured at 380 nanometers.

In contrast, the population of experiments studied in an alkaline medium tended to favor a larger proportion of metarhodopsin III formed from metarhodopsin II and even less evidence of retinal. The extreme category of experiments which exhibited only metarhodopsin II decay at 380 nanometers occurred exclusively in alkaline environments, predominantly in substrate-deprived, anoxic retinas. These observations suggest that a non-acidic environment favors the formation of large amounts of metarhodopsin III and that, furthermore,

	Total	A	B	C	D	E
pH: 5.5	4	0	0	0	2	2
7.3	15	0	3	9	3	0
8.2	29	8	10	3	2	6
Metabolic substrate:						
Glucose	23	1	7	8	2	5
2-deoxyglucose	25	7	6	4	5	3
Respiration:						
Oxygen	22	2	5	9	4	2
Nitrogen	26	6	8	3	3	6
Totals	48	8	13	12	7	8

Table V

Table V. Relative photoproduct categories as function of perfusate compositions. Number of experiments in each category, based on Figure 12, is classified as function of pH, substrate availability, and respiratory state.

progressively less retinal is observed in the absence of metabolic activity.

Summary

Before proceeding to a discussion of the implications and significance of these results, it is helpful to conclude this section with a brief review of the important observations which have been made concerning the nature of the photoproduct processes which have been studied.

It has been shown that the kinetics of formation and decay of metarhodopsin III exhibit consider variability as a function of the pH and metabolic composition of the surrounding medium. The ratio between the half-times of formation and decay, however, has been shown to remain relatively unchanged, regardless of environmental conditions. This suggests that the formation and decay processes might be affected similarly by the pH, substrate availability, and respiratory state of the retina.

Perhaps a more important observation has been the effect of these same variables on the pathways of photoproduct decay in isolated retinas. For example, evidence has been presented that metarhodopsin II almost always decays directly into retinal, bypassing the formation of metarhodopsin III, in conditions of acidic extracellular environment. Such acidic conditions are generally associated with an increased degree of scattering of light by the tissue, measured by the RMSP

as a larger baseline density. This condition is also observed in substrate-deprived retinas.

As the pH is increased, more metarhodopsin III is observed, accompanied by a progressive decrease in retinal formation. An anoxic, substrate-deprived retina, perfused with an alkaline solution, often produces a large amount of metarhodopsin III, without any evidence of retinal being part of the photoproduct sequence.

The remaining section of this dissertation discusses these experimental observations in detail. Two postulates are presented which explain the interaction and effects of pH, metabolism, and respiration on the sequence and kinetics of the photoproduct processes which influence the formation and decay of metarhodopsin III in isolated retinas.

DISCUSSION

Introduction

The kinetics of formation and decay of rhodopsin photoproducts have been the subject of a considerable number of experimental investigations as one means of elucidating the origins of electrical events in photoreceptors. The detection of certain photoproduct transformations, within the latency of the electrical response observed in photoreceptor cells, has led to the postulation that visual pigment molecules are somehow responsible for initiating the membrane excitation process (Fuortes and Hodgkin, 1964).

The study of photoproduct kinetics has been complicated by the rapidity of many of the potentially important transformations near physiological temperatures. Most of the early-appearing photoproducts have only been investigated either in solutions of purified rhodopsin or in suspensions of fragmented photoreceptor cells removed from an intact, physiological cellular environment. The result has been confusion and inconsistency in the reported literature.

Even the slower photoproduct transformations of rhodopsin have not been characterized uniquely. In addition to inconsistencies in kinetics which might be expected between rhodopsin studied in solution and *in situ*, it has also been difficult to interpret disparities in the photoproduct sequence reported in the various investigations carried out on intact retinas.

The fact that these experiments have been performed under a variety of extracellular conditions indicates one potential source for some of the discrepancies.

The possible effect of one environmental factor, the hydrogen ion concentration, on the chemical course of events of certain rhodopsin photoproducts has already been implicated (Falk and Fatt, 1966). Reversible phosphorylation of rhodopsin during illumination has also been observed, which suggests a potential role of metabolism in photoproduct physiology (Bownds, Dawes, Miller, and Stahlman, 1972; Miller and Paulsen, 1975).

For these reasons, the influences of the pH and the metabolic state of the preparation on the photoproduct transformations, involving metarhodopsins II and III and retinal, have been studied in the results which have been reported here. These later, slow photoproducts were investigated in order to provide a context in which to study, at a later date, the chemical pathways and kinetics of the earlier photoproducts that are involved in the transduction process. An additional aim was to gain information on the role of the microenvironment on visual pigment mechanisms in intact photoreceptor cells. Such information might provide insights into the normal and abnormal visual functions of the eye.

To these ends, a series of experiments were performed in which the environmental conditions of the isolated retina were varied in a systematic way from the normal, physiological conditions of ample glucose and oxygen at pH 7.3. Temporal

changes in optical density, which correspond to changes in photoproduct concentration, were measured, subsequent to flash photolysis, by means of rapid microspectrophotometry. Evidence has been presented which indicates that both the sequence and the kinetics of the slow photoproduct transformations are affected by hydroden ion concentration as well as by metabolic factors.

Identification of Photoproducts

Due to the similarity between the absorption maxima of metarhodopsins I and III and of metarhodopsin II and retinal, it is important to establish that the kinetics which have been measured in these experiments are, in fact, those of metarhodopsin III-retinal and not of metarhodopsins I-II. This has occasionally caused some confusion in the past (Donner and Reuter, 1969), even though metarhodopsin I presumably disappears within milliseconds at physiological temperatures. In the context of the studies reported here, however, an identification of photoproduct species can be made with little difficulty.

This identification is described most effectively by the relationships between photoproduct kinetics shown previously in Figure 12. In experiments exhibiting relatively large optical density changes at 470 nanometers, the decay measured at 380 nanometers could be resolved into two distinct phases (Figure 12(b) and (c)). Since the rapid decay phase is of

similar duration as the optical density increase centered at 470 nanometers, these rapidly changing photoproducts are identified to be metarhodopsins II and III, respectively, based on the scheme shown in Figure 1(c). Since the later process, measured at 380 nanometers, has similar kinetics to the decay of metarhodopsin III, it is identified as retinal. In these examples, metarhodopsin II kinetics were not obscured by the contribution of retinal to the optical density changes measured at 380 nanometers.

A similar line of reasoning holds for the experiments in which little or no metarhodopsin III formation was observed (Figure 12(d) and (e)). In these cases, the decay measured at 380 nanometers could not be resolved into two phases and, apparently, exhibited only a slow phase. It is not immediately obvious whether this is attributable to metarhodopsin II or to retinal. However, since the rate of pigment formation and decay measured at 470 nanometers both increase as less pigment is formed (Table IV), it is likely that metarhodopsin II kinetics are obscured by an increased contribution of retinal at 380 nanometers. Thus, metarhodopsin III and retinal would be the primary species whose kinetics were being measured.

Mechanisms of pH Effects

There is a considerable body of evidence that indicate hydrogen ions are important cofactors in certain rhodopsin photoproduct transitions. Matthews, Hubbard, Brown, and

Wald (1963) observed that the relative extent of a quasi-equilibrium between metarhodopsins I and II, in solution, was dependent upon pH. Since acid conditions favored the greater formation of metarhodopsin II, this photoproduct transition was postulated to be associated with the uptake of a hydrogen ion. Subsequently, Falk and Fatt (1966) produced electrochemical evidence in support of this hydrogen uptake during the formation of metarhodopsin II.

Other photoproduct transitions have been found to depend on proton availability. Reactions leading to the formation of free retinal plus opsin are known to be favored by high hydrogen ion concentration, in order to break the carbon-nitrogen double bond of the Schiff-base linkage between the two chemical moieties (DePont, Daemen, and Bonting, 1970). In addition, a pH indicator, N-retinylidene opsin (NRO), is observed as a photoproduct in solutions of extracted rhodopsin (Ostroy, Erhardt, and Abrahamson, 1966).

Thus, it is seen that the photoproduct precursors of metarhodopsin III, as well as its successors, are directly affected by pH, at least in solubilized rhodopsin preparations. It is not unreasonable to question whether metarhodopsin III itself might also be dependent on the pH of the surrounding medium. Evidence has already been presented that alternate pathways of metarhodopsin II decay, other than through metarhodopsin III, are present in isolated retinas (see Figure 1(c)). It is possible that the choice of pathway is somehow dependent on pH.

Figure 13 illustrates possible mechanisms involving hydrogen ions which might affect metarhodopsin III formation and decay in isolated retinas. For example, the metarhodopsins II-III transition might entail the release of the proton acquired in the metarhodopsins I-II transformation. Based upon the observation described previously that retinal formation favors acidic conditions, a pH hypothesis would postulate that the pathway through metarhodopsin III would be more important only in alkaline surroundings. Conversely, the direct formation of retinal from metarhodopsin II would be more likely to occur in acidic media.

Since observations of variable metarhodopsin III formation have already been made in certain studies of isolated retinas at differing pH's (Frank, 1969; Bowmaker, 1973; Gyllenberg, Reuter and Sippel, 1974), a pH mechanism has been postulated in an attempt to describe the extent to which metarhodopsin III is formed from metarhodopsin II. This mechanism, illustrated schematically in Figure 14, is presumed to cause a smaller proportion of metarhodopsin II to decay via metarhodopsin III as the intracellular pH of the preparation becomes more acidic. The arrows in this figure, which point toward less acidic conditions in which greater formation of metarhodopsin III would be predicted, are determined by examination of the cellular biochemical scheme presented previously and repeated in Figure 15.

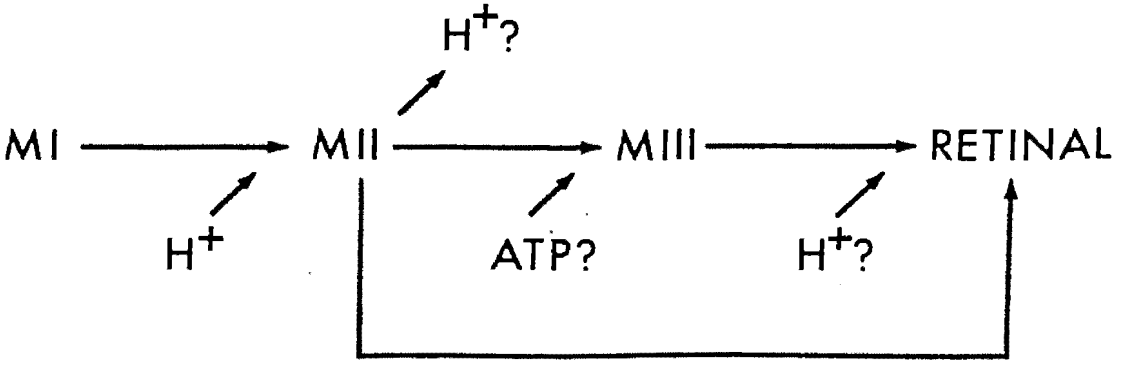

Figure 13

Figure 13. Possible mechanisms affecting metarhodopsin III. See text for explanation.

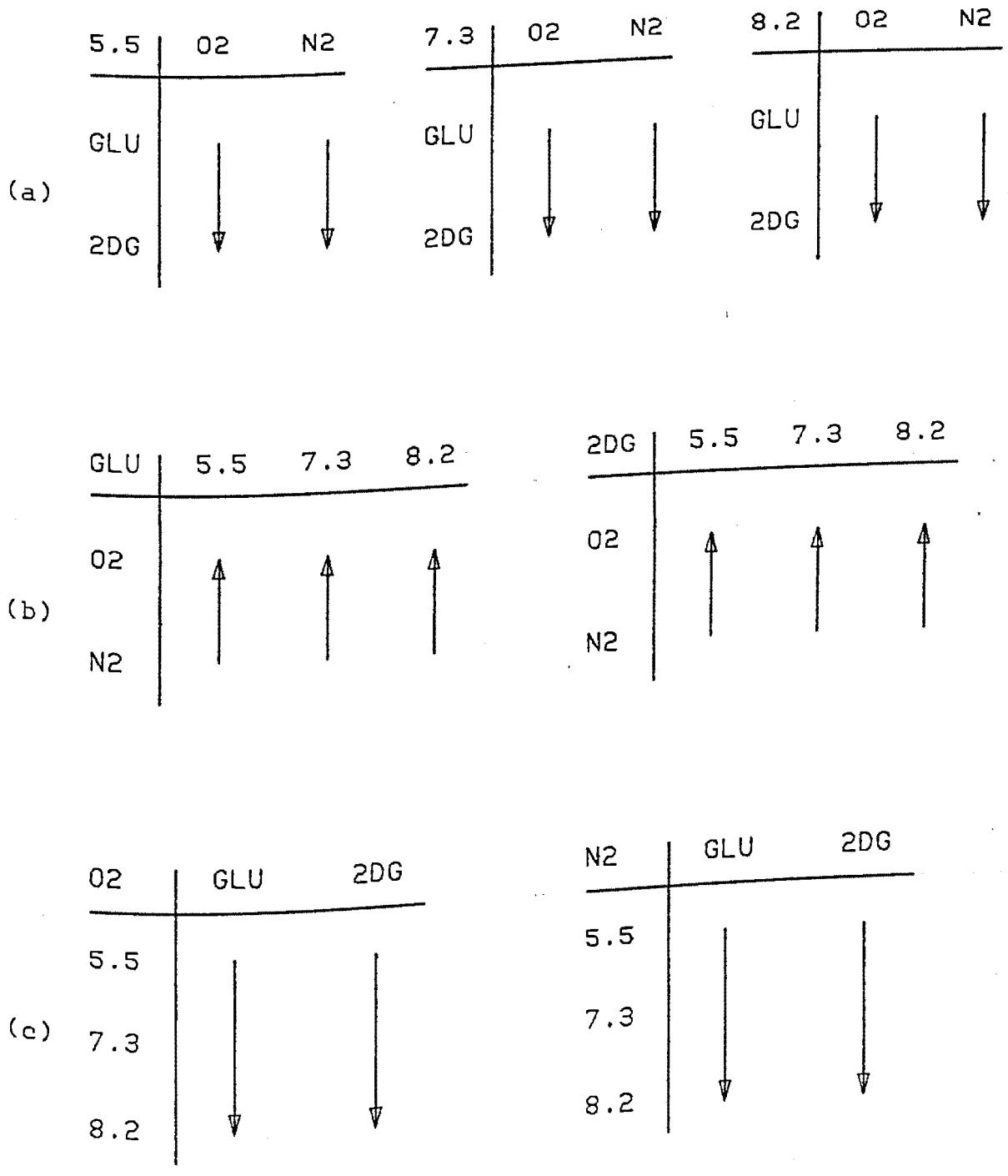
(a)
5.5
O2
N2
GLU
2DG
7.3
O2
N2
GLU
2DG
8.2
O2
N2
GLU
2DG
(b)
GLU
5.5
7.3
8.2
O2
N2
2DG
5.5
7.3
8.2
O2
N2
(c)
O2
GLU
2DG
5.5
7.3
8.2
N2
GLU
2DG
5.5
7.3
8.2

Figure 14

Figure 14. Schematic diagram of pH mechanism. Arrows point in direction of increased alkalinity, or of predicted increased formation of metarhodopsin III. (a) Comparison between substrates, given pH and respiratory state. (b) Comparison between respiratory states, given pH and substrate. (c) Comparison among pH's, given substrate and respiratory state.

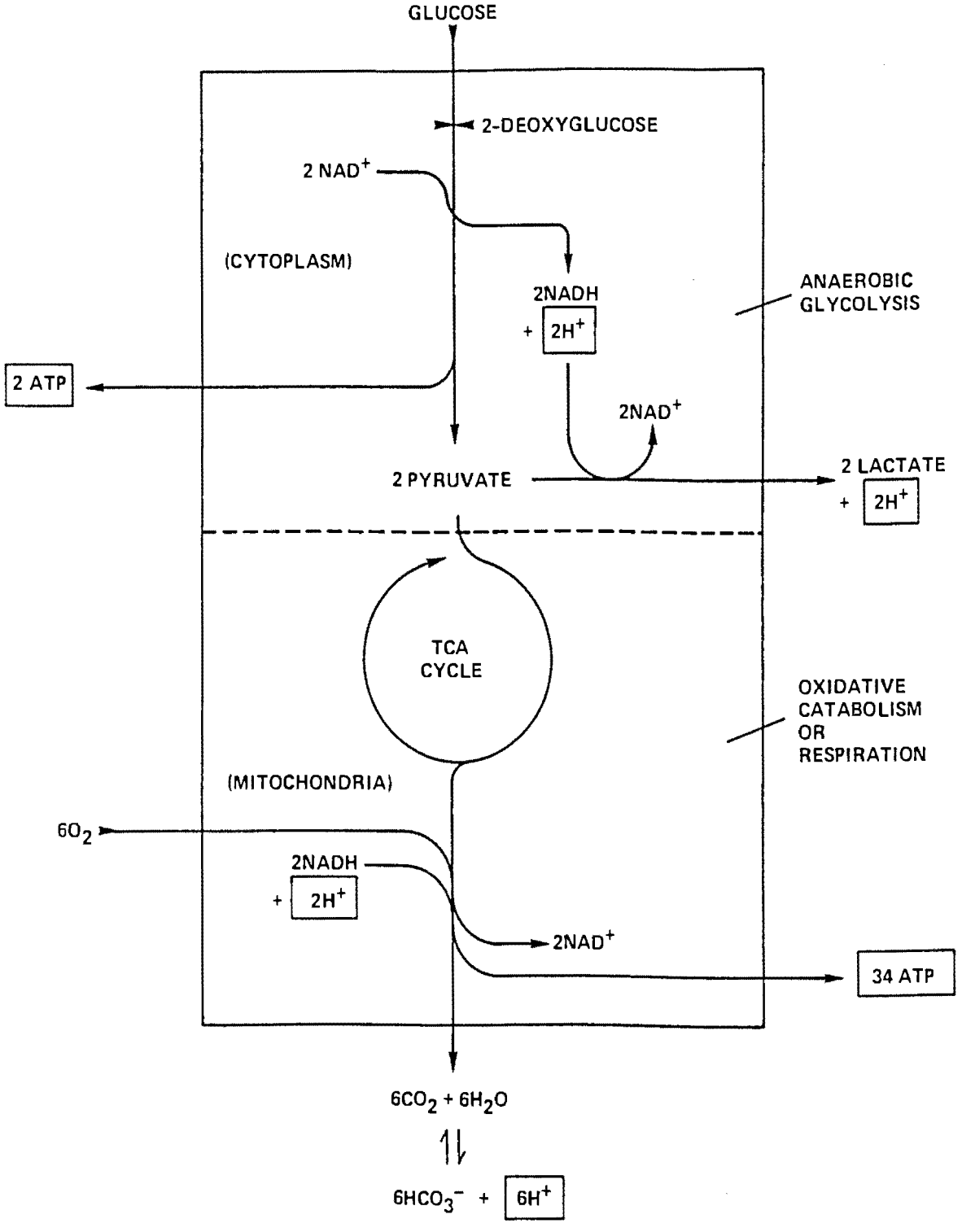
GLUCOSE
2-DEOXYGLUCOSE
2 NAD+
(CYTOPLASM)
2NADH
+ 2H+
ANAEROBIC
GLYCOLYSIS
2 ATP
2NAD+
2 PYRUVATE
2 LACTATE
+ 2H+
TCA
CYCLE
OXIDATIVE
CATABOLISM
OR
RESPIRATION
(MITOCHONDRIA)
6O2
2NADH
+ 2H+
2NAD+
34 ATP
6CO2 + 6H2O
6HCO3− + 6H+

Figure 15

Figure 15. Pathways of cellular metabolism. Figure 2 is repeated. Components of metabolic processes which are postulated to be potentially linked to metarhodopsin III formation are enclosed in boxes for emphasis.

For example, cells which are supplied with an adequate substrate, like glucose, will produce a greater quantity of acidifying products of catabolism, either lactic acid or carbon dioxide, than cells which have been deprived of any substrate. For this reason, comparisons in Figure 14(a) between perfusates containing either glucose or 2-deoxyglucose would predict a greater formation of metarhodopsin III in the presence of 2-deoxyglucose. Also, anoxia will create a more acidic intracellular environment than oxygenated conditions. In abundant oxygen, pyruvate is catabolized via the tricarboxylic acid cycle to produce carbon dioxide, which diffuses readily through the plasma membrane. Anoxia, on the other hand, blocks this breakdown pathway for pyruvate, whose conversion results in the production of lactic acid. Intracellular acidosis results, since the diffusion for the passive exit of lactate from a retinal cell is small, due to its low permeability (Lolley, 1972). Thus, metarhodopsin III formation would be predicted to be greater in concentration when abundant oxygen is available, which is represented in Figure 14(b). The predictions illustrated in Figure 14(c) need no further explanation, since straightforward comparisons between different pH environments are direct expressions of the pH mechanism.

Mechanisms of ATP Effects

In addition to the reported and postulated effects of hydrogen ions on rhodopsin photoproducts, ATP availability has

also been implicated as an important cofactor in events observed in photoreceptor cells. Rhodopsin molecules in outer segment suspensions are known to be phosphorylated following light stimulation (Kühn and Dreyer, 1972; Bownds, Dawes, Miller, and Stahlman, 1972). Presumably, the terminal phosphate group of ATP is transferred to opsin. In addition, decreased concentration of ATP in illuminated photoreceptor outer segments may occur through a combination of a light-activated GTPase and a GDP-ATP transphosphorylase (Robinson and Hagins, 1976).

The time course of rhodopsin phosphorylation has been determined to coincide with the occurrence of the metarhodopsins II-III-retinal transformations (Paulsen, Miller, Brodie, and Bownds, 1975), with the maximum rate occurring approximately 8 to 20 minutes subsequent to illumination at 21°C. However, there is some question as to any relationship, other than coincidence, between phosphorylation and photoproduct changes, at least in isolated outer segment preparations.

The significance of the simultaneity of the two phenomena warrants further consideration, especially in the context of an alternate experimental preparation other than suspensions of outer segments. For example, the enzymes and substrates of both glycolysis and oxidative phosphorylation have been found to be concentrated in the inner segments of photoreceptor cells (Matschinsky, 1970; Lowry, Roberts, Schulz, Clow, and Clark, 1961). Preparations of isolated photoreceptor outer segments, which are incomplete cells, only exhibit very low activity of these enzymes (Lolley and Hess, 1969).

Thus, it still remains possible that phosphorylation might be linked somehow to the photoproduct transitions occurring subsequent to metarhodopsin II in preparations where photoreceptor cells remain intact. For example, as illustrated in Figure 13, the molecular rearrangement which occurs during the metarhodopsins II-III transformation in intact retinas might require energy, obtained by means of phosphorylation. In contrast, the formation of free retinal, as a result of hydrolysis of its photoproduct precursors, would be an exergonic process. For these reasons, a mechanism of ATP influence has been postulated to explain the observed effects of metabolic factors on the photoproduct sequence described in this dissertation.

An ATP hypothesis would predict that the proportion of metarhodopsin II which decays via metarhodopsin III decreases under such conditions that ATP formation is lowered. Figure 16 illustrates this mechanism schematically, with the arrows pointing toward the condition in which greater metarhodopsin III is predicted. Since 2-deoxyglucose blocks glucose metabolism at the level of the first enzymatic step in glucose catabolism (Wick, Dury, Nakada, and Wolfe, 1957), it is assumed that little ATP is formed in its presence. Furthermore, any residual ATP supply which was formed prior to the application of 2-deoxyglucose is assumed to be depleted rapidly (Owen, Caplan, and Essig, 1975).

The comparisons in Figure 16(a) are straightforward applications of the ATP mechanism, based upon the increased

(a)

5.5	O2	N2
GLU	↑	↑
2DG		

7.3	O2	N2
GLU	↑	↑
2DG		

8.2	O2	N2
GLU	↑	↑
2DG		

(b)

GLU	5.5	7.3	8.2
O2			
	=	=	=
N2			

2DG	5.5	7.3	8.2
O2			
	=	=	=
N2			

(c)

O2	GLU	2DG
5.5		
	=	=
7.3		
	=	=
8.2		

N2	GLU	2DG
5.5		
	=	=
7.3		
	=	=
8.2		

Figure 16

Figure 16. Schematic diagram of ATP mechanism. Arrows point in direction of increased ATP production, or of predicted increased formation of metarhodopsin III. =: no difference in amount produced. (a) Comparison between substrates, given pH and respiratory state. (b) Comparison between respiratory states, given pH and substrate. (c) Comparison among pH's, given substrate and respiratory state.

availability of ATP in the presence of glucose. Two additional assumptions are invoked in the comparisons illustrated in Figure 16(b) and (c). First, it is assumed that anaerobic glycolysis can, within the duration of the experiments reported here, adequately provide as much ATP as the cells would normally produce if oxygen were available. This assumption is supported by observations that a high rate of glycolysis occurs in the retina in vivo, which suggests that the retina may function normally, for a considerable time, in a semi-anoxic state (Graymore, 1970; Lolley and Schmidt, 1974). Also, the amount of ATP produced at the three pH levels, in either respiratory state, is assumed to be adequate.

Extent of Metarhodopsin III Formation

The schemes illustrated in Figures 13 through 16 provide the framework in which the parameter, P', described previously in Table III, can be evaluated. As will be shown, the interaction of the pH and ATP mechanisms predicts satisfactorily the degree to which metarhodopsin III was formed in almost all of the various perfusate environments.

The bulk of the results of the experiments performed at pH 5.5 have indicated that less than 10 percent, and, more often, none of the metarhodopsin II photoproduct is transformed into metarhodopsin III, independent of the respiratory state or glucose availability in the retina. Experiments performed in an acidic medium represent a homogeneous category

in which the pH mechanism alone clearly predominates in predicting metarhodopsin III formation. This result is expected, based upon the scheme presented in Figure 13, since a large excess of hydrogen ions would favor the formation of retinal rather than of metarhodopsin III.

Results obtained from those experiments performed near the physiological pH, as well as in alkaline media, require a detailed evaluation in order to determine how the two mechanisms interact to determine metarhodopsin III formation. Figure 17 illustrates the results of t-test comparisons (see APPENDIX B) among the various perfusate compositions for the parameter, P', whose values were tabulated previously in Table III. The individual comparisons are discussed below in the context of the two mechanisms and their combined effort on metarhodopsin III formation.

1. Figure 17(a): pH 7.3 and 8.2, oxygen, glucose versus 2-deoxyglucose. A greater proportion of metarhodopsin II decays via metarhodopsin III in well-oxygenated, non-acidic media when abundant glucose is available. This observation is indicated in Table III by the magnitudes of P' in the presence of glucose and 2-deoxyglucose: .45 versus .15 and .66 versus .44, respectively, in pH 7.3 and 8.2. There is presumably no tissue acidosis incurred by the carbon dioxide produced in the presence of glucose, due to the ease of diffusion of this catabolic product across cell membranes. Likewise, since no tissue acidosis occurs in substrate-deprived

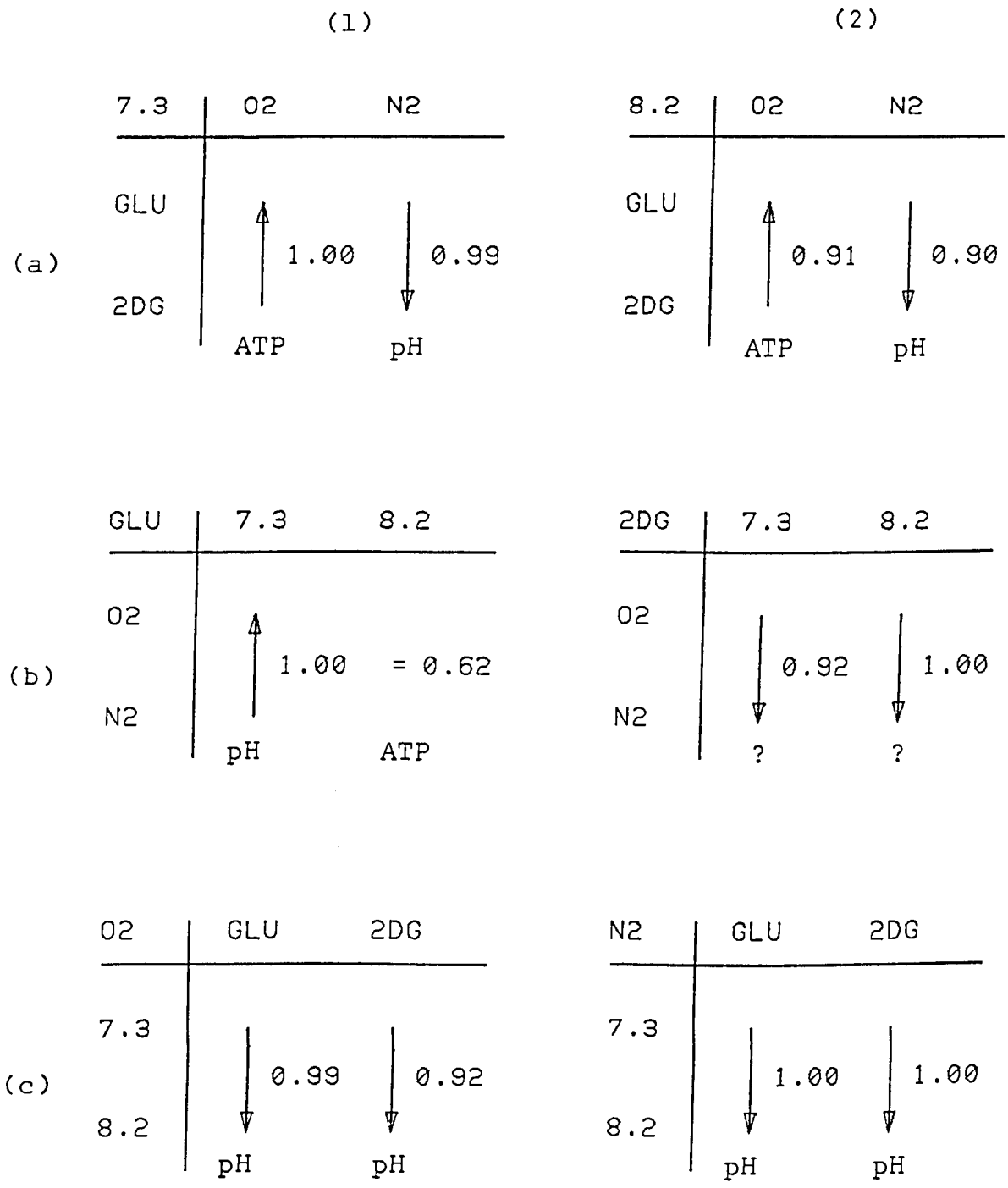
(1)
(2)
7.3
O2
N2
8.2
O2
N2
GLU
2DG
(a)
1.00
0.99
0.91
0.90
ATP
pH
ATP
pH
GLU
7.3
8.2
2DG
7.3
8.2
O2
N2
(b)
1.00
= 0.62
0.92
1.00
pH
ATP
?
?
O2
GLU
2DG
N2
GLU
2DG
7.3
8.2
(c)
0.99
0.92
1.00
1.00
pH
pH
pH
pH

Figure 17

Figure 17. Effects of perfusate media on amount of metarhodopsin III formation. Arrows point in direction of increased formation of metarhodopsin III, measured by t-tests on magnitudes of P' (see Table III and APPENDIX B). Numbers indicate probability values associated with each comparison. Comparisons between (a) substrates; (b) respiratory states; and (c) pH's. Predominating hypothesis is listed below each comparison.

preparations (Norberg, Nillson, and Siesjö, 1975), the intracellular pH is not significantly different as a function of substrate availability in oxygenated retinas. Thus, the ATP mechanism would cause greater metarhodopsin III to form in the presence of glucose.

2. Figure 17(a): pH 7.3 and 8.2, nitrogen, glucose versus 2-deoxyglucose. A greater amount of metarhodopsin III is formed in anoxic, non-acidic extracellular environments when glucose is lacking. In pH 7.3, the relative proportions are .14 in the presence of glucose, compared with .38 in its absence. In like manner, the magnitudes of P' in pH 8.2 are .66 versus .72. These observations are opposite to photoproduct behavior in well-oxygenated retinas, described above. Evidently, the production of lactate under anaerobic conditions is responsible for the difference.

It is not unexpected that lactate would tend to acidify cells intracellularly, since it does not diffuse readily out of the retina (Lolley, 1972). Intracellular lactic acidosis, produced when glucose supply is adequate, apparently cannot be buffered adequately by either external HEPES buffer, at pH 7.3, or external Tris buffer, at pH 8.2, in concentrations of 10 millimolar. This conclusion is supported in part by studies of snail neurones, in which intracellular pH was often found to be buffered inadequately, even by 20 millimolar concentrations of either of these particular extracellular buffering agents (Thomas, 1976). Thus, the actual intra-

cellular pH values are probably somewhat lower than 7.3 and 8.2, respectively, in cells metabolizing anaerobically.

On the other hand, metabolic degradation of 2-deoxyglucose cannot take place (Wick, Dury, Nakada, and Wolfe, 1957), since a bottleneck occurs at the first enzymatic steps of glycolysis when it is substituted for glucose as a substrate. This bottleneck diminishes the production of any metabolic waste products. Thus, intracellular acidosis, which might normally occur as a result of anaerobic glycolysis, would be protected against in substrate-deprived, anoxic preparations. As a result, hydrogen ions would be plentiful in anoxic retinas only when glucose substrate was available, favoring retinal formation rather than metarhodopsin III.

3. Figure 17(c)(1) and (2): oxygen and nitrogen, glucose and 2-deoxyglucose, pH 7.3 versus pH 8.2. A greater proportion of metarhodopsin II is transformed into metarhodopsin III in the more alkaline environment, regardless of the metabolic state of the retina. From Table III, the magnitudes of p' in the four comparisons between pH 7.3 and 8.2 are calculated to be .45 versus .66, .15 versus .44, .14 versus .66, and .38 versus .72, respectively. It is assumed from Figure 16(c) that there would be sufficient amounts of ATP produced within each of the four categories of comparison. Thus, the hydrogen ion concentration is the more important variable, and the differences in metarhodopsin III formation observed in Figure 17(c) are in direct agreement with the predictions

of the pH hypothesis.

4. Figure 17(b)(1): glucose, pH 7.3, oxygen versus nitrogen. A greater concentration of metarhodopsin III, .45, is observed in a respiring retina, near physiological pH, than in an anaerobic preparation, .14. Again, sufficient amounts of ATP are produced in either condition, so that hydrogen ion concentration is the important variable. An anoxic retina would probably exhibit lactic acidosis, producing an excess of hydrogen ions when compared with an aerobic preparation. Thus, the smaller formation of metarhodopsin III in anaerobic retinas is consistent with the pH mechanism described in Figure 13.

5. Figure 17(b)(1): glucose, pH 8.2, oxygen versus nitrogen. No difference in metarhodopsin III formation is observed in alkaline media, whether the cells are metabolizing aerobically or anaerobically. In each case, the magnitude of p' is .66. This observation is different from the results of the similar comparison discussed above in pH 7.3, although lactate production is most likely a by-product of glucose metabolism at either external pH. However, it is possible that any excess hydrogen ions accompanying lactate production at external pH 8.2 would not lower the intracellular pH enough to cause appreciable diversion of the metarhodopsin II decay process directly to retinal, relative to that observed in oxygenated preparations. Slight fluctuations in pH due to more or less accumulation of lactate are probably neutralized imme-

diately and exert no adverse effect on metarhodopsin III formation. Thus, either mechanism would be equally important in alkaline environments.

6. Figure 17(b)(2): 2-deoxyglucose, pH 7.3 and 8.2, oxygen versus nitrogen. When metabolic substrate is deprived from the tissue in either physiological or alkaline pH, a greater proportion of metarhodopsin II decays via metarhodopsin III in anoxic conditions than in an oxygenated preparation. The relative proportions, P', are .38 versus .15 and .72 versus .44 in pH 7.3 and 8.2, respectively. These two observations cannot be explained on the basis of either pH or ATP mechanisms.

In anoxic, substrate-deprived cells, it is presumed that metabolic activity would be markedly reduced. However, it has been shown that glucose-free brain tissue is capable of performing certain autolytic processes at high rates in the presence of oxygen (Nordström, Rehncrona, and Siesjö, 1976). This could result in the oxidation of tissue proteins and lipids (Abood and Geiger, 1955; Norberg and Siesjö, 1976), which would potentially damage the structural integrity of the cell. It is noteworthy that the photoreceptor membrane contains a high content of unsaturated fatty acids and is liable to oxidation by air (Farnsworth and Dratz, 1976). If such damage did occur, its effect on photoproduct formation would be difficult to predict. The explanation of potential cellular degradation in the presence of oxygenated, glucose-deprived extracellular media would not be incompatible

with any of the previously described comparisons, illustrated in Figure 17(a)(1) and (c)(1), involving this population of experiments.

The remaining experiments described in Table III are those, at other than pH 5.5, in which no metarhodopsin III formation was detected. These experiments are indicated in the table by the number of accepted experiments in each category which were not included in the curve-fitting statistics. All of the six experiments occurred in anoxic conditions at external pH 8.2. Based on the scheme presented previously in Figure 13, those experiments with glucose-supplied substrate probably were in a state of acidosis serious enough to divert metarhodopsin II decay through the alternate pathway directly to retinal. The other experiments, with 2-deoxyglucose replacing the substrate, presumably depleted all ATP reserves without replacement, so the probable cofactor required for metarhodopsin III formation was absent.

The alternate grouping of the experiments, based upon the pigment categories illustrated previously in Figure 12, can also be explained with respect to the interaction of the two mechanisms. As indicated in Table V, the majority of the experiments in which large concentrations of metarhodopsin III occurred were perfused by alkaline solutions. In fact, the distribution of experiments based upon decreasing amounts of metarhodopsin III formation correlated generally with the declining pH of the external medium. In contrast, the sub-classification of the five pigment

categories as functions of either respiratory state or substrate availability, individually, is not straightforward. This might be expected, in view of the fewer comparisons in Figure 17 in which the ATP mechanism predominated.

Thus, with the exception of the two comparisons in Figure 17(b)(2), the preferred pathways of metarhodopsin II decay, measured by the parameter, P', in Table III, are consistent with the mechanisms depicted in Figure 13. The availability of hydrogen ions seems to exert the primary influence in determining the photoproduct sequence subsequent to metarhodopsin II. The only conditions in which ATP availability is the predominant factor controlling metarhodopsin III formation are described in comparison 1 above, between glucose and 2-deoxyglucose in well-oxygenated conditions. With adequate supplies of both glucose and oxygen, the cells are metabolically in a healthy condition and quickly oxidize lactic acid, if any is formed. Thus, the pH of the cell is maintained at neutral or higher.

Conditions in which lactate accumulation, a lowering in the pH, is prevented appear to favor increased formation of metarhodopsin III. This strongly suggests that metarhodopsin III is a normal bleaching intermediate in a healthy retina.

Pathways of Metarhodopsin II Decay

The data presented here imply that multiple pathways of rhodopsin photoproduct decay exist in the isolated retina,

beginning at least as early as the decay of metarhodopsin II. Examination of the parameter, P', indicates that metarhodopsin II decays via at least two pathways near physiological temperatures, one of them through the metarhodopsin III photoproduct.

The phenomenon of multiple pathways of metarhodopsin II decay has been observed previously in isolated frog retinas (Baumann, 1972; Bowmaker, 1973; Gyllenberg, Reuter, and Sippel, 1974), as well as in suspensions of photoreceptor outer segments (Paulsen, Miller, Brodie, and Bownds, 1975). These earlier studies indicated that the only pathway of metarhodopsin II decay, other than through metarhodopsin III, is its hydrolysis directly to free retinal plus opsin. In addition, the decay of Hagins' (1957) "Intermediate B" in the living eye was reported to follow more than one pathway, although the identification of the alternate photoproduct sequence was not established.

In isolated retinas, the direct formation of free retinal in lieu of metarhodopsin III was observed to be more predominant, at 5°C, in a solution of low pH (Bowmaker, 1973; Gyllenberg, Reuter, and Sippel, 1974). Frank (1969) also detected a lower relative peak optical density of metarhodopsin III, at 22°C, in a pH 5.5 medium than at either pH 7.7 or 10.3, where he observed no significant difference in peak concentrations. These observations are consistent with the decreased influence of the pH mechanism, described in Figure 13, in non-acidic environments.

The direct influence of ATP availability on the pathway of metarhodopsin II decay has not been previously documented as extensively as the role of pH. In suspensions of photoreceptor outer segments, incubated at pH 7.5 with ATP, the rate of light-induced phosphorylation of rhodopsin was not a function of metarhodopsin III concentration, although the time course coincided with the phase of metarhodopsin II decay (Paulsen, Miller, Brodie, and Bownds, 1975). Donner and Reuter (1969) did not observe any effect of ADP or certain respiratory chain inhibitors on the metarhodopsins II-III transition. However, their preparation was enclosed in a non-perfused chamber with only a small volume of solution. To date, a systematic study of the effects of ATP on the photoproduct sequence in intact, perfused retinas has not been previously reported.

Pathways of Metarhodopsin III Decay

It is also likely that metarhodopsin III can decay via more than one pathway. In preparations of solubilized rhodopsin extracts, the formation of N-retinylidene opsin (NRO), the pH indicator, has been well-documented as an additional photoproduct, appearing in the decay sequence in between metarhodopsin III and retinal (see Figure 1). This substance exhibits characteristic absorption maxima at 440 nanometers in acid solution and at 365 nanometers in alkaline media. At neutral pH, NRO is rapidly hydrolyzed in solution to free retinal plus opsin, so it is not observed as a

photoproduct (Ostroy, Erhardt, and Abrahamson, 1966).

Alkaline NRO has been observed subsequent to metarhodopsin III in rod outer segment preparations (Pausen, Miller, Brodie, and Bownds, 1975) and even possibly in non-perfused, isolated retinas buffered with borate (Bowmaker, 1973). In contrast, alkaline NRO was not observed in other non-perfused (Gyllenberg, Reuter, and Sippel, 1974) or perfused, isolated retinas (Frank, 1969), up to a pH value of 10.3. Because of the measurement limitations of the RMSP in the near ultraviolet spectrum, it was not possible to establish whether alkaline NRO was formed in the experiments reported in this thesis.

Acid NRO has not been reported to date as a photoproduct in isolated retina preparations (Frank, 1969; Gyllenberg, Reuter, and Sippel, 1974), although its slow formation has been observed in suspensions of outer segments (Bridges, 1962). However, unlike its behavior in solution, acid NRO did not decay in the outer segment preparations, and, in fact, was implied to exist as a stable photoproduct in very acidic media of pH 4.6.

In general, metarhodopsin III decay in isolated retinas and in outer segment suspensions has been attributed exclusively to the formation of free retinal plus opsin (Baumann, 1972; Bowmaker, 1973; Gyllenberg, Reuter, and Sippel, 1974; Paulsen, Miller, Brodie and Bownds, 1975). However, at least one laboratory reports that metarhodopsin III in rat retinas decays directly into the reduced product, retinol, without an intermediate retinal stage (Cone and Brown, 1969; Cone and

Cobbs, 1969). Although retinal was observed in these experiments, its formation was assumed to be due exclusively to a direct transformation from metarhodopsin II.

Evidence of alternate pathways of metarhodopsin III decay has been presented in this research as well. For example, the category of experiments in which only a single, rapid decay phase was measured at 380 nanometers (see Figure 12(a)) indicates that very little retinal was formed in this population of experiments. The apparent sequence is that metarhodopsin II decayed primarily into metarhodopsin III, which, in turn, decayed to some photoproduct other than retinal that was undetectable by the RMSP. This could be either retinol or alkaline NRO, which absorb maximally in the far and near ultraviolet regions, respectively, out of the spectral range of the RMSP. Alkaline NRO can probably be ruled out, since its finite absorption bandwidth, centered at 365 nanometers, would cause it to contribute significantly to the extreme blue end of the visible spectrum. As pointed out previously, the RMSP did not detect optical density changes in this region, other than the single rapid decay phase, so that retinol was more likely the final photoproduct.

Although the mechanism responsible for the direct reduction of metarhodopsin III to retinol is not known, it is interesting to note the similarities between the environmental conditions in Cone's experiments and in this research. Cone's retinas

were enclosed in a non-perfused chamber with only a single drop of pH 6.8 Ringer, which was unoxygenated and included no glucose. Table V indicates that this category of experiments was observed here in the presence of buffers of exclusively pH 8.2, usually in metabolically-deprived retinas.

The fact that none of the experiments in external pH 7.3 exhibited direct reduction to retinol is somewhat at odds with Cone's results in pH 6.8, although the effects of a perfusion flow might be contributory. The results described here could also be influenced, in part, by the action of the Tris buffer, used at pH 8.2 (see METHODS), which has been shown previously to be capable of interfering with certain enzyme-catalyzed reactions (Mahler, 1961). Although the effects of Tris, if any, on the enzymatic reduction of photoproducts to retinol is not known, this buffering agent cannot be ruled out as a determining factor of the pathway of metarhodopsin III decay in isolated retinas.

Photoproduct Formation in Incompletely Controlled Environments

If the metabolic state of the retina truly affects the course of photoproduct transformations, it is not unreasonable to expect experimental results to depend on the manner in which the preparation is maintained during a measurement sequence. If nutrients are not continually supplied and the pH is not adequately buffered, one might expect variations in magnitudes of photoproduct formation such as those illustrated

in Table III, depending upon the actual state of the retina at any given time.

For this reason, experiments performed under conditions where any of the controlling variables are time-varying in an unknown way might yield misleading results. The use of air-tight, non-perfused chambers to house isolated retinas is an extreme example of an incompletely controlled extracellular environment. Not only is the preparation gradually depleting endogenous glucose and oxygen supplies, but it is also accumulating metabolic waste products which cannot be removed due to the lack of superfusing flow. The detrimental effects of no perfusion are supported by observations of rapidly deteriorating electrical activity of the retina, which is worst in small volume chambers (Sickel, 1972).

The observation of somewhat unexpected results with respect to metarhodopsin III decay under these conditions has already been pointed out (Cone and Brown, 1969). At least two other studies utilizing non-perfused, air-tight chambers have indicated unusual metarhodopsin III formation as well. Matthews, Hubbard, Brown, and Wald (1963) reported no formation of metarhodopsin III at 22°C in isolated frog retinas enclosed in such a chamber and questioned whether potentially increased acidity was responsible. Donner and Reuter (1967) noted substantially less metarhodopsin III formation at 15°C after the retina had been incubated in a closed chamber for 30 minutes prior to bleaching, rather

than if it were measured immediately.

Additional experiments performed for this dissertation, other than those already reported in the RESULTS section and discussed previously, were devised to learn more about metarhodopsin III behavior in uncontrolled, time-varying extracellular environments. The first group of studies were done in an air-tight, non-perfused chamber of much the same type as in the experiments discussed above. Since the volume of the experimental chamber was not much greater than that of the retina itself (see METHODS), the preparation remained sealed in the chamber with only approximately one milliliter of the fluid in which the dissection was performed.

Two sets of closed chamber experiments were performed, both with solutions buffered at pH 8.2. In the first case, no glucose was present in the dissecting Ringer solution. In these experiments, no formation of metarhodopsin III was ever observed, no matter how soon measurements began after surgery. In the second population of experiments, the Ringer solution contained 20 mM of glucose, as in the perfusion experiments. These preparations exhibited a consistently repeatable sequence of events. The first few 10-minute measurements always produced observable amounts of metarhodopsin III, while measurements taken much after the retina had been enclosed for about 20 minutes in the chamber never detected any metarhodopsin III.

Presumably, both types of closed chamber experiments were manifestations of the same phenomenon. The retina was utilizing its remaining substrate until it was depleted, forming lactate, in the meantime, due to the anoxic chamber. The intracellular region became increasingly acidotic, due to lactate waste accumulation. Such acidosis was magnified due to the lack of a perfusion to remove the lactate. This effect was coupled with the diminishing supply ATP, as the glucose was gradually consumed. The result of this combination of events was the observed absence of metarhodopsin III in favor of the alternate pathway of metarhodopsin II decay directly to retinal, in agreement with the interaction of the hydrogen ion and ATP cofactors illustrated in Figure 13. Additional, exogenous glucose did not prevent the deterioration of the metarhodopsin III pathway but merely delayed its onset.

The results of the closed chamber experiments led to a series of studies of uncontrolled substrate levels in perfused preparations. Twelve retinas were used for a total of 58 experiments, in which the pH and respiratory state were controlled as described previously in the METHODS section. However, neither exogenous glucose nor 2-deoxyglucose were added to the perfusate in these experiments.

The amount of metarhodopsin III formed in such "ambient" substrate experiments is summarized in Table VI as a function of the relative pigment categories described previously in Figure 12. If the data for P' in Table VI are compared with

		Total	A	B	C	D	E
pH:	5.5	2	0	0	0	1	1
	7.3	15	1	3	4	5	2
	8.2	16	2	7	6	1	0
Respiration:							
	Oxygen	21	2	6	5	6	2
	Nitrogen	12	1	4	5	1	1
Totals		33	3	10	10	7	3

Table VI

Table VI. Relative photoproduct categories as function of perfusate composition in ambient substrate. See legend for Table V.

that of controlled substrate levels in Table V, it is seen that the distributions of experiments among the five categories are much the same as a function of pH, regardless of substrate availability. That is, more metarhodopsin III is observed in more alkaline conditions. It is also noted that the distribution of the 33 ambient experiments among the five categories is more like the distribution of the 23 glucose experiments than the 25 2-deoxyglucose experiments. Since no glucose was being supplied to the preparation in ambient experiments, the retina would be expected to deplete gradually whatever endogenous energy substrates were present in the cells at the time of surgical isolation of the preparation. Thus, the range of metarhodopsin III behavior in ambient experiments ought to fall intermediate between experiments performed in either glucose or 2-deoxyglucose environments, depending upon the extent to which the endogenous substrate has been exhausted.

Although this expectation is borne out in five kinetics categories, it is not always in agreement with the experimental observations of P', tabulated as a function of perfusate compositions in Table VII. It is apparent from comparisons described in Figure 18(a) that experiments with ambient substrate cannot be expected to behave predictably toward either extreme condition. The differences observed in the ambient state suggest that the interaction between ATP availability

	(1)	(2)	(3)	C_f	C_d	$\overline{C}$	P'	T_f	T_d	$\frac{T_f}{T_d}$
8.2-O_2	13	8	8	.71±.30	.62±.24	.66±.26	.64±.24	35±11	297±104	.13±.04
8.2-N_2	9	8	8	.67±.17	.54±.16	.60±.16	.53±.14	45± 4	236± 50	.20±.05
7.3-O_2	14	11	10	.33±.15	.44±.19	.39±.15	.31±.15	36±14	208± 93	.24±.23
7.3-N_2	6	4	3	.33±.16	.25±.11	.29±.13	.29±.13	30± 6	315± 72	.10±.02
5.5-O_2	10	2	1	.08	.12	.10	.08	21	94	.22
5.5-N_2	6	0	0	0	0	0	0	--	--	--
Totals	58	33	30							

Table VII

Table VII. Summary of metarhodopsin III parameters for ambient substrates. See legend for Table III.

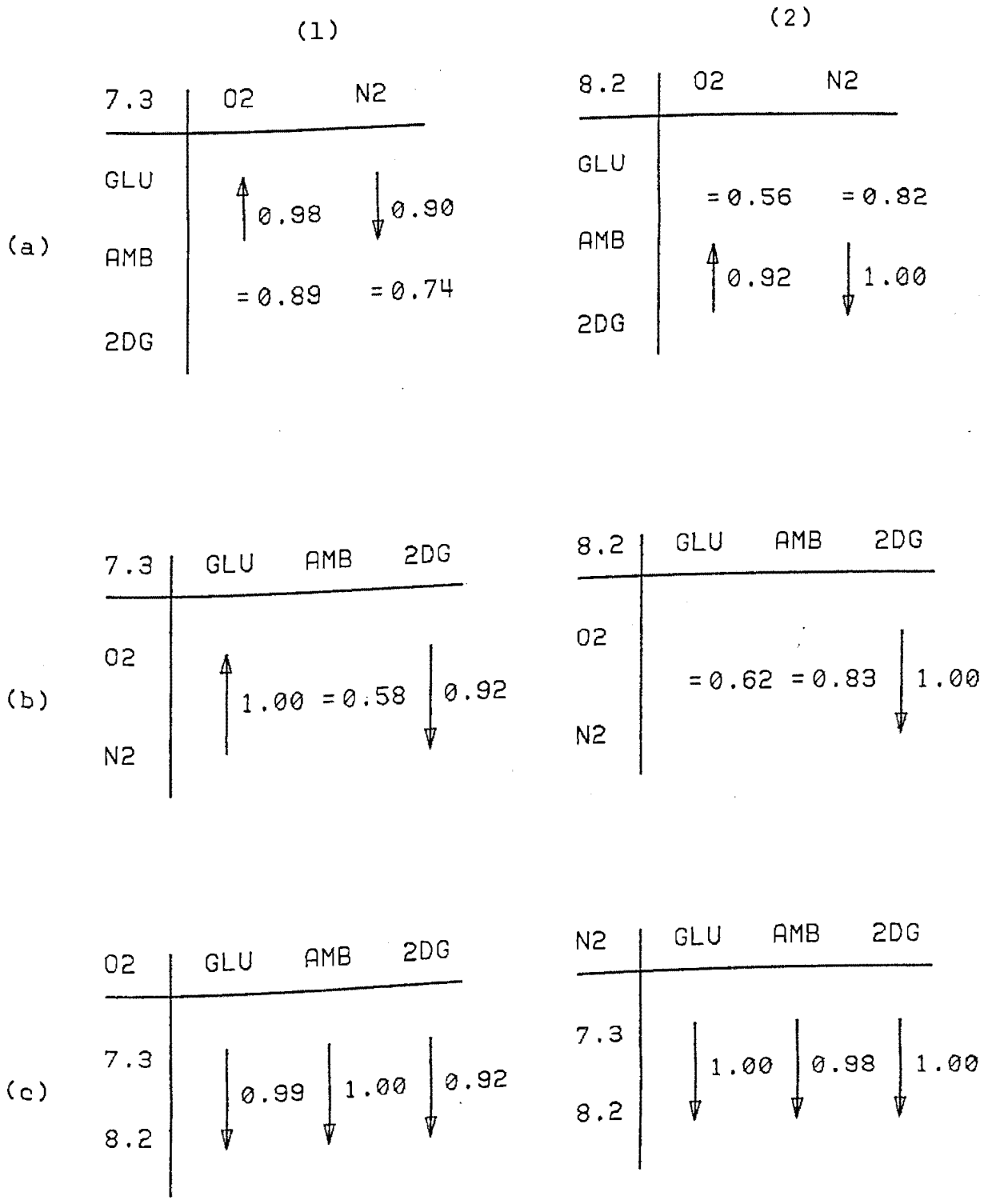
(1)
(2)
(a)
7.3
O2
N2
GLU
AMB
2DG
0.98
0.90
=0.89
=0.74
8.2
O2
N2
GLU
AMB
2DG
=0.56
=0.82
0.92
1.00
(b)
7.3
GLU
AMB
2DG
O2
N2
1.00
=0.58
0.92
8.2
GLU
AMB
2DG
O2
N2
=0.62
=0.83
1.00
(c)
O2
GLU
AMB
2DG
7.3
8.2
0.99
1.00
0.92
N2
GLU
AMB
2DG
7.3
8.2
1.00
0.98
1.00

Figure 18

Figure 18. Comparisons of metarhodopsin III concentration in different substrate conditions. Arrows point in direction of increased formation of metarhodopsin III, measured by magnitudes of P'. Comparisons between (a) substrates; (b) respiratory states; and (c) pH's. Results for glucose and 2-deoxyglucose are repeated from Figure 17.

and intracellular pH is more complicated to evaluate when glucose is in the process of being depleted during the course of a measurement.

This is even more evident when one attempts to evaluate the differences between P' magnitudes as functions of either pH or respiratory state in the presence of ambient substrate, illustrated in Figure 18(b) and (c), respectively. When comparing between extracellular pH's (Figure 18(c)), the ambient substrate exhibits significant differences in the same direction as both the glucose and 2-deoxyglucose states, in either state of respiration.

However, the comparisons of Figure 18(b), made between the two respiratory states, are not as straightforward. For example, no difference is observed in P' in ambient conditions at pH 7.3, although there are significant differences in the presence of both excess glucose and 2-deoxyglucose (Figure 18(b)(1)). In contrast, ambient behavior of P' in pH 8.2 is consistent only with observations made in a glucose-supplied medium (Figure 18(b)(2)). The time-dependent changes in the state of the preparation obviously make it more difficult to predict observed results on the basis of the scheme presented in Figure 13.

To emphasize further how incomplete control of all environmental factors can affect the parameters of metarhodopsin III, a comparison is summarized in Table VIII between results reported in literature references for frog retinas and results,

Reference	pH, buffer	Temp °C	Preparation	Substrate Supplied	Respiration	Norm. MIII	T_f sec.	T_d sec.
Frank, 1969	5.5, phosphate	22	perfused	glucose	saturated O_2	.10	--	540
Table III	5.5, acetate	21	perfused	glucose	saturated O_2	0	--	--
Frank, 1969	7.7, bicarb.	22	perfused	glucose	saturated O_2	.43	--	780
Baumann, 1972	7.5, phosphate	21	perfused	glucose	atmosphere O_2	.47	49	490
Gyllenberg et al., 1974	7.3, phosphate	20	non-perf.	none	aerated	--	--	294
Table III	7.3, HEPES	21	perfused	glucose	saturated O_2	.45	43	231
Bowmaker, 1973	7.2, phosphate	25	non-perf.	none	none	--	--	725
Paulsen et al. 1975	7.5, HEPES	22	outer seg.	none	none	.40	--	690
Table III	7.3, HEPES	21	perfused	2DG	saturated N_2	.38	35	166
Frank, 1969	10.3, phosphate	22	perfused	glucose	saturated O_2	.46	--	600
Table III	8.2, Tris	21	perfused	glucose	saturated O_2	.43	41	329

Table VIII

Table VIII. Comparison of published values for metarhodopsin III parameters. Literature references are tabulated, along with comparable conditions from Table III. pH and buffering agent are listed at temperature of study. Preparation was either perfused or non-perfused, isolated retina, or photoreceptor outer segment suspensions. Substrate availability and respiratory state are outlined for each reference.

in comparable environments, described in this dissertation. Only those published results of experiments performed around 21°C are included in this table. It can be seen that there is general agreement among the various comparisons as to the amount of metarhodopsin III formed, if the experiments are classified according to extracellular environment. The disparities in the half-times of formation and decay of metarhodopsin III, however, are noted at this time and will be discussed to a greater extent below.

Kinetics of Metarhodopsin III Formation and Decay

As with the relative amounts of formation of metarhodopsin III, both the half-times of formation and decay of metarhodopsin III, tabulated previously in Table III, are affected by the environment in which the experiments are performed. This is illustrated in the comparisons of Figures 19 and 20. Larger concentrations of metarhodopsin III were often associated with longer half-times of its formation. Thus, many of the significant differences between environmental conditions are observed to be the same for T_f (Figure 19) as for P' (Figure 17). In comparison, T_d was less likely to be influenced by environment in the same manner.

However, certain similarities can be noted between the two half-times if they are categorized as a function of the relative pigment categories (see Table IV). Figure 21 illustrates comparisons among these categories for both T_f and

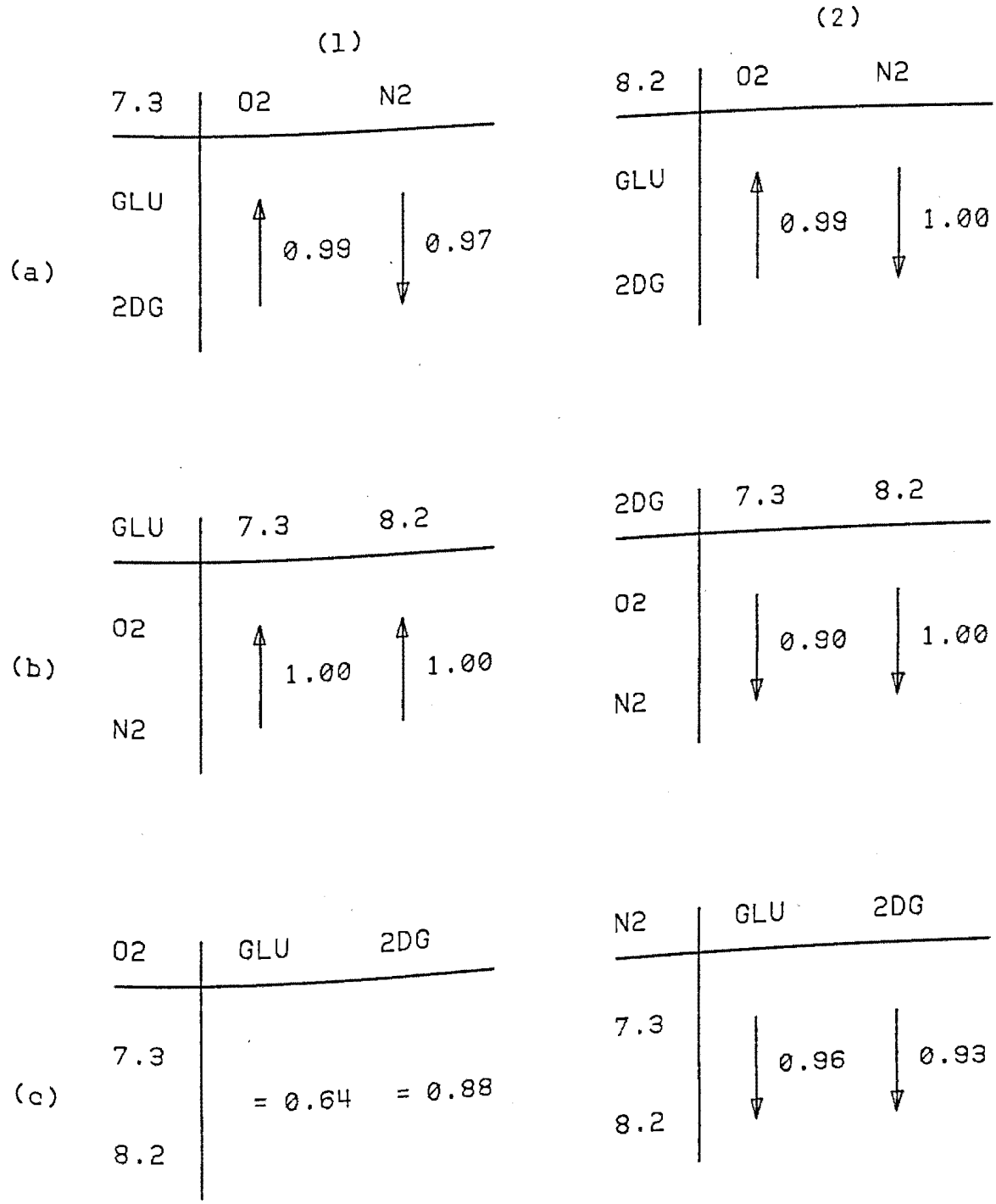
(1)
(2)
7.3
O2
N2
GLU
2DG
0.99
0.97
8.2
O2
N2
GLU
2DG
0.99
1.00
(a)
GLU
7.3
8.2
O2
N2
1.00
1.00
2DG
7.3
8.2
O2
N2
0.90
1.00
(b)
O2
GLU
2DG
7.3
8.2
= 0.64
= 0.88
N2
GLU
2DG
7.3
8.2
0.96
0.93
(c)

Figure 19

Figure 19. Effects of perfusate media on rate of metarhodopsin III formation. Arrows point in direction of longer half-time of formation of metarhodopsin III, T_f. See legend for Figure 17.

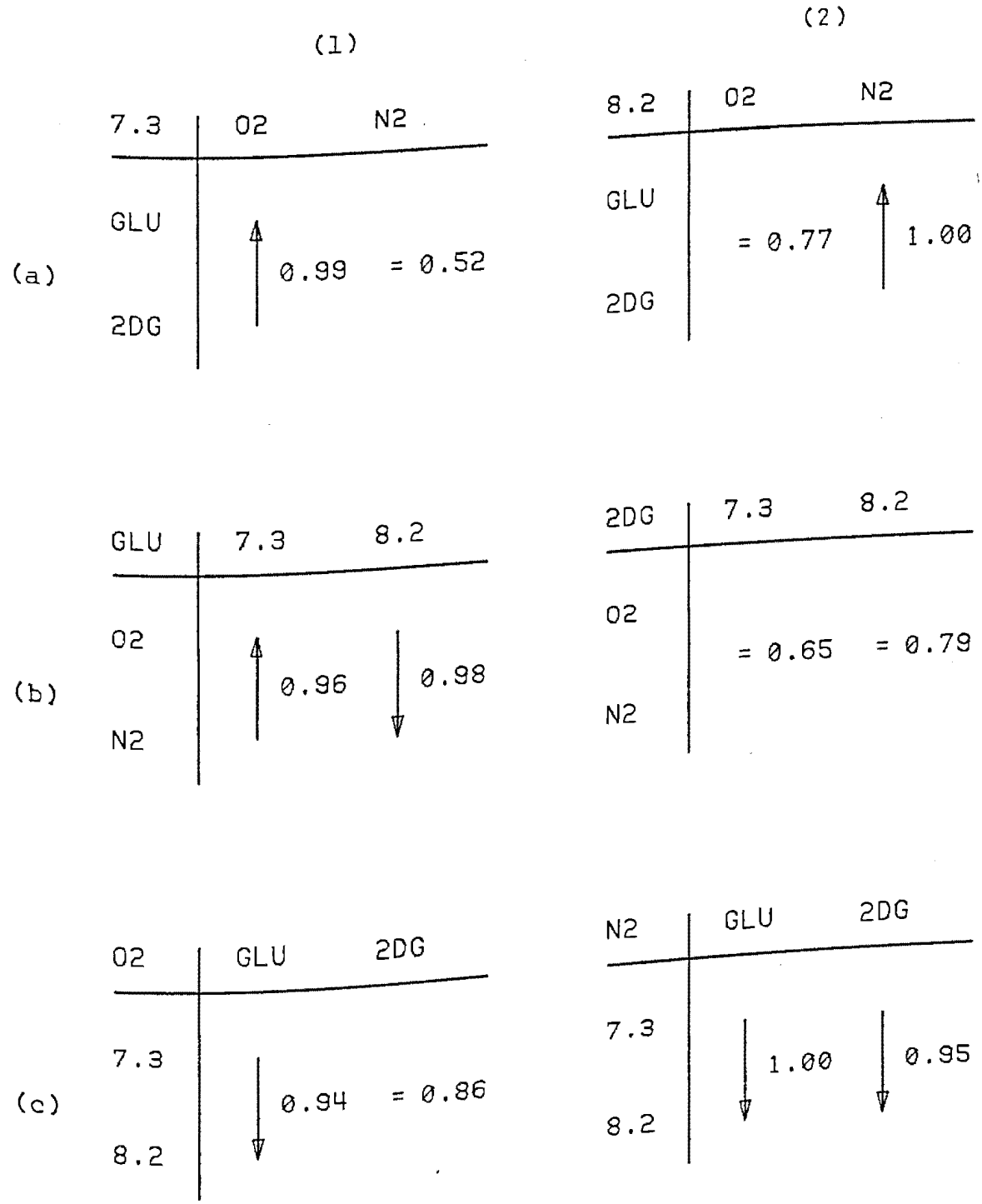
(1)
(2)
7.3
O2
N2
GLU
2DG
0.99
= 0.52
8.2
O2
N2
GLU
2DG
= 0.77
1.00
(a)
GLU
7.3
8.2
O2
N2
0.96
0.98
2DG
7.3
8.2
O2
N2
= 0.65
= 0.79
(b)
O2
GLU
2DG
7.3
8.2
0.94
= 0.86
N2
GLU
2DG
7.3
8.2
1.00
0.95
(c)

Figure 20

Figure 20. Effects of perfusate media on rate of metarhodopsin III decay. Arrows point in direction of longer half-time of decay of metarhodopsin III, T_d. See legend for Figure 17.

(a)

T_F	A	B	C
B	= 0.54	--	--
C	= 0.73	= 0.80	--
D	↑ 1.00	↑ 1.00	↑ 1.00

(b)

T_D	A	B	C
B	= 0.71	--	--
C	= 0.77	↑ 0.93	--
D	↑ 0.99	↑ 1.00	↑ 0.94

Figure 21

Figure 21. Comparisons of metarhodopsin III half-times as function of pigment categories. Arrows point in direction of longer half-times of formation, T_f (a), and decay, T_d (b). Numbers indicate probability value associated with each comparison. Categories A through D are defined in Table IV.

T_d. In each comparison involving the "D" category of experiments in which only a small amount of metarhodopsin III was observed, both T_f and T_d were significantly shorter. Thus, the metarhodopsin III photoproduct has a shorter existence when metarhodopsin II decays primarily into retinal, a process which has previously been shown to depend on hydrogen ion availability.

An even greater appreciation of the relationship between the formation and decay processes of metarhodopsin III is obtained from Figure 22, in which the ratios of the two half-times, T_f/T_d, have been compared. Differences in the magnitude of this ratio are significant only in comparisons in which at least one of the environmental conditions was anoxic. From Figure 22(a) and (b), it might be postulated that the accumulation of lactate somehow prolongs the decay phase with respect to the formation of metarhodopsin III. It is unclear why this effect would be stronger in alkaline media, illustrated in Figure 22(c). However, the potential involvement of enzymatic processes might complicate any explanation.

It has been observed that the net synthesis of lactate is restricted in <u>in vitro</u> conditions which mimic the <u>in vivo</u> state of the retina (Matschinsky, Passonneau, and Lowry, 1968). This could be interpreted to imply that the control of lactate levels is important to the normal function of the retina (Lolley and Schmidt, 1974). If so, the data in Figure 22 lend

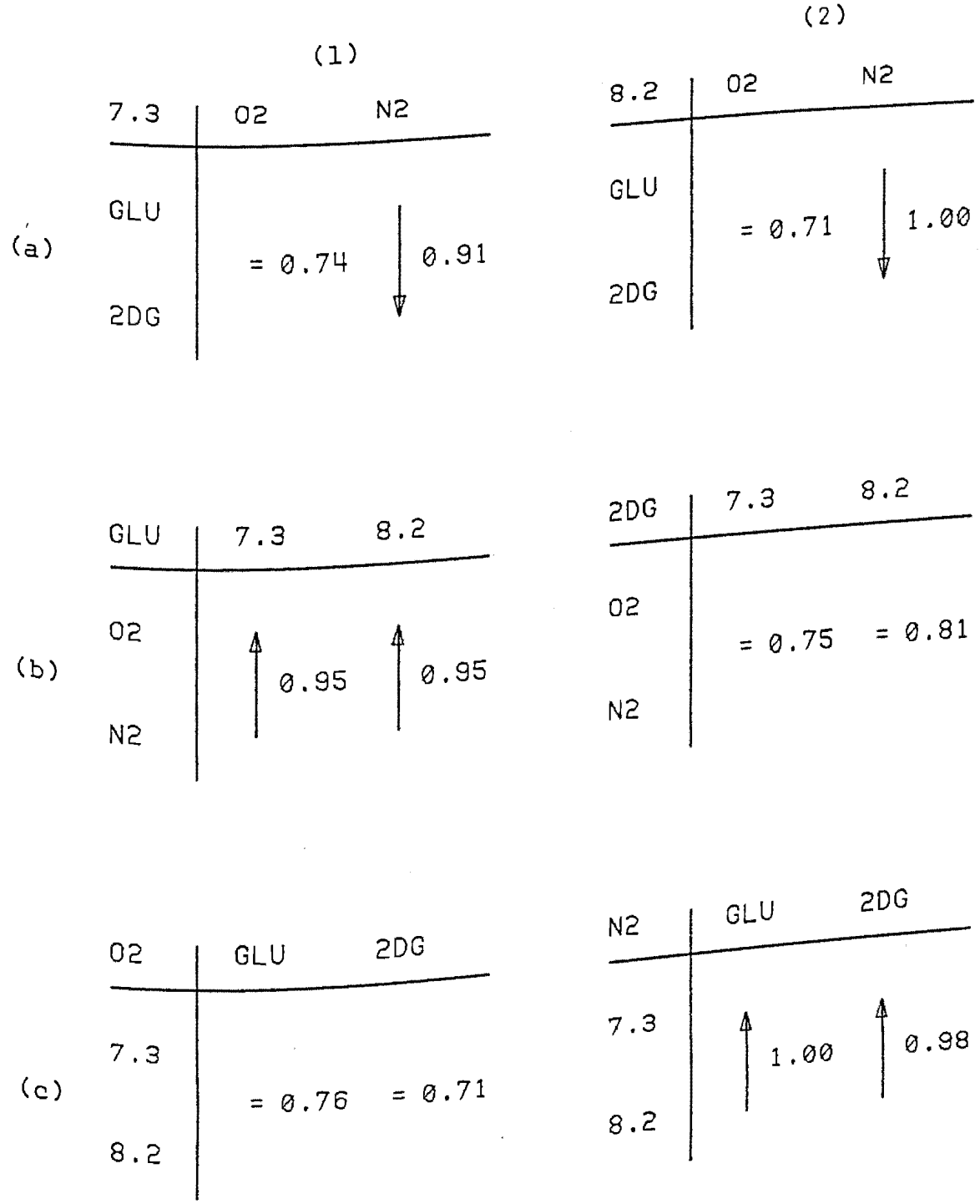
(1)
(2)
(a)
7.3
O2
N2
GLU
2DG
= 0.74
0.91
8.2
O2
N2
GLU
2DG
= 0.71
1.00
(b)
GLU
7.3
8.2
O2
N2
0.95
0.95
2DG
7.3
8.2
O2
N2
= 0.75
= 0.81
(c)
O2
GLU
2DG
7.3
8.2
= 0.76
= 0.71
N2
GLU
2DG
7.3
8.2
1.00
0.98

Figure 22

Figure 22. Effects of perfusate media on ratio of metarhodopsin III half-times. Arrows point in direction of larger magnitude of ration, T_f/T_d. See legend for Figure 17.

support to a narrow range of lactate concentration outside which at least one physiological process in the retina, the metarhodopsin III photoproduct kinetics, becomes significantly modified.

Evidence has been presented previously that metarhodopsin III kinetics are influenced by pH. The rate of metarhodopsin III formation was found to be acid-catalyzed in preparations of solubilized rhodopsin (Ostroy, Erhardt, and Abrahamson, 1966). Metarhodopsin III formation in isolated retinas was also found to occur most rapidly in low pH, at least at low temperatures (Bowmaker, 1973; Gyllenberg, Reuter, and Sippel, 1974). However, this rate, measured at 4°C, was reportedly independent of hydrogen ion concentration in the region between pH 6.0 and 8.0 (Gyllenberg, Reuter, and Sippel, 1974).

As indicated previously in Table VIII, Bowmaker's experiments were performed with unperfused retinas, enclosed in a chamber. These conditions are probably approximated by anoxic experiments described in this research. If the effect of lowered temperature on the photoproduct transformations is simply a prolonging of the processes involved, then the trends observed by Bowmaker at 5°C are consistent with the comparisons for T_f made in nitrogen-saturated perfusates, illustrated in Figure 19(c)(2).

The experiments of Gyllenberg *et al.* were likewise performed in a closed chamber, without any superfusion of the preparation. However, the fluid surrounding the retina was aerated prior to the sealing of the chamber. The oxygen thus provided probably prevented the preparation from becoming totally anoxic prior to the formation of metarhodopsin III, especially at 4°C where metabolic activity was presumably slower. These experiments would probably be most like the oxygenated conditions of Figure 19(c)(1). Thus, the similarity of the rates of metarhodopsin III formation between pH 6.0 and pH 8.0 is consistent with the results described here for T_f.

The decay of metarhodopsin III has also been observed to be influenced by the pH of the surrounding medium. The decay of metarhodopsin III is most rapid at low pH, with pK of 6.5 at 5°C (Frank, 1969; Bowmaker, 1973; Gyllenberg, Reuter, and Sippel, 1974). Injection of hydrochloric acid or sodium hydroxide into the fluid surrounding the tissue during the decay of metarhodopsin III eventually increased or decreased the rate of decay, respectively (Gyllenberg, Reuter, and Sippel, 1974).

These observations, too, are in general agreement with corresponding trends presented here for T_d, illustrated in Figure 20(c), in which metarhodopsin III decay was usually slower in alkaline surroundings. The only conditions where this difference was not observed in this research was in

substrate-deprived, oxygenated media. However, this exception does not mimic the experimental conditions of any of the three previous investigations.

For example, the Ringer solution used by Frank included glucose at all pH levels. Neither Bowmaker nor Gyllenberg et al. added glucose to their bathing solutions, although their observations were made at low temperatures where endogenous substrate supplies were probably not depleted rapidly. Therefore, the trends reported previously in the literature with respect to metarhodopsin III kinetics under the influence of pH are not inconsistent with this research.

However, even though trends in T_d do not seem to vary from investigator to investigator as a function of pH, the magnitudes of metarhodopsin III decay half-times near 21°C are quite diverse, as illustrated previously in Table VIII. It is possible that a rate-limiting step might be involved in the decay of metarhodopsin III, or of photoproducts subsequent to it, such as an enzyme-mediated chemical reduction (Futterman, 1963; Koen and Shaw, 1966; Donner and Reuter, 1969). Such a process might be affected preferentially by the intracellular pH, which perhaps would be manifested by a characteristic pK (Bridges, 1962).

Exceptions to the Model

As described previously in the RESULTS, there was one combination of metabolic and pH constituents in the extra-

cellular perfusate solution in which unusual metarhodopsin III parameters were observed. That is, when the data points for this population of experiments were fit on the computer to the modified model (Equation (5)), a statistically significant difference was found between the coefficients of metarhodopsin III formation and decay, C_f and C_d. For this reason, the average of the two coefficients, $\bar{C}$ (Equation (6)), could not be calculated to represent a single concentration parameter of the fundamental model quantitated by Equation (4).

The particular conditions in which this observation was made were those four experiments performed in pH 8.2 medium containing glucose and saturated with nitrogen gas (see Table III). It is not immediately obvious why this perfusate concentration was the only one in which this phenomenon was observed. However, there are certain recent reports in the literature of the central nervous system which relate to cellular behavior in the presence of particular components of this perfusate. Since metabolic control mechanisms for maintaining electrical activity in the retina are similar to those described for the brain (Matschinsky, 1970), a comparison between these two tissues does not seem unreasonable.

For example, it has been observed that a lack of oxygen, when the supply of glucose substrate is still plentiful, can irreversibly damage brain tissue in the cerebral cortex of rats (Salford, Plum, and Siesjö, 1973). Such damage was assessed by the inability of the tissue to recover normal levels of metabolic function after physiological oxygen levels

were restored. Also, glucose consumption in similar preparations increases only briefly after the onset of hypoxia, returning to its former, lower level within 15 minutes (Borgström, Norberg, and Siesjö, 1976). These results suggest that anoxic tissue might somehow not be fully capable of producing enough energy to keep up with the demands imposed on the metabolic system.

It is possible that this lack of capacity is only manifested in the retina in non-physiological pH environments in which more stress is presumably placed on the tissue. Such a possibility could explain why similar discrepancies in metarhodopsin III parameters were not noted in media buffered at pH 7.3. Also, since metarhodopsin III formation was rarely observed in pH 5.5 media, regardless of metabolic factors, unusual behavior in metarhodopsin parameters might not be noticed due to the overriding predominance of the pH mechanism.

Another reason that the unusual kinetics were only observed in anoxic, alkaline extracellular environments with adequate metabolic substrate might be due to possible side effects of the buffering agent, Tris (see METHODS). It has been implicated previously that Tris is capable of interacting with pyruvate, inhibiting its reduction to lactate (Mahler, 1961). The extent of such behavior in the retina, if any, is not known. Any contribution of Tris in causing the unusual results could be evaluated by repeating experiments at alkaline pH using a different buffering agent, such as phosphate.

Although a combination of these and other mechanisms might contribute to an understanding of the environmental factors leading to the unusual behavior, it is still unclear what a two-coefficient metarhodopsin III model signifies physiologically or chemically. In a mathematical context, such a model implies that the formation and decay phases are independent processes. That is, the pigment formed is not identical to the pigment which decays, and, in fact, two processes are occurring with the same spectral characteristics.

One could devise an explanation of the independent-process hypothesis in the following manner. Two separate "isochromic" pigments, possessing the same absorption peak, with unequal rates of formation and decay, respectively, could be described by a four-coefficient model if separate linear first-order processes were postulated. A simplified two-pigment model might be approximated by only three exponentials if, for example, the rate of formation of one of the pigments were considerably faster than that of the second. In fact, the population of experiments with the unusual coefficient properties were fit to such a three-coefficient, three-exponential model. This procedure was attempted because Table III indicated that C_f was significantly less than C_d, which suggested the possibility of a second, undetected formation phase faster than the resolution of the RMSP.

The interesting result of this curve-fitting process was that the best mathematical fit of each of the four experiments yielded identical decay rates for both isochromic pigment processes. In other words, the three-exponential model was no better than the two-coefficient model in describing metarhodopsin III kinetics. This observation could be interpreted to mean that two separate pigments were formed at different rates, one of those being faster than the measurement resolution, but were decaying with the same rate. The difference between C_f and C_d would thus represent the concentration of the rapidly-forming second pigment. The identical decay rates could indicate a rate-limiting step subsequent to metarhodopsin III decay, such as an enzymatic chemical reduction described previously.

Evidence has already been presented in the literature that multiple isochromic forms of certain early rhodopsin photoproducts have been observed in preparations of photoreceptor cell outer segment suspensions and in solutions of extracted rhodopsin (see INTRODUCTION). Three isochromic forms of metarhodopsin III, with differing kinetics, have also been observed recently in solubilized rhodopsin (Shichi, Muellenberg, Hárosi, and Somers, 1977). Even though multiple photoproduct forms have not been observed in intact retinas, three forms of the parent rhodopsin pigment have been implicated (Bowmaker and Loew, 1976). The significantly longer decay time in the unusual population of experiments than in other perfusates (Table III)

lends additional support to the possibility of more than one form of metarhodopsin III. Thus, this explanation of the unusual data cannot be ruled out at the present time.

Baseline Density and Photoproduct Cofactors

As indicated previously in Table II, the magnitude of the baseline optical density, measured at 640 nanometers for every experimental variation, was observed to be larger in acidic media or in states of deprived metabolic substrate. These observations are supported by t-test comparisons in Figure 23, which indicate statistically significant differences between the means at the three pH values as well as between the two extremes of substrate availability. In contrast, the respiratory state of the preparation was not a factor in producing any differences in baseline magnitude.

Sickel (1972) noticed similar increases in overall optical density in perfused frog retinas deprived of glucose. He suggested that the decreased transmittance was due to an increase in light scattering caused by the chemical reduction of the pyridine nucleotide, NAD. Thus, an increased baseline correlates with greater concentrations of NADH. Sickel also observed that withdrawal of glucose affects the gross electrical activity of the retina more drastically than lack of oxygen. This is in agreement with the absence of significant differences in the baseline as a function of respiratory state found here.

(a)

PH	5.5	7.3
7.3	↑ 1.00	--
8.2	↑ 1.00	↑ 0.95

(b)

SUB	GLU	AMB
AMB	= 0.86	--
2DG	↓ 1.00	↓ 1.00

(c)

RESP	02
N2	= 0.51

Figure 23

Figure 23. Comparison of baseline optical densities. Arrows point in direction of greater optical density, measured at 640 nanometers, tabulated in Table II. Experiments are classified by means of (a) pH value of extracellular buffer; (b) state of substrate availability; and (c) respiratory state. Numbers indicate probability value associated with each comparison.

The observation of larger baseline magnitudes in acidic, substrate-deprived media is in agreement with the conditions, described previously, which prevented the formation of metarhodopsin III. This correlation can also be noted in Table IX, in which the baseline values have been classified according to the relative pigment categories illustrated in Figure 12. With the exception of experiments in category "A," in which no retinal was observed, it can be seen that the baseline shows significant increases as metarhodopsin formation becomes progressively less. Perhaps the optical density of the baseline can be used as an indicator of the photoproduct decay sequences expected under various metabolic conditions. This might lead to a better understanding of the nature of the rhodopsin photoproduct transformations and their relation to the overall condition of the retina.

Significance

The results described in this dissertation have concentrated on the effects of metabolic factors and pH on the sequence and kinetics of photoproduct transformations involving metarhodopsin III. The roles of these variables have been discussed as they relate to their involvement in the chemical transformations of slow rhodopsin photoproducts. These results are of potential importance in several regards.

(a)

A:	$.38 \pm .14$
B:	$.29 \pm .10$
C:	$.37 \pm .10$
D:	$.42 \pm .12$
E:	$.53 \pm .11$

(b)

	B	C	D	E
A	← 0.99	= 0.61	= 0.85	↑ 1.00
B	--	↑ 1.00	↑ 1.00	↑ 1.00
C	--	--	↑ 1.00	↑ 1.00
D	--	--	--	↑ 1.00

Table IX

Table IX. Optical density of baseline as function of kinetics categories. (a) Mean value ± standard deviation of optical density, measured at 640 nanometers, is tabulated as function of kinetics categories defined in Table IV. (b) Results of t-test comparisons. Arrows point toward category in which baseline optical density was greater. Numbers represent probability values associated with each comparison.

First, it is not known precisely what roles the slower rhodopsin intermediates play in the physiological and pathological functioning of photoreceptor cells. For example, it is likely that the photoproduct decay sequence, subsequent to the onset of electrical activity, is involved in the recovery processes in the retina (Ernst and Kemp, 1972), thereby affecting the course of dark-adaptation or altering the overall visual sensitivity. There is some evidence to this effect; namely, the time course of regeneration of rhodopsin has been observed to follow temporally the decay of metarhodopsins II and III into free retinal plus opsin (Paulsen, Miller, Brodie, and Bownds, 1975).

In addition, there are a variety of abnormal conditions, both pathologic and toxic, which affect the functions of the eye either focally or throughout the retina. A knowledge of how the primary function of the eye, visual excitation, is affected by these abnormalities is likely to be necessary not only to understand them but also to develop rational therapies for their prevention and treatment. The development of instrumentation of the kind reported in this dissertation, but applicable to the in vivo retina, might provide the means to that knowledge and understanding.

Furthermore, the development of such a rapid scanning spectrophotometer (RSP) might find use in a variety of diseases that have generalized effects on the central nervous system. Assessment of the functional state of the brain is usually difficult and rarely direct. Since the brain and the

eye are often affected similarly in disease states, the eye has a venerable history in providing a means of assessing the state of the brain, for example, by retinoscopy. Such techniques, however, are not very precise. An instrument, such as an RSP, might provide the means of assessing the metabolic or other functional states of the eye, and by inference, of the brain, with more precision and insight.

From the point of view of photoreception, this research establishes a context in which to study the metarhodopsin I photoproduct and its potential involvement in phototransduction. If factors which influence slower photoproducts can be determined, this might contribute to a better understanding of parameters to be evaluated in studying molecular events occurring within the latency of the photoreceptor excitation process.

In addition, several problems associated with experiment methodology have been noted. This information is valuable in establishing the types of controls and experimental protocols which are necessary to obtain meaningful quantitative results. The elimination of as many insufficiently controlled metabolic, ionic, and other conditions as possible is a virtual necessity in quantitative studies of the photoproduct sequence and kinetics in isolated retinas.

Future Plans

It is apparent from the results presented in this dissertation that much remains to be learned about the rhodopsin photoproduct transformations in isolated retinas.

The interaction of metabolic and ionic factors, as they affect the photoproduct sequence and kinetics, is certainly complicated. Further investigations are required in order to clarify the potential roles of these photoproducts in the overall physiological function of photoreceptors.

A first step in the continuation of the present studies would be an examination of the metarhodopsin I-metarhodopsin II-metarhodopsin III sequence of transformations in healthy, isolated retinas supplied with glucose and oxygen at pH 7.3. This investigation could be accomplished by a minor modification in the optics of the RMSP, to shorten the duration of the bleaching interval, coupled with slight cooling of the preparation.

The RMSP could be further improved by redesigning the perfusion chamber to incorporate microelectrodes for recording gross electrical activity of the retina, simultaneously or sequentially with absorption changes. In this manner, the general metabolic state of the retina could be correlated with the photoproduct sequence and kinetics observed with any variations of the perfusate medium.

Effects of monovalent ions (sodium, potassium, chloride, etc.) and divalent ions (calcium, strontium, barium, etc.) could be readily evaluated by modifying the perfusate accordingly. Chelating substances, which selectively bind free ions, could be included in the perfusion medium. These experiments might be useful in clarifying the roles, if any of certain ions in the photoreceptor transduction

and recovery processes.

In addition to these studies of the isolated retina preparation, similar measurements could be taken both from rod outer segment suspensions and from solutions of purified rhodopsin, obtained from the same species, Rana pipiens. In this manner, similarities and differences between kinetics observed with the different types of preparations could be compared for a better understanding of environmental factors on the physiology of the rhodopsin photoproducts.

Summary

A rapid scanning microspectrophotometer has been developed and utilized to study the photoproducts resulting from the bleaching of rhodopsin in the isolated retina of the frog. The results discussed in this dissertation have shown that hydrogen ion availability is a primary cofactor in determining the relative concentration of the metarhodopsin III photoproduct, with less appearing, in lieu of greater free retinal formation, at low pH levels. Metabolic factors have also been shown to influence the pathways of photoproduct decay. The most significant effect has been observed in non-acidic intracellular environments, with deficiencies in metabolic energy production also favoring the direct formation of free retinal from metarhodopsin II.

The half-times of formation and decay of metarhodopsin III

have also been observed to vary, depending on the extracellular environment of photoreceptor cells. In general, both half-times tend to be greater when proportionately more metarhodopsin III is formed. The ratio of the two half-times, however, remains relatively constant, except in anoxic conditions, in which the decay half-time is significantly prolonged with respect to the formation half-time.

Several problems associated with the control of experimental conditions have been discussed as they relate to photoproduct sequence and kinetics. The elimination of as many metabolic, ionic, and other insufficiently controlled conditions as possible has been pointed out as a necessary requirement for obtaining meaningful quantitative results.

In addition, the baseline magnitude of the optical density of the retina, which is, in part, a quantification of light scattering, has been shown to be significantly larger in conditions of low intracellular pH or insufficient substrate supply. The utilization of this parameter as an indirect indicator of the probable sequence of photoproducts has been discussed.

In conclusion, this research has provided a greater insight into the mechanisms affecting the later, slow photoproduct processes in isolated retinas. In particular, the interaction of hydrogen ions and metabolic factors influences the pathways of photoproduct decay in isolated retinas, subsequent to metarhodopsin II. The results and methods described

here should be useful in establishing a context in which to study the faster mechanisms involved in photochemical and electrical transduction in photoreceptor cells. In addition, these results may become important in understanding the normal and pathological functionings of the eye.

APPENDIX A:

Rapid Scanning Microspectrophotometer

INTRODUCTION

In order to investigate the kinetics of formation and decay of visual pigment photoproducts, a novel rapid scanning microspectrophotometer (RMSP) has been developed to measure photon absorption and resulting optical density changes of an isolated vertebrate retina. This Appendix summarizes the structure, function, and performance characteristics of the instrument.

INSTRUMENTATION

A block diagram of the RMSP is presented in Figure A1. An unusual characteristic of this instrument is the use of a special cathode ray tube (CRT) as a measuring light source, a design first described by Koszewski, Jasny, and Grabowski (1968). The light-emitting screen of the CRT consists of a mixture of three phosphors of differing spectral properties such that their combined emission in the visible range is nearly white (Figure A2). Each phosphor compound exhibits a characteristic emission decay-time, to 10 percent, of less than 1 microsecond.

The CRT replaces the usual light source and entrance slit of a 0.25 meter Ebert monochromator. The vertical axis of the CRT is positioned so as to correspond to the long or vertical dimension of the monochromator entrance slit. A diffraction

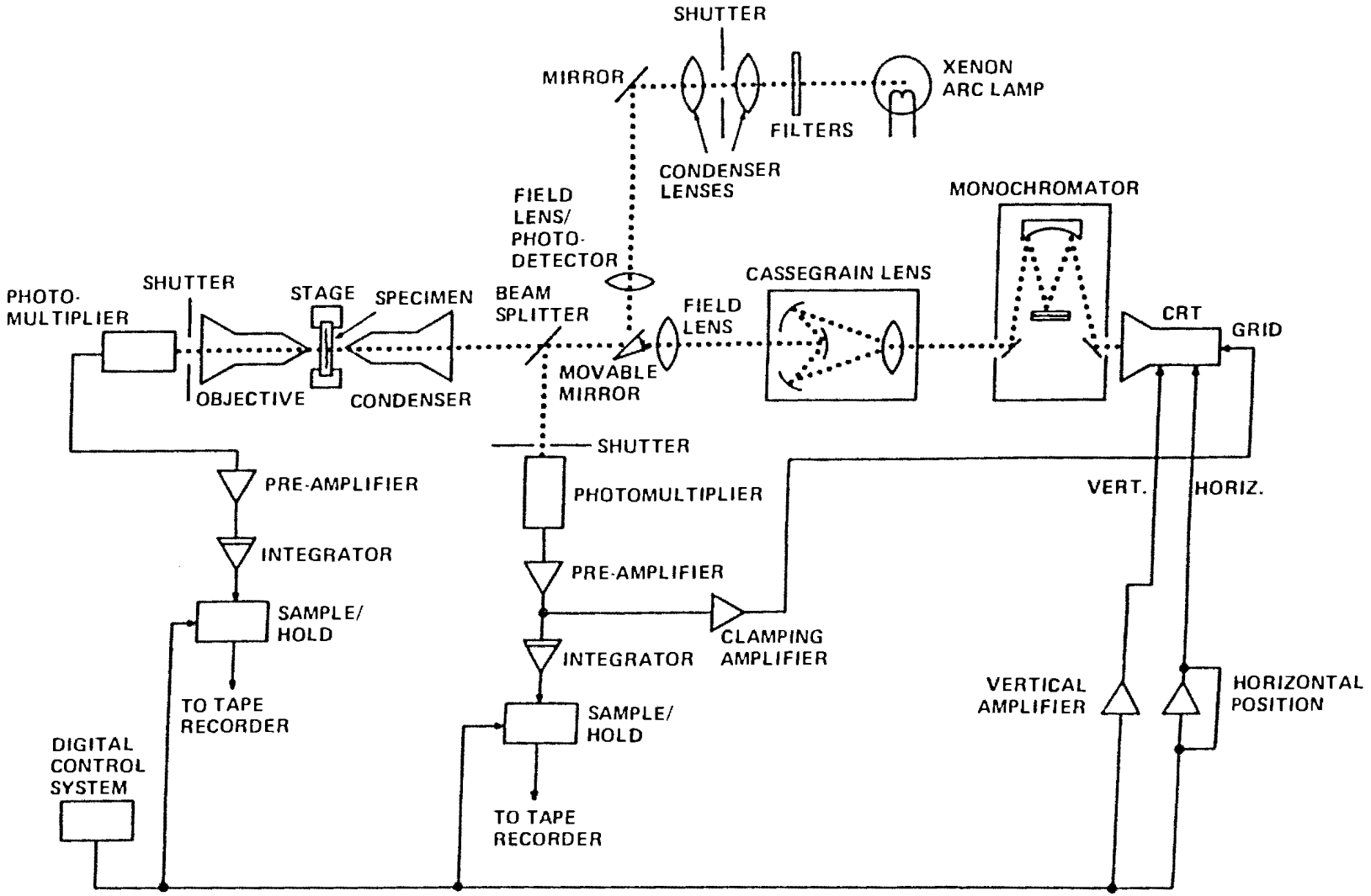
SHUTTER
MIRROR
XENON
ARC LAMP
FILTERS
CONDENSER
LENSES
FIELD
LENS/
PHOTO-
DETECTOR
MONOCHROMATOR
CASSEGRAIN LENS
PHOTO-
MULTIPLIER
SHUTTER
STAGE
SPECIMEN
BEAM
SPLITTER
FIELD
LENS
CRT
GRID
OBJECTIVE
CONDENSER
MOVABLE
MIRROR
SHUTTER
PRE-AMPLIFIER
PHOTOMULTIPLIER
VERT.
HORIZ.
INTEGRATOR
PRE-AMPLIFIER
SAMPLE/
HOLD
CLAMPING
AMPLIFIER
INTEGRATOR
VERTICAL
AMPLIFIER
HORIZONTAL
POSITION
TO TAPE
RECORDER
SAMPLE/
HOLD
DIGITAL
CONTROL
SYSTEM
TO TAPE
RECORDER

Figure A1

Figure A1. Diagram of rapid scanning microspectrophotometer. See text for explanation.

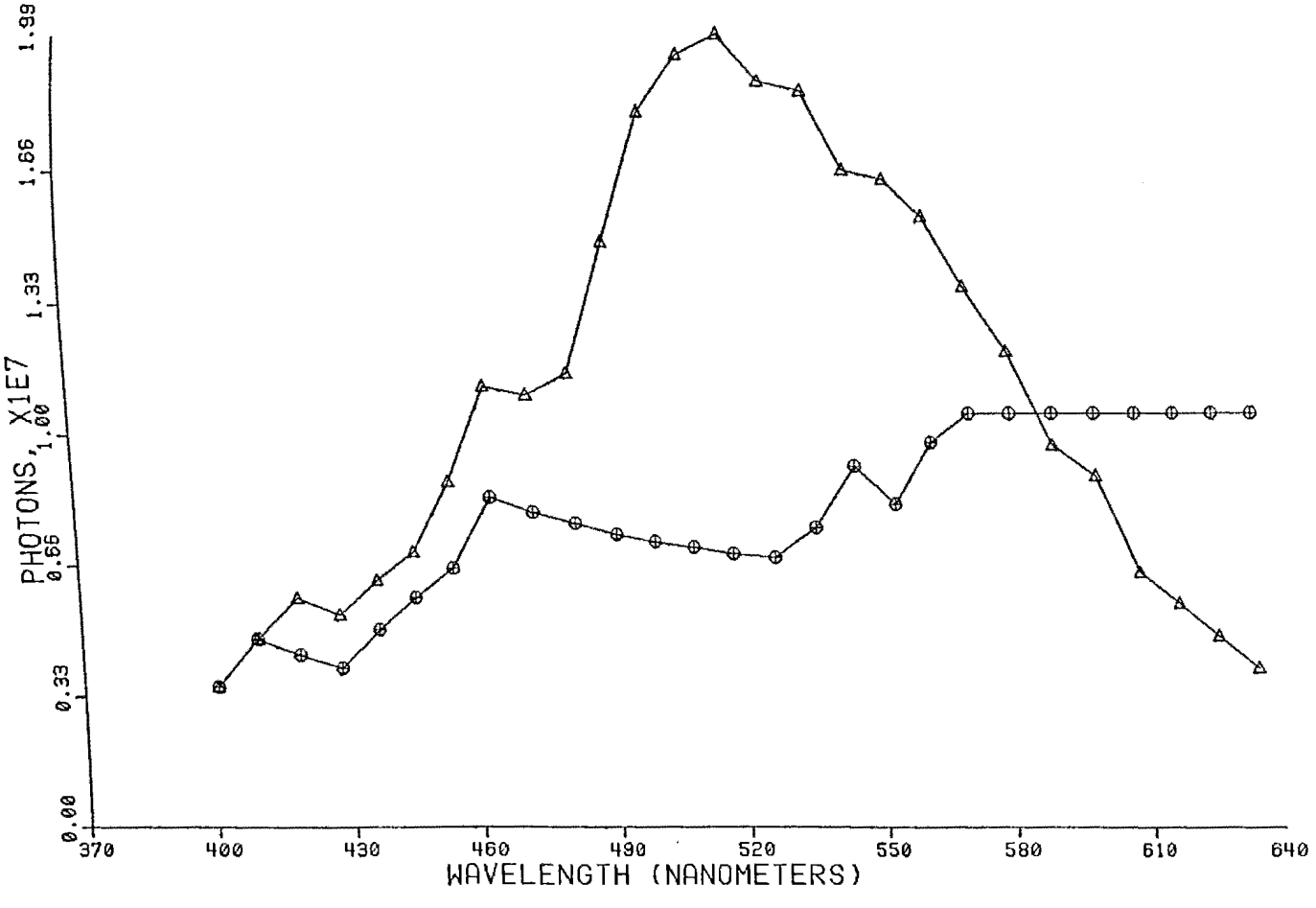
PHOTONS, X1E7
0.00
0.33
0.66
1.00
1.33
1.66
1.99
370
400
430
460
490
520
550
580
610
640
WAVELENGTH (NANOMETERS)

Figure A2

Figure A2. Emission spectrum of cathode ray tube. Ordinate represents photons (X 10^7) delivered to preparation during measurement interval (600 microseconds) at each wavelength. Triangles: cathode ray tube unclamped. Circles: cathode ray tube clamped. (See text and Figure A9 for description of clamping operation.) Calibration was performed with United Detector #5183.

grating, within the monochromator (1180 grooves/mm; 64 x 64 mm), disperses light from a spot on the CRT screen across a 1 millimeter exit slit, which allows an approximately 10-nanometer band of light to emerge from the monochromator. The vertical position of the CRT spot is aligned with respect to the entrance aperture of the monochromator. Initial alignment is performed mechanically and then electrically by adjustment of the voltage applied to the CRT vertical deflection plates, as shown in Figure A3.

The central wavelength of light passing through the exit slit is determined jointly (a) by the angle of the diffraction grating with respect to the optical axis of the RMSP and (b) by the horizontal position of the CRT spot. For a fixed mechanical alignment of the diffraction grating, a horizontal movement of the CRT spot changes the angle of incidence of the light with respect to the grating, thereby dispersing a different waveband of light across the exit slit of the monochromator. In practice, the grating is mechanically set so that, when the CRT spot is in the center of the optical axis, the monochromator output is at 500 nanometers. Spectral scanning is achieved by and at the rate of incremental voltage steps applied to the horizontal deflection plates of the CRT. The circuit diagram of the horizontal amplifier is illustrated in Figure A4.

Quasi-monochromatic light from the exit slit is collected by Cassegrain and field lenses and is then demagnified by a

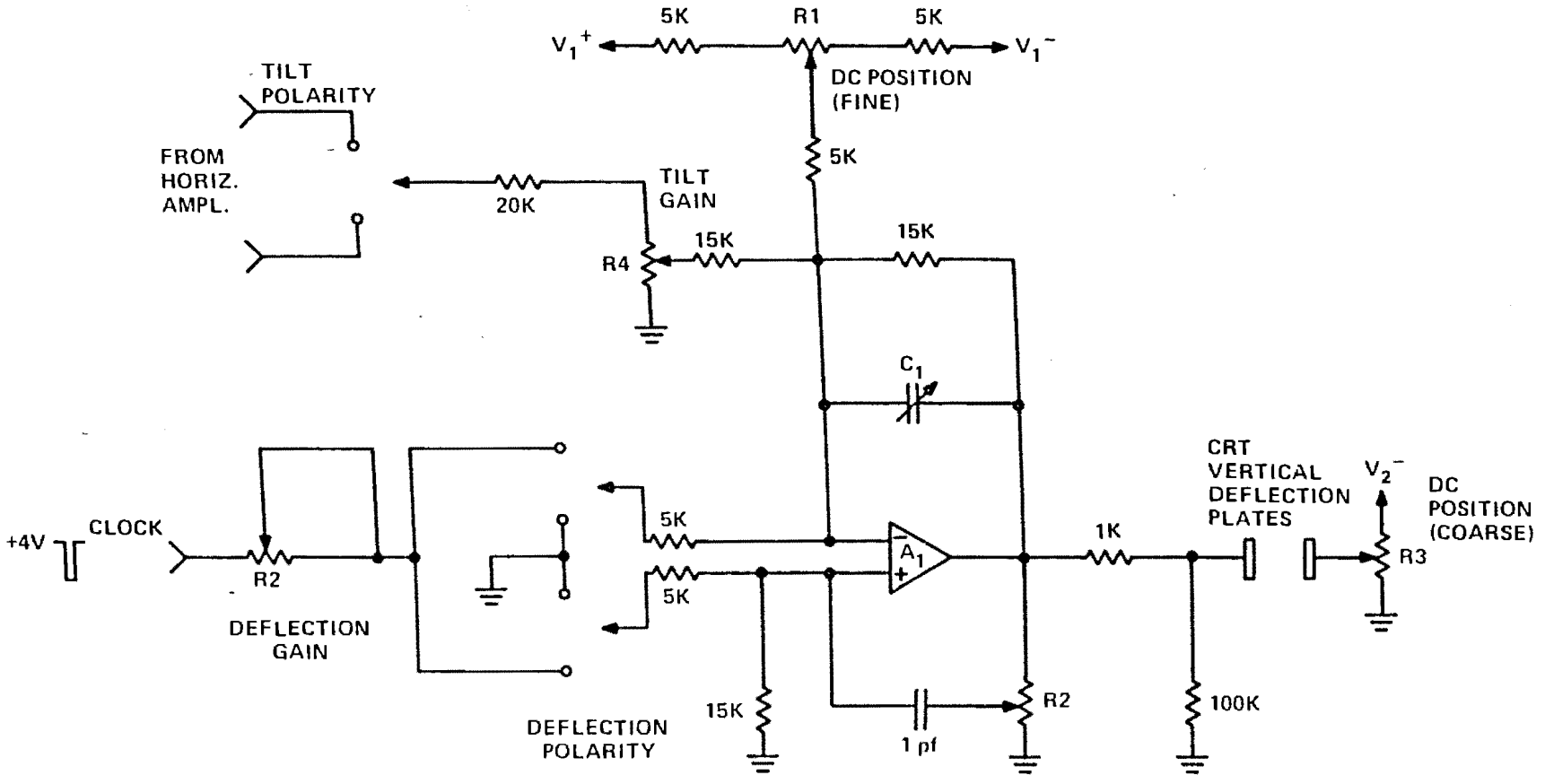
5K
R1
5K
V_1^+
V_1^-
DC POSITION
(FINE)
TILT
POLARITY
FROM
HORIZ.
AMPL.
20K
TILT
GAIN
5K
15K
R4
15K
C_1
CRT
VERTICAL
DEFLECTION
PLATES
V_2^-
DC
POSITION
(COARSE)
+4V
CLOCK
R2
DEFLECTION
GAIN
5K
5K
A_1
1K
R3
15K
DEFLECTION
POLARITY
1 pf
R2
100K

Figure A3

Figure A3. Circuit diagram of CRT vertical amplifier. DC Position potentiometers (R_1 and R_3) provide means of optical alignment of vertical position of CRT spot with respect to optical axis of the RMSP. Deflection gain potentiometer (R_2) and Deflection Polarity switch control, respectively, the amplitude and direction of vertical deflections of CRT spot. The signal which drives vertical plates is derived from RMSP clock (Figure A8), and is described in text. Tilt controls (Polarity and Gain) allow for fine adjustment of rotation of CRT output around the horizontal axis of RSMP. This adjustment is necessary since adequate alignment cannot be achieved mechanically, and is refined by applying to CRT vertical plates a portion of the signal applied to horizontal plates.

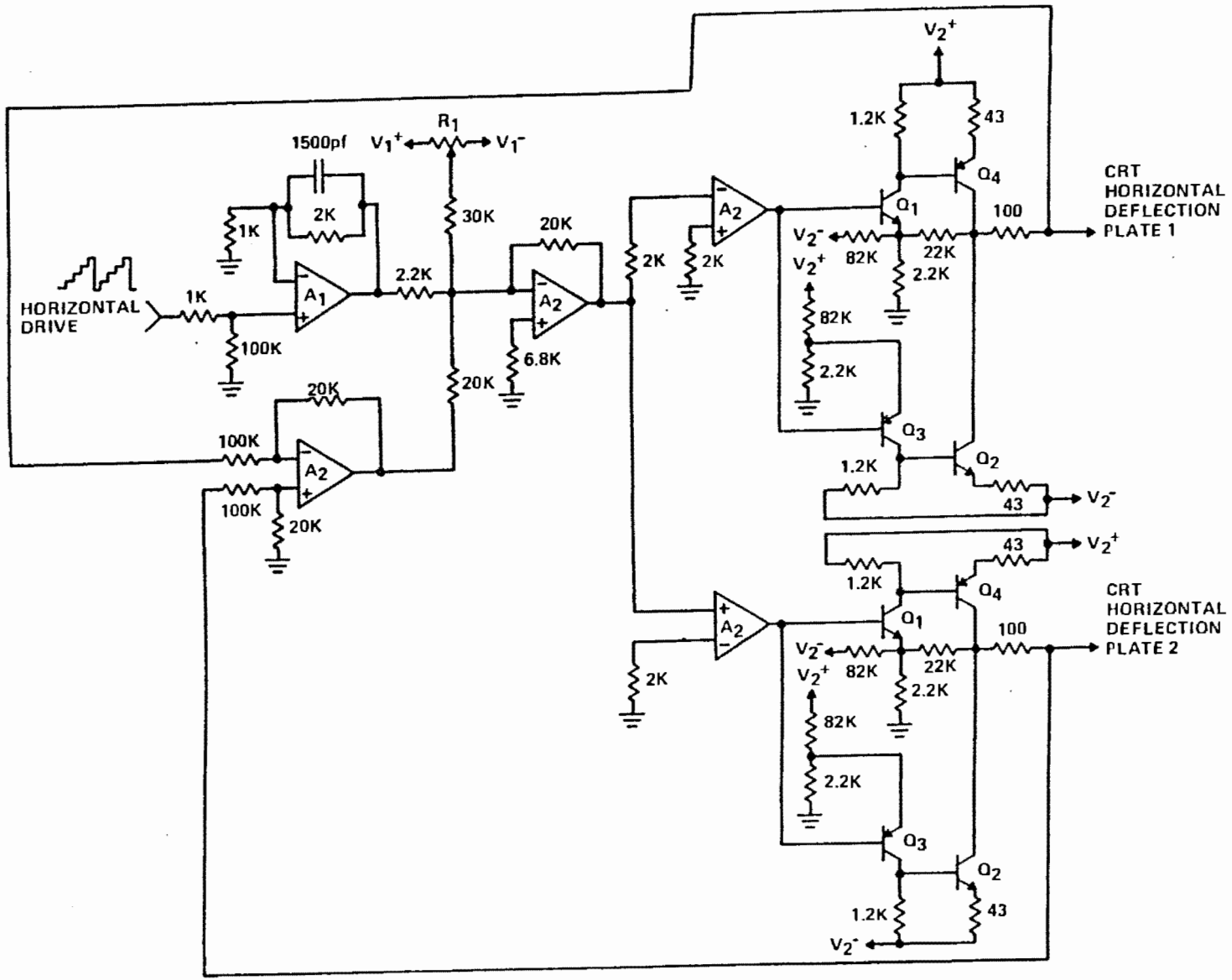
HORIZONTAL DRIVE
1K
100K
1500pf
2K
1K
A_1
2.2K
R_1
V_1^+
V_1^-
30K
20K
20K
A_2
6.8K
20K
100K
A_2
100K
20K
2K
A_2
2K
V_2^+
1.2K
43
Q_4
Q_1
100
CRT HORIZONTAL DEFLECTION PLATE 1
V_2^-
V_2^+
82K
22K
2.2K
82K
2.2K
Q_3
Q_2
1.2K
43
V_2^-
V_2^+
43
1.2K
Q_4
Q_1
100
CRT HORIZONTAL DEFLECTION PLATE 2
V_2^-
V_2^+
82K
22K
2.2K
82K
2.2K
Q_3
Q_2
1.2K
43
V_2^-

Figure A4

Figure A4. Circuit diagram of CRT horizontal amplifier. A_1: μA740 operational amplifier. A_2: μA715 operational amplifier. Q_1: 2N4927. Q_2: 2N3440. Q_3: 2N4929. Q_4: 2N5415. R_1: 5 KΩ. V_1^+: +15 volts. V_2^+: +70 volts. V_1^-: -15 volts. V_2^-: -70 volts. Horizontal drive signal, described in Figures A6 and A8, is amplified through push-pull amplifier, to be applied to CRT horizontal deflection plates.

20X, 0.5 numerical-aperture, apochromatic microscope condenser to illuminate a 400 micron diameter cross-section of retina (Figure A1). The retina is mounted in a special chamber which is placed on the stage of the microscope (see METHODS). Light flux which is transmitted through the specimen is collected by a 20X, 0.65 numerical-aperture, apochromatic microscope objective. A sliding prism in the microscope tube deflects the transmitted flux into an eyepiece for the purpose of viewing the specimen. For photometry, the prism is moved aside, which permits the transmitted flux to fall upon the cathode of an EMI 9558-QAM, 11-stage photomultiplier tube, a high quantum efficiency device whose cathode is of S-20 tri-alkali composition.

A beam splitter diverts approximately 10 percent of the primary CRT light to the cathode of a second, matched photomultiplier. By correlating the output of this second photomultiplier with that of the first photomultiplier attached to the microscope, in the absence of a specimen, the second photomultiplier provides an indirect but reliable measure of the light flux incident to the specimen. The locations of the photomultipliers along their respective optical axes are such that the flux which falls upon each photocathode is defocused, in order to minimize any error due to spectral inhomogeneities in the photocathode.

The anode current of each photomultiplier is further amplified by a preamplifier, after the photomultiplier gain has been adjusted to utilize the full dynamic range of the preamplifier. Each preamplifier output is then integrated and sent to a sample-and-hold system, which operates for 19 cycles of a 33-kilohertz square-wave clock command. A circuit diagram of the signal amplifier system is shown in Figure A5. One additional clock cycle is used to reset the integrators and to operate the sample-and-holds of the two amplifiers, so that a single sampling interval of 20 cycles has a duration of 0.6 milliseconds for each wavelength band, as illustrated in Figure A6.

A spectral measurement scan begins with the application of a brightening pulse between the grid and cathode of the CRT, as shown in Figure A7. The voltage of the CRT horizontal plates is then incrementally stepped synchronously with the conclusion of each sampling interval. This operation moves the CRT spot and thus changes the waveband of light exiting from the monochromator. The voltage outputs of both sample-and-hold amplifiers (Figure A5) and the horizontal drive signal (Figures A6, A8) are recorded for subsequent data reduction (see APPENDIX B).

A block diagram of the digital wavelength scanning system is illustrated in Figure A8. The bandwidth, location, and number of wavebands in each scan are selectable via appropriate settings of control panel switches, which permit one to 128

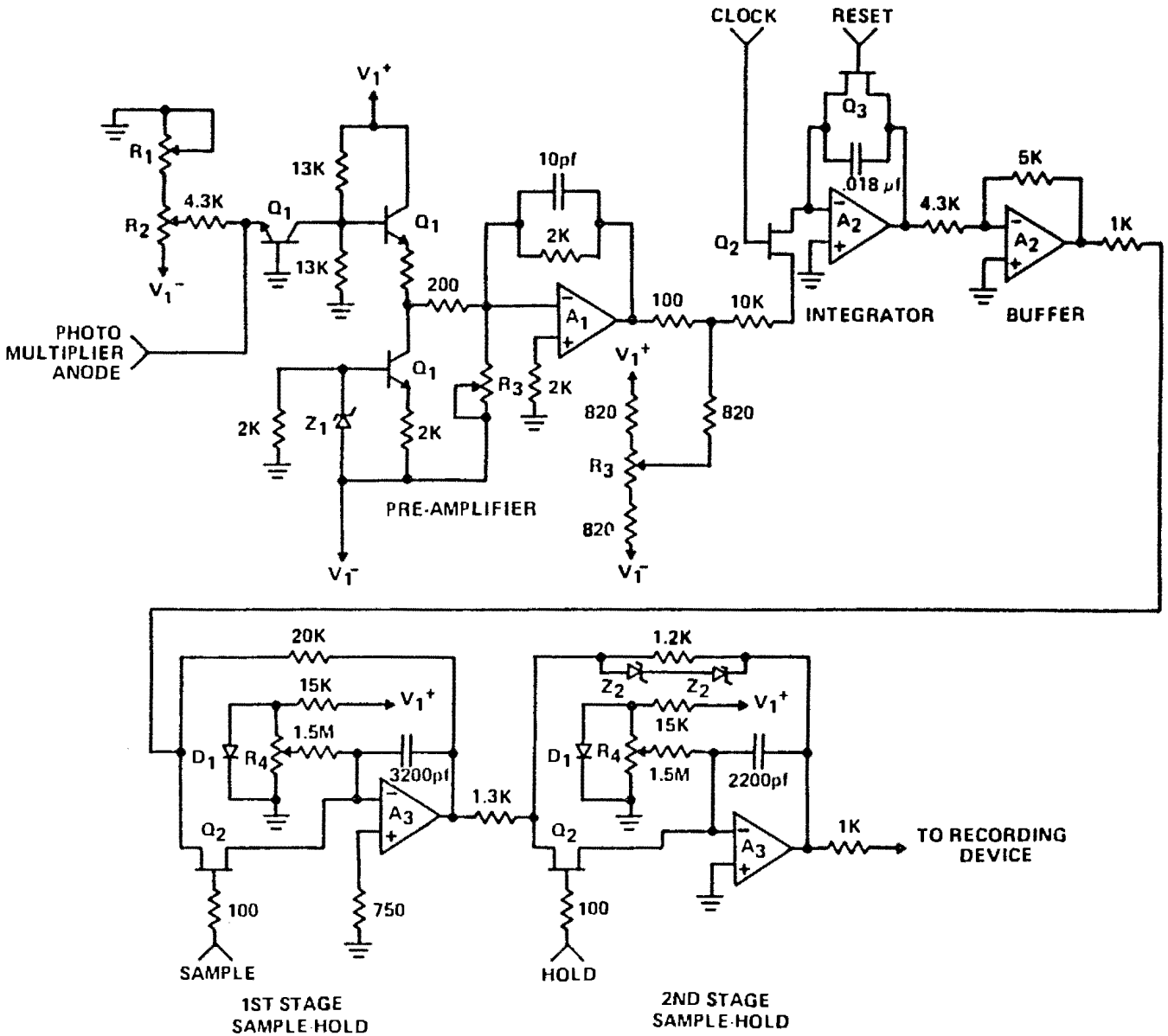
CLOCK
RESET
V_1^+
R_1
4.3K
R_2
V_1^-
Q_1
13K
Q_1
13K
200
10pf
2K
A_1
100
10K
Q_2
Q_3
.018 μf
A_2
4.3K
5K
A_2
1K
INTEGRATOR
BUFFER
PHOTO MULTIPLIER ANODE
Q_1
2K
Z_1
2K
R_3
2K
V_1^+
820
820
R_3
820
PRE-AMPLIFIER
V_1^-
V_1^-
20K
15K
V_1^+
1.5M
D_1
R_4
3200pf
A_3
1.3K
Q_2
100
750
SAMPLE
1ST STAGE SAMPLE-HOLD
1.2K
Z_2
Z_2
V_1^+
15K
D_1
R_4
1.5M
2200pf
Q_2
A_3
1K
TO RECORDING DEVICE
100
HOLD
2ND STAGE SAMPLE-HOLD

Figure A5

Figure A5. Circuit diagram of signal amplifier. A_1: Burr-Brown 3342/15C fast line driver FET operational amplifier. A_2: μA740 operational amplifier. A_3: μA715 operational amplifier. Q_1: 2N3904. Q_2: 2N3819. Q_3: 2N5397. Z_1: 6-volt zener diode. Z_2: 12-volt zener diode. D_1: 1N914. R_1: 500 KΩ. R_2: 5 KΩ. R_3: 10 KΩ. R_4: 20 KΩ. V_1^+: +15 volts. V_1^-: -15 volts. Photomultiplier anode current is preamplified and applied to integrating amplifier in synchrony with RMSP clock signal (Figure A8). This operation is described in greater detail in Figure A13. Amplifier operation and gating signals (reset, sample, hold) are illustrated graphically in Figure A6.

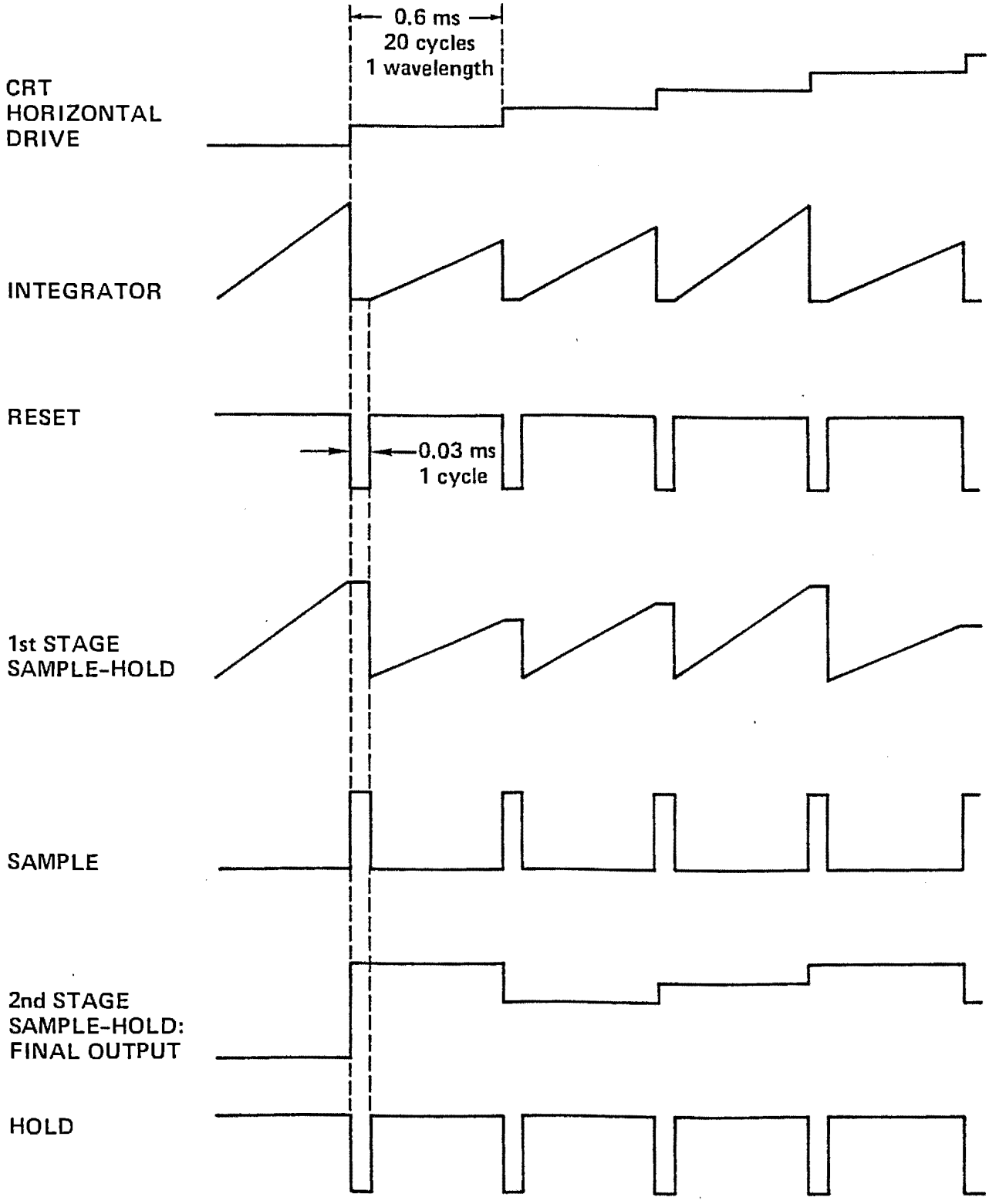
0.6 ms
20 cycles
1 wavelength
CRT
HORIZONTAL
DRIVE
INTEGRATOR
RESET
0.03 ms
1 cycle
1st STAGE
SAMPLE-HOLD
SAMPLE
2nd STAGE
SAMPLE-HOLD:
FINAL OUTPUT
HOLD

Figure A6

Figure A6. Timing diagram of sampling process. RMSP square wave clock operates at 33 kHz, so that one cycle has 0.03 millisecond duration. Integration and first-stage sampling occur during first 19 clock cycles. During 20th cycle, integrator is reset, and first-stage output is sampled by second-stage amplifier. Second-stage amplifier holds this voltage level for total of 20 clock cycles (0.6 milliseconds) for each wavelength, gated by "hold" signal. Drive voltage to CRT horizontal plates is synchronized with sampling procedure via "reset" signal.

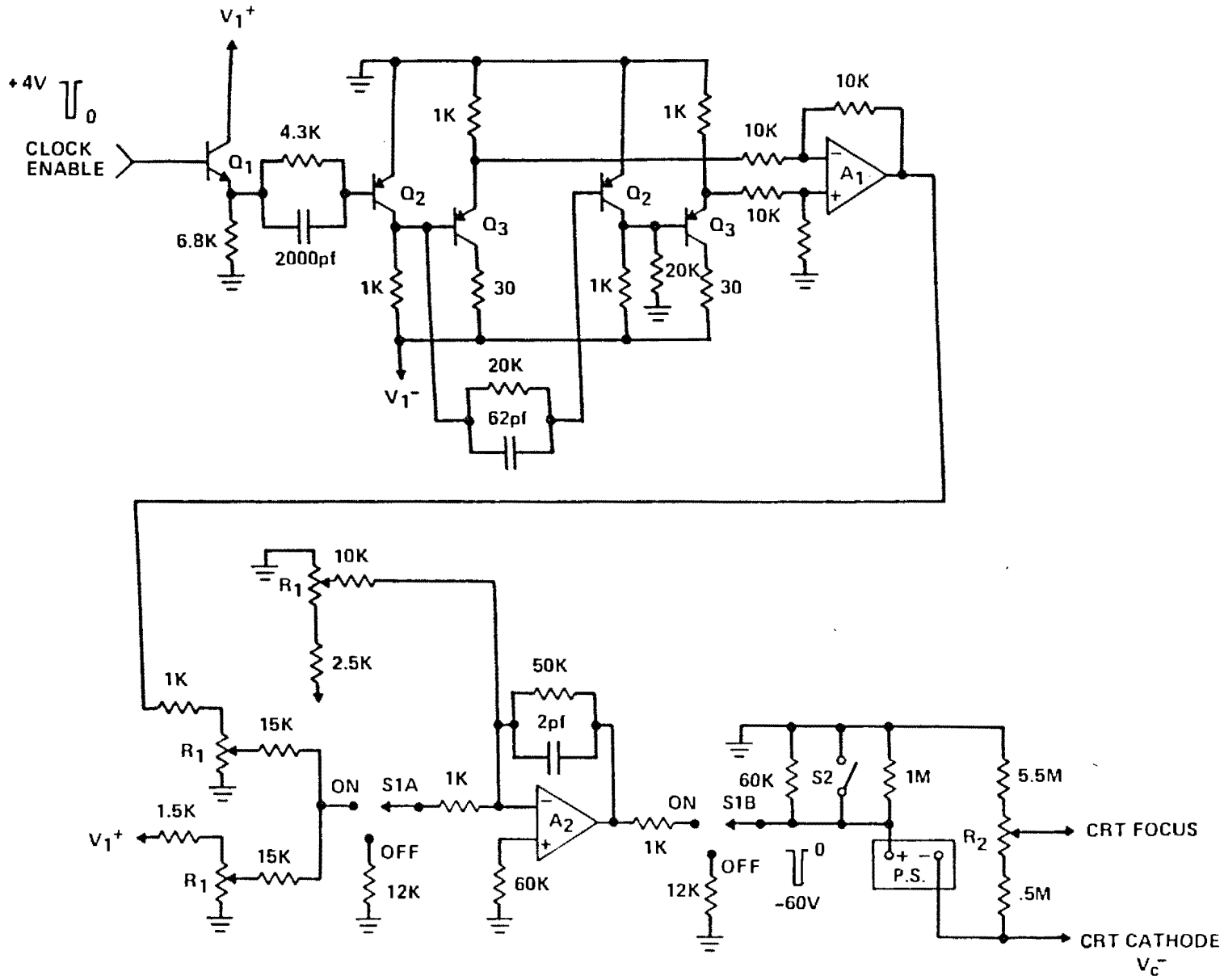
+4V
CLOCK ENABLE
V_1^+
Q_1
4.3K
6.8K
2000pf
Q_2
Q_3
1K
30
20K
62pf
V_1^-
10K
A_1
R_1
2.5K
1K
15K
1.5K
ON
S1A
OFF
12K
50K
2pf
A_2
60K
S1B
S2
1M
5.5M
R_2
P.S.
.5M
-60V
CRT FOCUS
CRT CATHODE
V_c^-

Figure A7

Figure A7. Circuit diagram of CRT brightening amplifier. A_1: μA715 operational amplifier. A_2: Philbrick TP1022 high voltage FET operational amplifier. Q_1: 2N3643. Q_2: 2N3906. Q_3: 2N3645. R_1: 10 KΩ. R_2: 2 MΩ. PS: Hewlett-Packard 6110A DC power supply. V_1^+: +15 volts. V_1^-: -15 volts. V_c^-: -2545 volts. Signal which drives CRT brightening amplifier ("clock enable") is described in Figure A8. In quiescent state, prior to CRT brightening, CRT cathode is held at V_c^- by grounding positive terminal of cathode power supply (Switch 2). V_c^- is adjusted to be less negative than grid voltage, V_g^- (Figure A9), so that CRT remains unlit. (Anode voltage is +5000 volts). Switch S_2, protective grounding switch for CRT power supplies during initial RMSP warm-up and standby, remains open at all times during instrument operation. Switches S1A and S1B, which are used to isolate high-voltage amplifier A_2 during warm-up, are also placed in "on" position during instrument operation. During "clock enable" signal, negative output pulse from A_2 is applied to positive terminal of cathode power supply. This results in CRT cathode becoming more negative than grid for duration of "clock enable" signal, thus beginning CRT emission. Potentiometer R_3 provides means for fine focus of CRT spot.

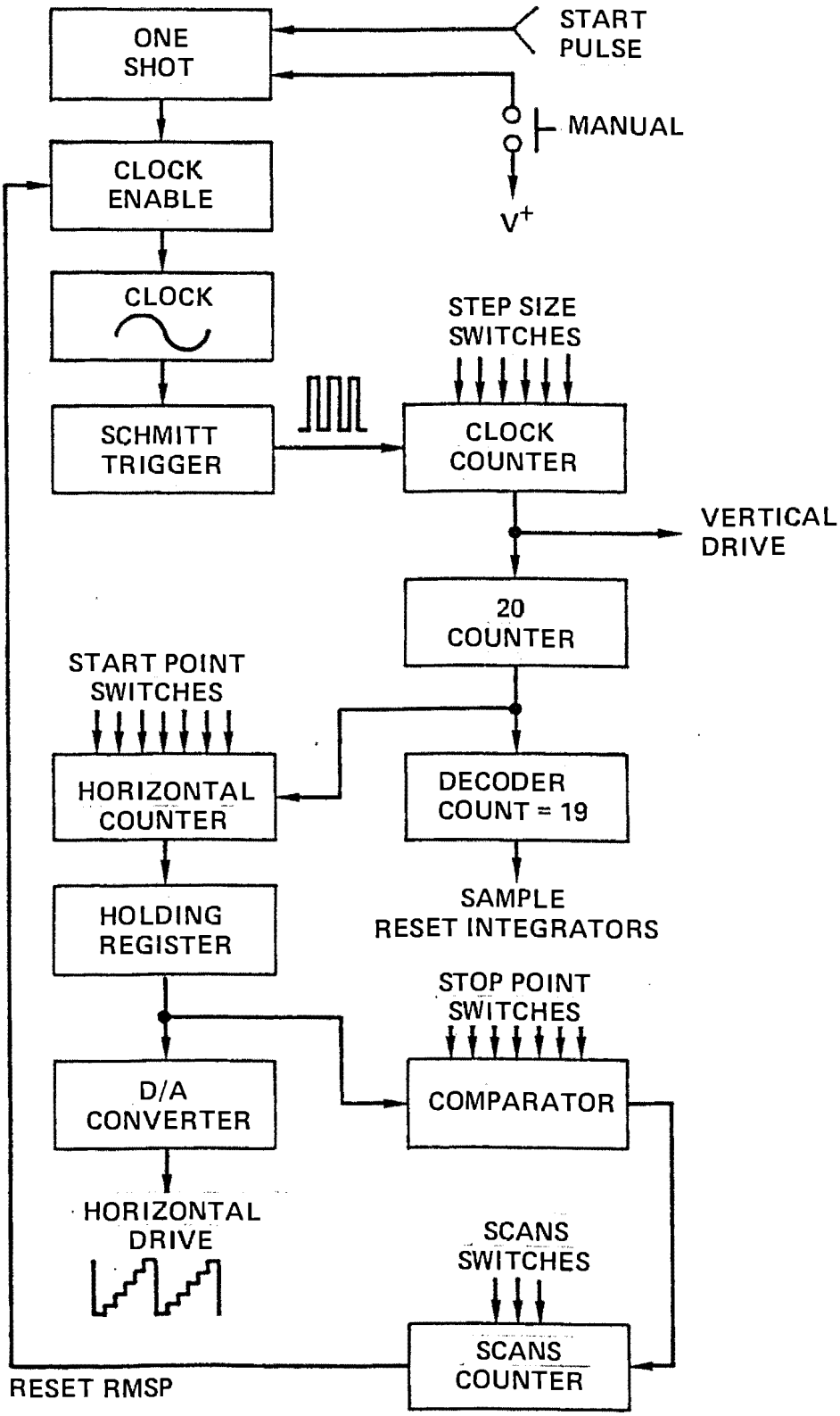
ONE SHOT
START PULSE
MANUAL
V+
CLOCK ENABLE
CLOCK
STEP SIZE SWITCHES
SCHMITT TRIGGER
CLOCK COUNTER
VERTICAL DRIVE
20 COUNTER
START POINT SWITCHES
HORIZONTAL COUNTER
DECODER COUNT = 19
HOLDING REGISTER
SAMPLE RESET INTEGRATORS
STOP POINT SWITCHES
D/A CONVERTER
COMPARATOR
HORIZONTAL DRIVE
SCANS SWITCHES
SCANS COUNTER
RESET RMSP

Figure A8

Figure A8. Block diagram of wavelength scanning system. Scanning operation begins either manually or automatically through one-shot by enabling Schmitt trigger, which produces square-wave clock signal at 33 kHz. Vertical amplifier drive signal, used as input in Figure A3, is described in text. Duration of single sampling interval is 20 clock cycles (600 msec). Sampling and integrator reset are performed after 19th clock cycle in each interval. Horizontal counter is incremented from preset start-point magnitude by step-size amount at conclusion of each sampling interval. Output of horizontal counter is converted to analog voltage, which is applied to horizontal deflection plates of CRT to change wavelength. Scan is completed when horizontal count reaches preset stop-point magnitude. One scan consists of (stop point - start point)/(step size) sampling intervals. Entire process is repeated until scans count equals preset number of scans, whereupon clock enable is reset.

wavebands to be studied for wavelengths between 370 and 640 nanometers.

A refinement in the emission characteristics of the CRT is achieved by diverting a fraction of the incident-light photomultiplier-preamplifier output through a high-voltage operational amplifier, which is fed back to the grid of the CRT (Figure A1). This process partially equalizes the average light flux which is emitted at each waveband during a sampling interval. In addition, the average total flux, which is emitted during a scan of several wavebands, is made more uniform. One important consequence of such uniformity is that the photomultipliers can be operated at a higher gain. A circuit diagram of the clamping feedback amplifier is shown in Figure A9.

Each photomultiplier is housed in a separate, light-tight enclosure with an electromagnetic shutter in front of the window of the tube (Figure A1). These shutters protect the photomultipliers during the bleaching of the retina by intense flashes of light. A 75-watt xenon short arc lamp is utilized as the bleaching light source. This light is delivered via a second optical pathway, shown in Figure A1. A photodetector-amplifier, which is mounted near the field lens of the bleaching light pathway, functions as an interlock to disable the photomultiplier protection shutters whenever the bleaching light is detected. This protection system is illustrated in Figure A10.

A third electromagnetic shutter controls the bleaching light onset and duration, as desired. Operation of this shutter

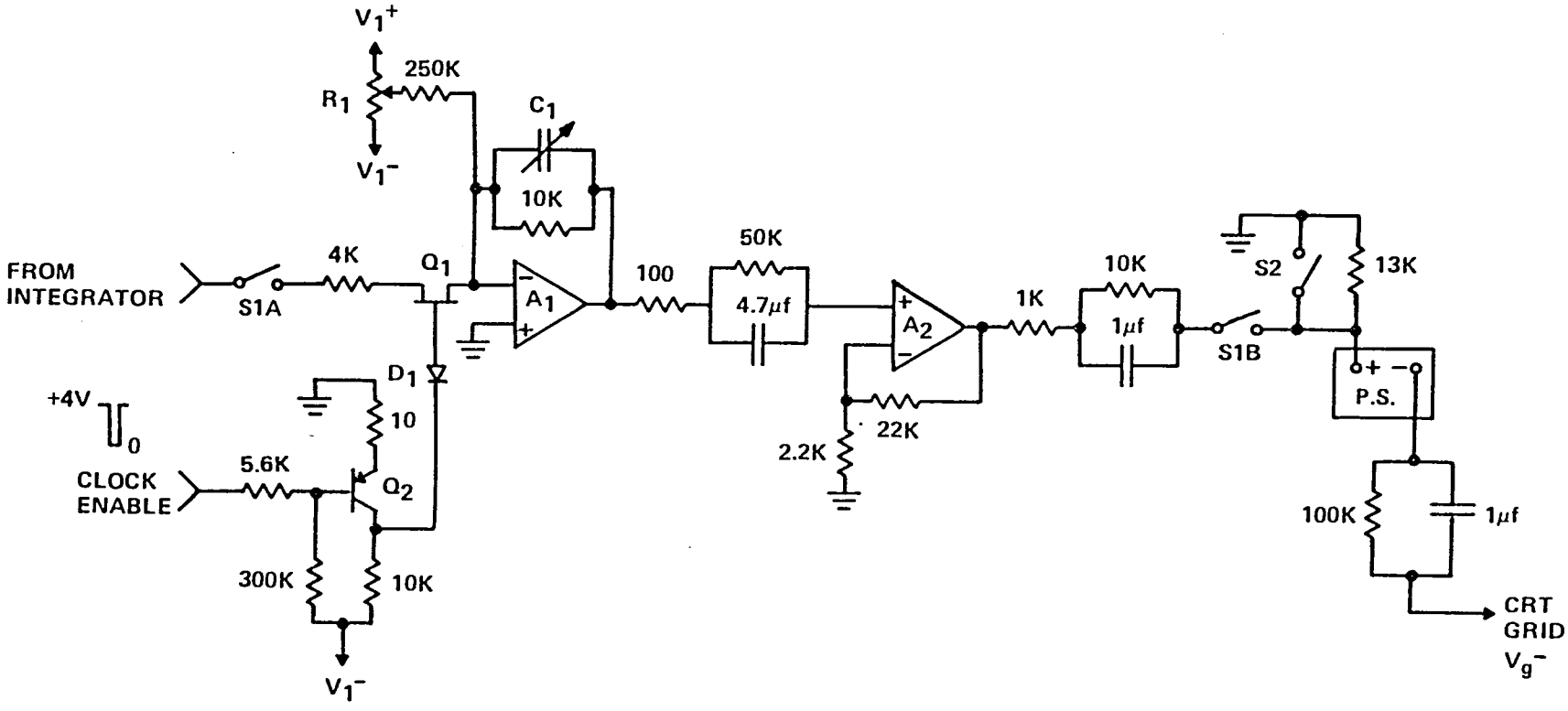
V_1^+
250K
R_1
V_1^-
C_1
10K
FROM
INTEGRATOR
4K
Q_1
S1A
A_1
100
50K
4.7μf
A_2
1K
10K
1μf
S1B
S2
13K
P.S.
+4V
0
D_1
10
5.6K
CLOCK
ENABLE
Q_2
300K
10K
2.2K
22K
100K
1μf
CRT
GRID
V_g^-

Figure A9

Figure A9. Circuit diagram of CRT clamping amplifier. A_1: Intronics A502 very fast inverting operational amplifier. A_2: Philbrick TP1022 high voltage FET operational amplifier. Q_1: 2N3819. Q_2: 2N4122. D_1: 1N914. R_1: 1 MΩ. C_1: 10 pF. PS: Fluke 415B high voltage power supply. V_1^+: +15 volts. V_1^-: -15 volts. V_g^-: -2565 volts. Signal to modulate CRT grid voltage is derived from output of integrator (Figure A5). Control signal (clock enable) to synchronize clamping operation with sampling process is described in Figure A8. Switch S_2, protective grounding switch for CRT power supplies described in Figure A7, remains open at all times during RMSP operation. Switches S1A and S1B, which are used to isolate high-voltage amplifier A_2 during warm-up, are also closed during instrument operation.

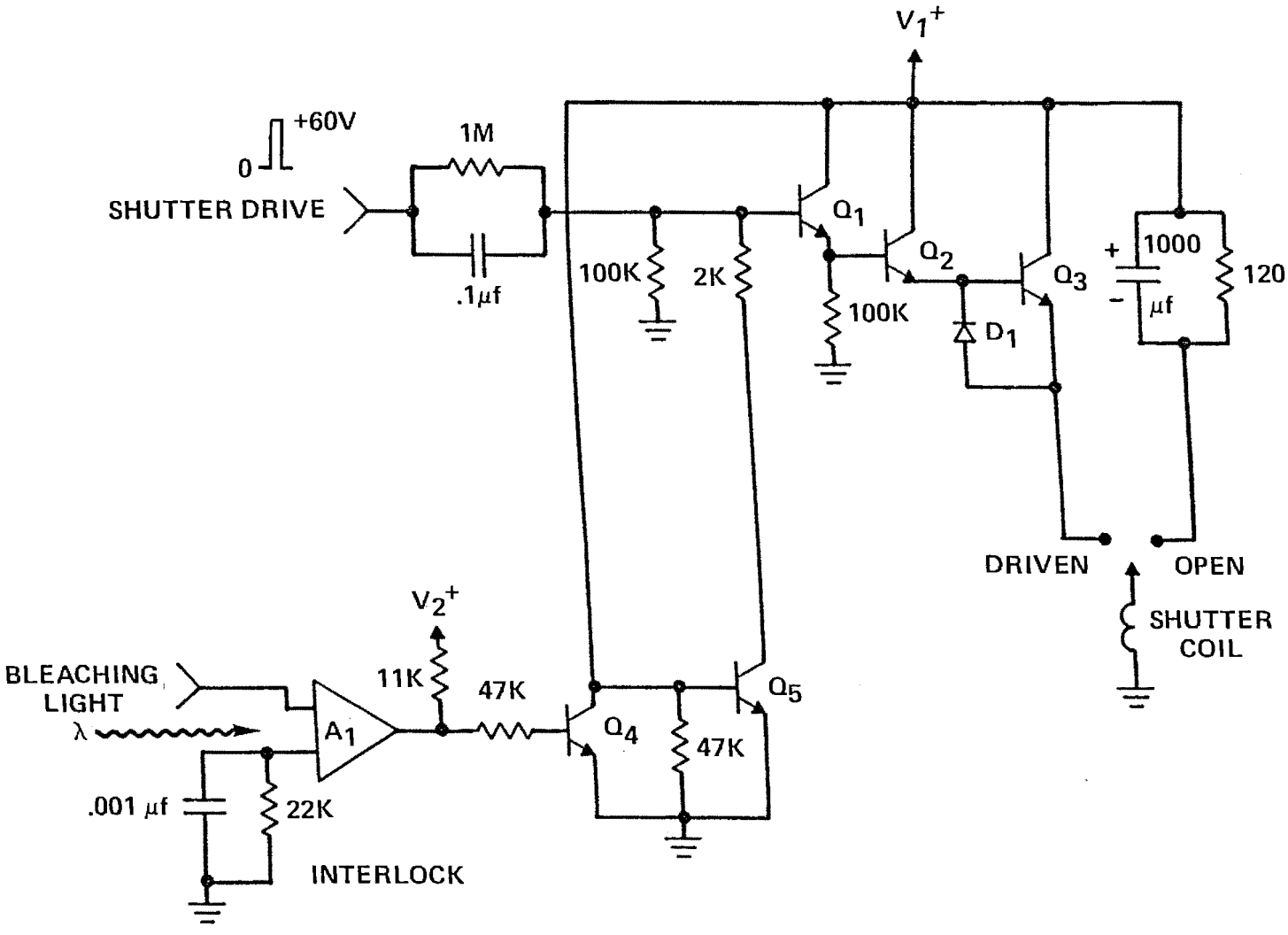
V_1^+
+60V
0
SHUTTER DRIVE
1M
.1μf
100K
2K
Q_1
Q_2
Q_3
100K
D_1
+
1000
μf
-
120
DRIVEN
OPEN
SHUTTER
COIL
V_2^+
BLEACHING
LIGHT
λ
A_1
11K
47K
Q_4
Q_5
47K
.001 μf
22K
INTERLOCK

Figure A10

Figure A10. Circuit diagram of photomultiplier shutter driver and interlock. A_1: RCA CA3062 photodetector/amplifier. Q_1: 2N2102. Q_2: 2N4927. $Q_3$3. Q_4: 2N3642. Q_5: 2N2484. D_1: 1N4004. V_1^+: +50 volts. V_2^+: +15 volts. Shutter drive signal is controlled by "clock enable" (Figure A8) and is derived from output of high voltage amplifier similar to circuit shown in Figure A7 (through amplifier A_2). When switch to shutter coil is in "driven" position, photomultiplier shutter is opened for duration of shutter drive signal only if interlock is deactivated. When switch is in "open" position, shutter remains open regardless of state of interlock or shutter drive signal.

is electrically synchronized with the mechanical movement of a mirror into the optical pathway of the bleaching light (Figure A1). The mirror, which is mounted on the rotor of a DC motor, is initially placed at an angle of 45° with respect to the main, measuring axis of the RMSP. Thus located, an image of the xenon arc is focused at the plane of the specimen and illuminates the same 400 micron diameter area from which measurements are taken by the CRT system.

Within a few milliseconds following the cessation of the bleaching light pulse, the mirror is automatically moved and held out of the main optical axis, thereby allowing the measuring light from the CRT to be delivered to the preparation. The circuitry used to drive the field windings of the DC motor is illustrated in Figure A11.

Shutter function, spectral scanning, and amplifier operation are synchronized by a digital control system which controls a repeatable operational procedure. A summary of the timing of a complete measurement sequence is shown in Figure A12.

In addition to the components of the RMSP described above, there is an additional feature of the instrument which is utilized for on-line operation during an experiment but whose output is not collected for data analysis. As illustrated in Figure A3, the RMSP clock signal is amplified and applied to the vertical deflection plates of the CRT. This modulates the position of the CRT spot along the vertical axis, causing

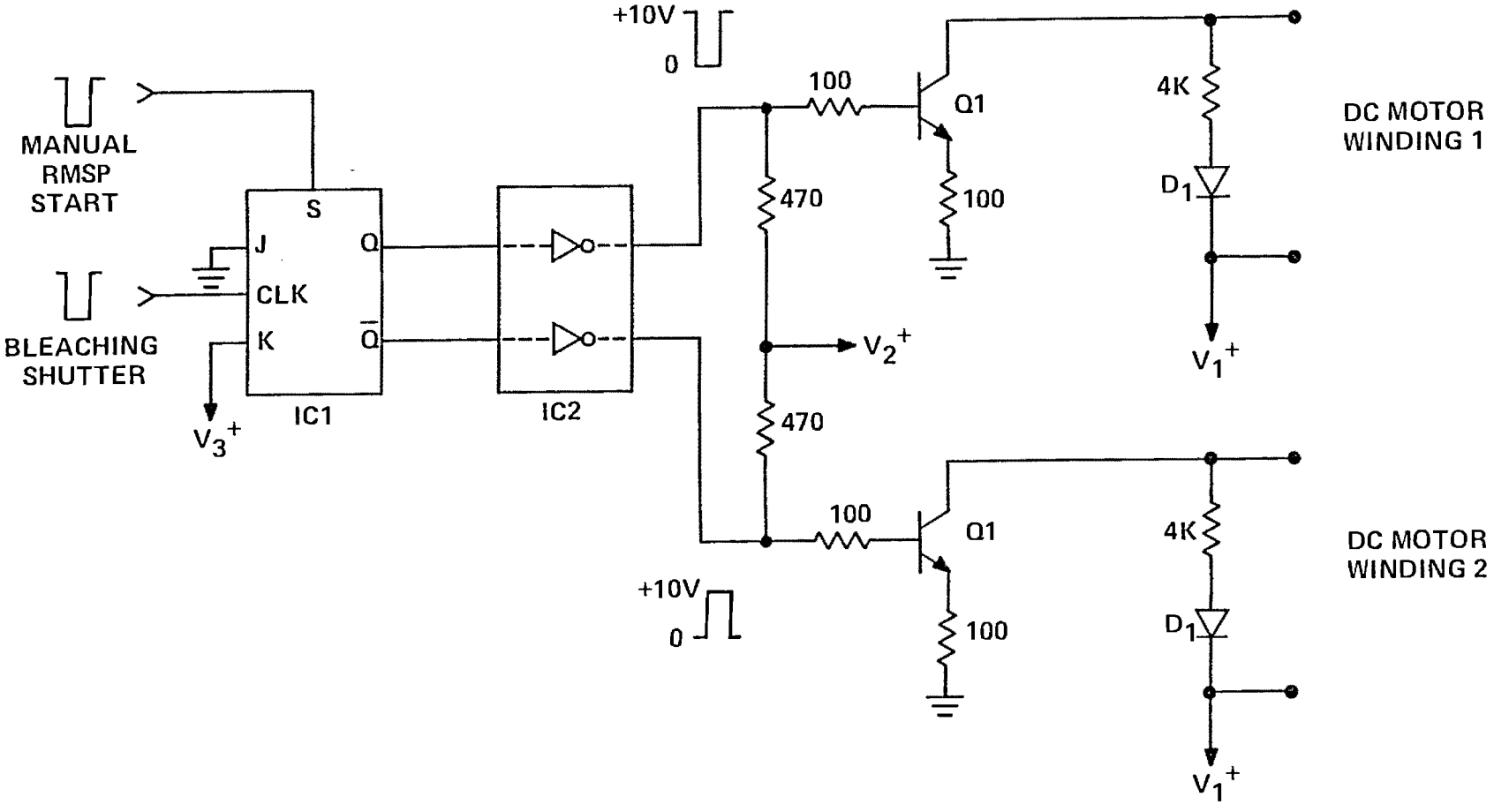
MANUAL
RMSP
START
BLEACHING
SHUTTER
S
J
CLK
K
Q
$\overline{Q}$
IC1
IC2
V_3^+
+10V
0
100
Q1
100
470
V_2^+
470
4K
D_1
V_1^+
DC MOTOR
WINDING 1
100
Q1
100
+10V
0
4K
D_1
V_1^+
DC MOTOR
WINDING 2

Figure All

Figure A11. Circuit diagram of movable mirror driver. Q_1: MJ413. D_1: 1N4004. Z_1: 130-volt zener diode. IC1: SN7476 J-K flip-flop. IC2: SN7406 open-collector inverter. V_1^+: +129 volts. V_2^+: +14 volts. V_3^+/: +5 volts. Mirror control signal onset is initiated by manual RMSP start pulse (Figures A8, A12). For duration of control signal, voltage V_1^+ is applied across field winding 1 of DC motor and removed from field winding 2. This operation moves mirror fully into position, at 45^o angle with respect to measuring axis of RMSP. Control signal is reset by closure of bleaching light shutter (Figure A12). At this time, V_1^+ is removed from winding 1 and applied across winding 2, to hold mirror out of measuring axis.

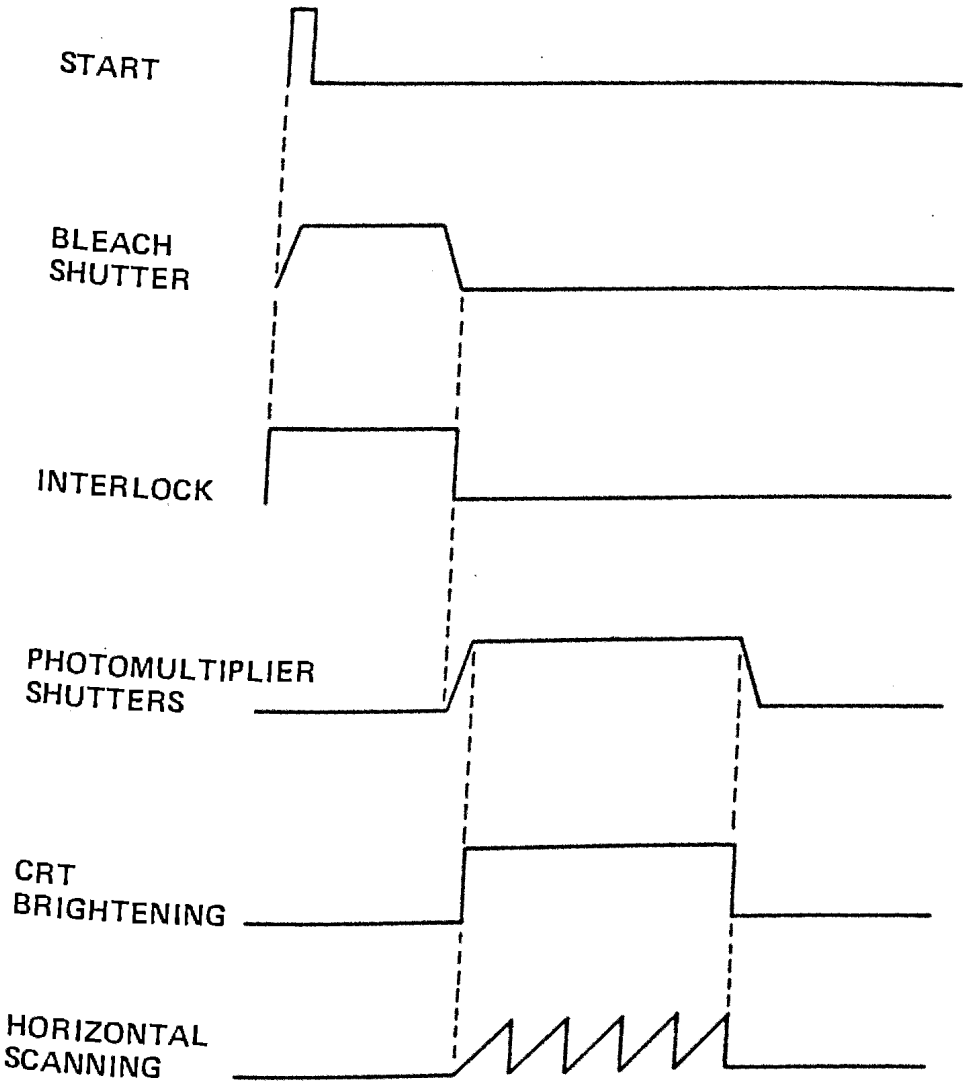
START
BLEACH SHUTTER
INTERLOCK
PHOTOMULTIPLIER SHUTTERS
CRT BRIGHTENING
HORIZONTAL SCANNING

Figure A12

Figure A12. Timing diagram of RMSP operation. Start pulse enables opening of bleach shutter. Photomultiplier shutters, disabled by interlock during bleaching, do not open until bleach shutter has closed completely. After suitable delay to insure photomultiplier shutters are completely open, CRT brightening and horizontal scanning are begun. Photomultiplier shutters close upon completion of scanning operation.

two spatially separate light fluxes to exit alternately from the monochromator, chopped 180° out of phase.

Both fluxes are collected by the Cassegrain and field lenses and are demagnified by the condenser, as described above. The "sample" flux illuminates the 400 micron diameter cross-section of retina which is aligned with the bleaching optics. The "reference" flux illuminates a separate cross-section of retina which is not in the pathway of the bleaching light.

The fluxes transmitted by both cross-sections of retina are collected by the objective and fall upon the cathode of the primary photomultiplier. The resulting anode current is proportional to the sample transmittance during one-half of the clock cycle and to the reference transmittance during the other half. A lock-in amplifier employs a gating signal at the same frequency and in phase with the vertical axis modulating clock command. This operation allows each of the two respective photomultiplier signals to be recovered and integrated separately. The circuitry of the lock-in amplifier, shown in a simplified manner in Figure A5, is illustrated schematically in Figure A13.

The output of the sample integrator is processed directly, as described above, and recorded for later data analysis. In addition, the difference between the sample integrator and the reference integrator is amplified through an additional sample-and-hold system and is displayed on a cathode ray oscilloscope.

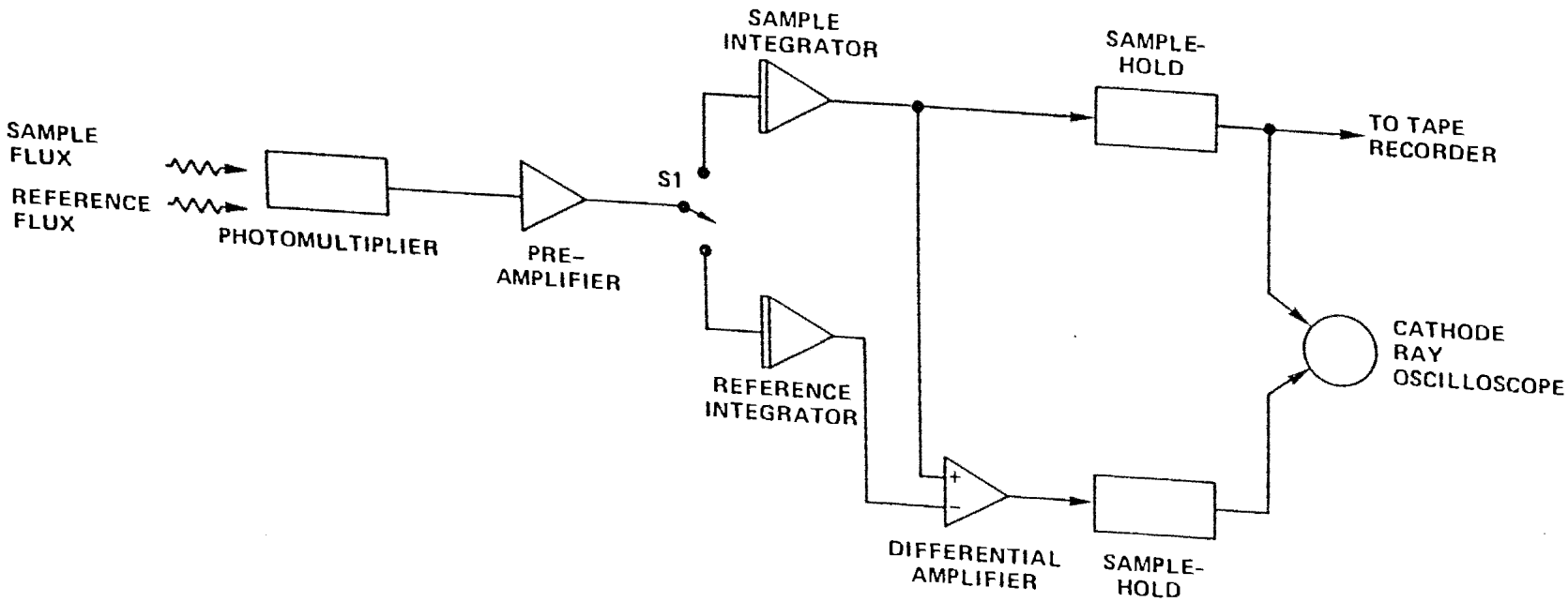
SAMPLE
FLUX
REFERENCE
FLUX
PHOTOMULTIPLIER
PRE-
AMPLIFIER
S1
SAMPLE
INTEGRATOR
REFERENCE
INTEGRATOR
SAMPLE-
HOLD
TO TAPE
RECORDER
CATHODE
RAY
OSCILLOSCOPE
DIFFERENTIAL
AMPLIFIER
SAMPLE-
HOLD

Figure A13

Figure A13. Block diagram of dual-beam operation. Photomultiplier anode current, consisting of summation of out-of-phase transmittances from both sample and reference spots, is preamplified in composite form. Output of preamplifier is switched between two integrators synchronously with application of square-wave deflection voltage to CRT vertical plates (Figure A3). This procedure recovers sample and reference signals separately. Switch S_1 is driven by RMSP clock signal. Output of sample integrator system is recorded, to be used in data reduction. Difference between sample and reference integrator outputs is amplified and monitored on peripheral cathode ray oscilloscope.

This procecure allows the investigator to monitor differences occurring after a bleach by comparing the unstable bleached spot with a steady-state reference spot. In this manner, by subtracting out common-mode transmittance between the two spots, such differences can be observed on a more sensitive scale than by merely monitoring the sample integrator output directly. The differential output, which is utilized solely for purposes of qualitative on-line monitoring, is not required for data reduction operations described in APPENDIX B and is therefore not recorded.

APPENDIX B:

Data Reduction and Analysis

INTRODUCTION

A microspectrophotometer measures light fluxes which are incident upon and transmitted through a specimen. Although the flux which is absorbed by a specimen at a particular wavelength is not directly available for detection, its value can be inferred from detection of these flux magnitudes, according to the approximation,

$$\text{absorptance} \approx 1 - \frac{\text{transmitted flux}}{\text{incident flux}} \quad ; \qquad (1)$$

given certain assumptions about the combined optical characteristics of the instrument and the preparation.

In addition to being absorbed or transmitted, light flux, which is incident upon an object, can also be reflected or scattered. Reflection in a microspectrophotometer occurs primarily at the glass boundaries of the specimen chamber and usually amounts to approximately five percent of the incident light. Thus, it does not appear to be an unreasonable assumption that the undetected flux due to reflection is insignificantly small.

In contrast, there is no known way to measure or to quantify accurately the amount of light flux which is scattered by a preparation. This is true not only of the rapid scanning microspectrophotometer (RMSP) but of any absorptance photometer as well. If a microscope objective with a large numerical aperture is selected as the collecting lens, some of the

scattered light can be recovered, rather than being lost to the surroundings. However, the inability to separate the scattered light fraction from the total transmitted light, coupled with the wavelength dependency of scattering, results in considerable distortion of the transmittance measurement.

A further complication arises from studying visual cell preparations, since a certain amount of light-absorbing impurity is usually present (due to blood vessels, retinal tissue other than photoreceptor cells, etc.) in addition to the absorbing visual pigment. Such non-specific absorption, like the wavelength-dependent scattering, also causes distortion in the transmittance measurement. Thus, the actual transmitted flux which is detected represents the combined effect of the distortions as well as the actual characteristics of the pigment alone. If the absorptance is calculated from this measurement, as defined by Equation (1), this value will also reflect the distortions.

The spectral characteristics of the light-absorbing impurities are known or assumed to be unchanged by light, so that they contribute equally to measurements taken before and after bleaching. If scattering likewise remains constant, then the common background density due to the various distortions can be eliminated by calculating a difference spectrum, in which one absorption spectrum is subtracted from another (Dartnall, 1962). The advantage of studying difference spectra, therefore, is that only photolabile species are displayed.

The data reduction scheme for RMSP measurements consists of calculating absorptances, using Equation (1), preceding the calculation of difference spectra. The two sample-and-hold voltage outputs of the RMSP (see APPENDIX A) thus provide all the necessary information required to study photoproduct kinetics.

SIGNAL PROCESSING

During each sampling interval of the RMSP, light with central wavelength λ emerges from the exit slit of the monochromator with average flux $\phi(\lambda)$ (Figure B1). An amount, $\phi_S(\lambda)$, of this flux passes through the beam splitter undeflected and is the incident flux to the preparation. The photomultiplier, with wavelength-dependent gain $P_S(\lambda)$, senses the flux $\phi_S'(\lambda)$ which is transmitted through the preparation and generates an electrical anode current, $P_S(\lambda)\phi_S'(\lambda)$. This signal is amplified by a photomultiplier preamplifier with wavelength-independent gain G_S.

In order to use the dynamic range of this preamplifier optimally, two steps are taken. First, a constant bias current, I_S, is applied to its input. This current, which is of much greater amplitude than the photomultiplier dark current, displaces the preamplifier output to near one extreme of its dynamic range. Second, the gain of the photomultiplier, $P_S(\lambda)$, is adjusted such that the maximum transmitted light

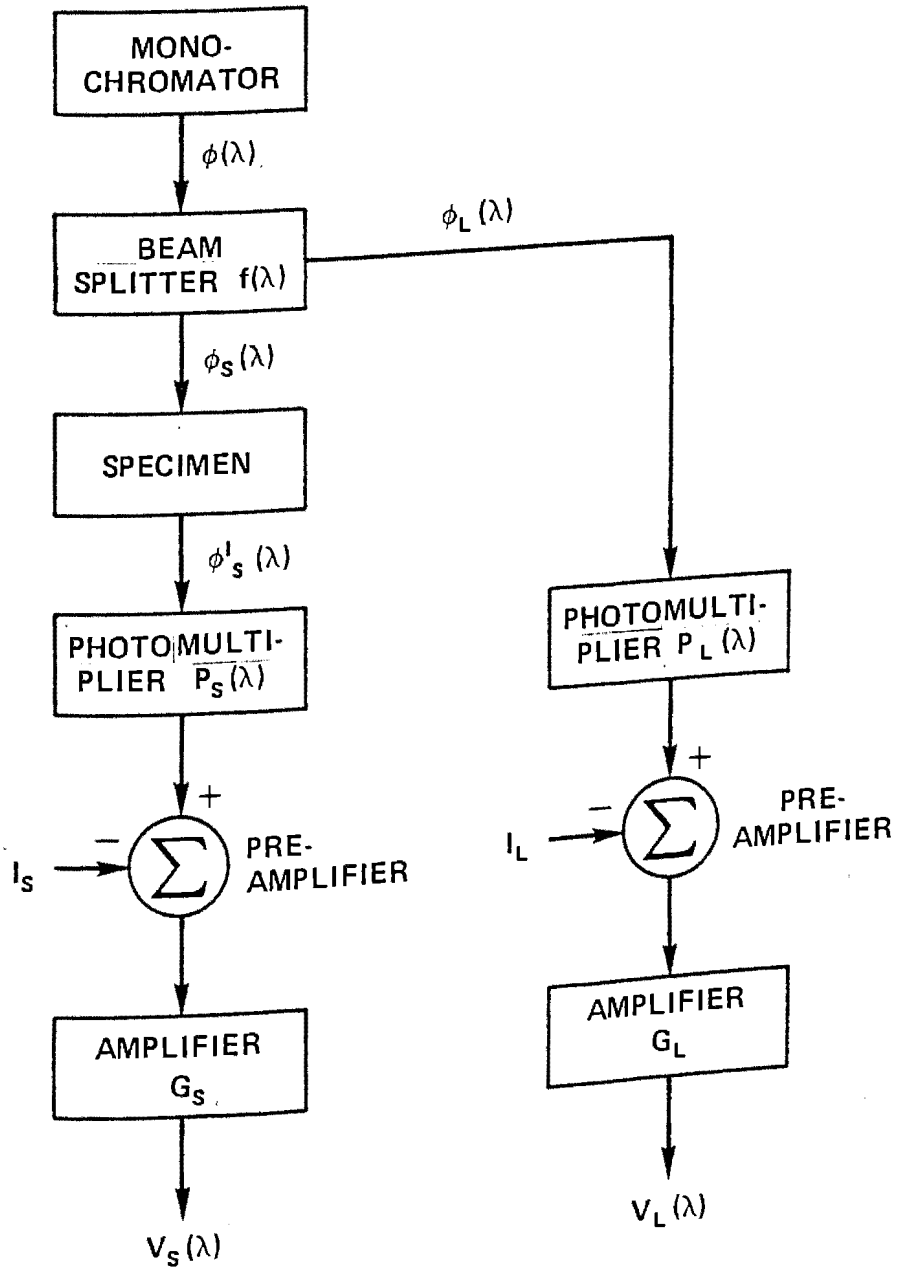
MONO-
CHROMATOR
$\phi(\lambda)$
BEAM
SPLITTER f(λ)
$\phi_L(\lambda)$
$\phi_S(\lambda)$
SPECIMEN
$\phi'_S(\lambda)$
PHOTOMULTI-
PLIER $P_S(\lambda)$
PHOTOMULTI-
PLIER $P_L(\lambda)$
+
−
I_S
Σ
PRE-
AMPLIFIER
+
−
I_L
Σ
PRE-
AMPLIFIER
AMPLIFIER
G_S
AMPLIFIER
G_L
$V_S(\lambda)$
$V_L(\lambda)$

Figure B1

Figure B1. Block diagram of RMSP signal processing. See text for explanation.

signal, $P_S(\lambda)\phi_S'(\lambda)$, approaches the other extreme of the preamplifier dynamic range. Thus, the output of the preamplifier is given by

$$V_S(\lambda) = G_S\,[P_S(\lambda)\phi_S'(\lambda) - I_S] \quad . \quad (2)$$

The remainder of the light from the monochromator, $\phi_L(\lambda)$, which is diverted by the beam splitter and similarly processed, ultimately generates a corresponding output voltage, by a second photomultiplier,

$$V_L(\lambda) = G_L\,[P_L(\lambda)\phi_L(\lambda) - I_L] \quad . \quad (3)$$

Because of spectral differences in the separate optical pathways of the transmitted and diverted lights (beam splitter, microscope lenses, etc.), an additional wavelength-dependent factor, $f(\lambda)$, is determined such that

$$f(\lambda) = \frac{\phi_L(\lambda)}{\phi_S(\lambda)} \quad . \quad (4)$$

In practice, $f(\lambda)$ is computed from simultaneous measurements of the outputs of the two photomultiplier preamplifier systems in the absence of a preparation in the microscope of the RMSP. This procedure allows Equation (3) to be rewritten,

$$V_L(\lambda) = G_L\,[P_L(\lambda)f(\lambda)\phi_S(\lambda) - I_L] \quad . \quad (5)$$

If the amplifier electronics are operated with the CRT unlit (subscript 0), where $\phi_0(\lambda) = \phi_{SO}(\lambda) = \phi_{LO}(\lambda) = 0$, then the dark, baseline voltages are

$$V_{SO}(\lambda) = -G_S I_S = V_{SO} \quad ; \quad (6a)$$

$$V_{LO}(\lambda) = -G_L I_L = V_{LO} \quad ; \quad (6b)$$

(ignoring constant and small photomultiplier dark current), so that

$$V_S(\lambda) - V_{SO} = G_S P_S(\lambda)\phi'_S(\lambda) \quad ; \quad (7a)$$

$$V_L(\lambda) - V_{LO} = G_L P_L(\lambda)\phi_S(\lambda)f(\lambda) \quad ; \quad (7b)$$

The absorptance of the specimen is thus

$$A_S(\lambda) = 1 - \phi'_S(\lambda)/\phi_S(\lambda)$$

$$= 1 - \frac{G_L P_L(\lambda)f(\lambda)}{G_S P_S(\lambda)} \cdot \frac{V_S(\lambda) - V_{SO}}{V_L(\lambda) - V_{LO}} \quad . \quad (8)$$

A measurement taken through a blank area of the chamber, outside the boundary of the retina (subscript B), can be utilized in order to determine the absorptance directly from the magnitudes of voltage outputs alone. This is possible since the drifts of the DC levels and gains of the RMSP have been determined to be insignificant in magnitude for the duration of time that a retinal spot was studied. If the reflection of the blank glass cell is assumed to be small, so that $\phi_{SB}(\lambda) = \phi'_{SB}(\lambda)$, then

$$V_{SB}(\lambda) - V_{SO} = G_S P_S(\lambda)\phi_{SB}(\lambda) \quad ; \quad (9a)$$

$$V_{LB}(\lambda) - V_{LO} = G_L P_L(\lambda)f(\lambda)\phi_{SB}(\lambda) \quad . \quad (9b)$$

By substituting Equations (9a) and (9b) into Equation (8), the absorptance calculation of Equation (1) is reduced to:

$$A_S(\lambda) = 1 - \frac{V_{LB}(\lambda) - V_{L0}}{V_{SB}(\lambda) - V_{S0}} \cdot \frac{V_S(\lambda) - V_{S0}}{V_L(\lambda) - V_{L0}} \quad ; \qquad (10)$$

or, in units of optical density,

$$D_S(\lambda) = -\log [1 - A_S(\lambda)]$$

$$= -\log \frac{V_{LB}(\lambda) - V_{L0}}{V_{SB}(\lambda) - V_{S0}} \cdot \frac{V_S(\lambda) - V_{S0}}{V_L(\lambda) - V_{L0}} . \qquad (11)$$

The practical consequence of this calculation procedure is that a knowledge of the actual numerical values of all of the wavelength-dependent components of the RMSP (beam splitter, lens, photomultiplier, etc.) is not required to calculate the absorptance of the preparation.

ABSORPTION SPECTRA AND KINETICS

A comparison among several measurements, taken prior to and at various times subsequent to bleaching, yields a qualitative description of the kinetics of the on-going processes. The implicit assumption is that the change in concentration of a particular photoproduct, which possesses a characteristic wavelength of maximum absorption, is proportional to the optical density change measured at that wavelength. By locating the wavelengths where the maximum optical density changes occur from measurement to measurement, the active photoproducts during any particular time interval can be identified. Furthermore, the kinetics of photoproduct transformations can be quantitatively deduced

by calculating the magnitude of the optical density changes at these specific wavelengths as a function of time.

With the ultimate objective of determining these kinetics in mind, the first step in data reduction was the calculation of absorption spectra from unprocessed data such as that shown in Figure B2. These computations were accomplished by means of computer software programs on a PDP-11/10 computer, which evaluate Equation (11). Figure B3, which was obtained via a PDP-11/40 computer with a peripheral Versatek printer-plotter, demonstrates three examples of absorption spectra which were calculated from a set of measurements made on a typical retina.

Figure B3 indicates that the retina has a finite, non-zero optical density at all times across the visible spectrum, although the purified visual pigment and its photoproducts are known to absorb only a negligible amount of light at the red end of the spectrum (Collins, Love, and Morton, 1952). Thus, the absolute magnitude of the optical density at 640 nanometers is an indirect measure of the distortion-causing impurities described previously.

Although it has been the general practice of other microspectrophotometrists to re-zero the absorption curves based on the 640 nanometer optical density, this practice has not been followed in the experiments reported in this dissertation. The re-zeroing procedure presumably loses no information about the visual pigment. However, it does discard valuable information concerning the degree of

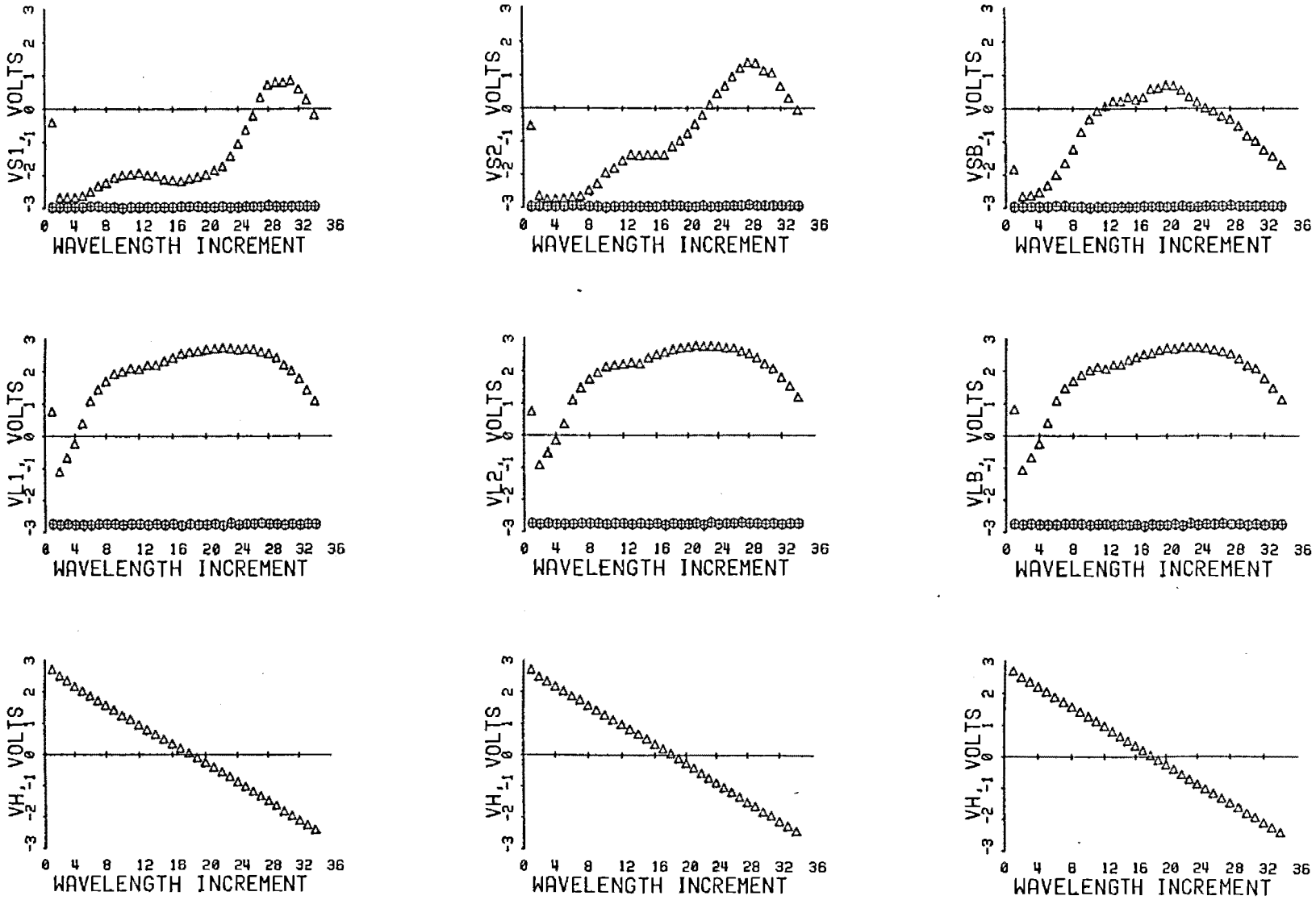
VS1, VOLTS
VS2, VOLTS
VSB, VOLTS
VL1, VOLTS
VL2, VOLTS
VLB, VOLTS
VH, VOLTS
3
2
1
0
-1
-2
-3
0 4 8 12 16 20 24 28 32 36
WAVELENGTH INCREMENT
(a)
(b)
(c)

Figure B2

Figure B2. Record of typical raw data output voltages. Typical example of RMSP horizontal deflection and sample-and-hold output voltages, which have been digitized by PDP-11/10 digital computer. Analog data was input either directly from RMSP, via remote on-line connection, or from Honeywell 5600C analog FM tape recorder. Software programs, written in assembly language, utilized RMSP reset voltage pulse (see APPENDIX A) to synchronize analog-to-digital sampling procedures, storing data on floppy disks. Reconstruction of raw data, in digitized form, and graphical display, on oscilloscope screen peripheral to computer, were mediated by subroutines written in FORTRAN programming language. (a) Record of raw data voltages from typical 400 micron diameter retinal patch, measured prior to bleaching. $V_{S1}(\lambda)$ and $V_{L1}(\lambda)$ (triangles) represent digitized waveforms from transmitted-light and incident-light sample-and-hold amplifiers, respectively. Also shown are V_{SO} and V_{LO} (circles), which represent baseline levels of the respective electronics. Wavelength changes are indicated by $V_H(\lambda)$, the record of CRT horizontal deflection voltage. Wavelength range is 370 to 640 nanometers. (b) Typical record of raw data voltages from same retinal patch, measured subsequent to bleaching. (c) Typical records of respective sample-and-hold amplifier outputs, $V_{SB}(\lambda)$ and $V_{LB}(\lambda)$, measured and recorded through blank area of chamber.

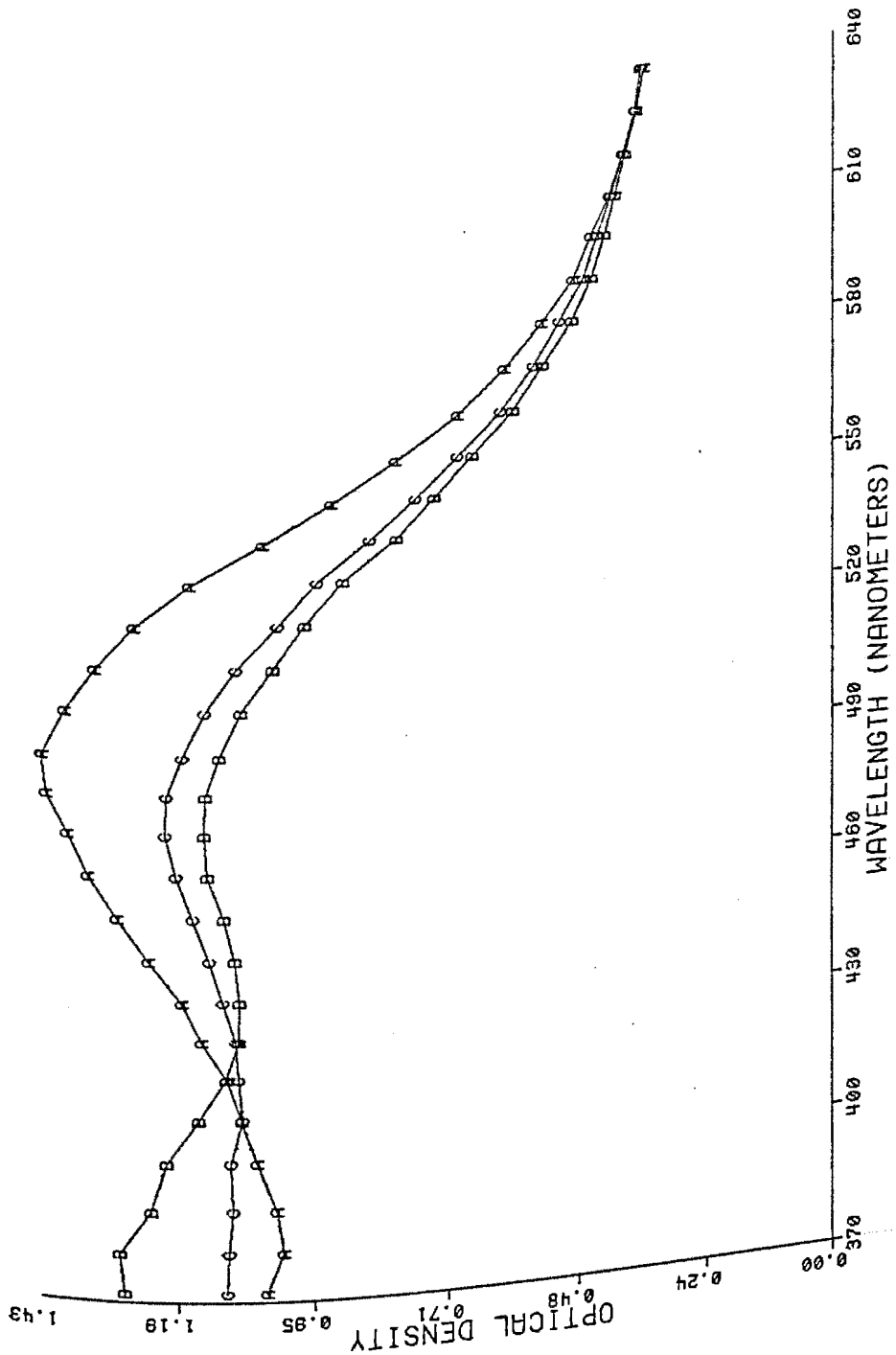
OPTICAL DENSITY
0.00
0.24
0.48
0.71
0.95
1.18
1.43
370
400
430
460
490
520
550
580
610
640
WAVELENGTH (NANOMETERS)

Figure B3

Figure B3. Record of typical absorptance spectra. Record A represents absorptance, in optical density units, of patch of retina in dark-adapted, unbleached condition. Record B illustrates optical density measured 100 milliseconds after completion of 300 millisecond bleach. Record C portrays measurement 650 seconds post-bleach. Wavelength calibration is achieved on PDP-11/40 computer by FORTRAN software programs. Raw data from three interference filter measurements (see METHODS) are searched for location of maximum transmittance of each scan. These three locations correspond to positions in scan of 400, 500, and 600 nanometer wavelength, respectively. Calculation of numerical wavelength values for each step of scan is achieved by interpolation. Optical density values are calculated by FORTRAN programs, which evaluate Equation (11) of APPENDIX B for each wavelength in scan. These values, which are permanently stored in files on floppy disk, are displayed on peripheral oscilloscope screen by means of FORTRAN software programs. The lines connecting data points in this and all subsequent figures were generated by linear interpolation.

scattering by the retina, which is an important parameter in this research (see RESULTS).

Proceeding to the time-dependent changes which are illustrated in Figure B3, several observations can be made. For example, a comparison between an unbleached patch of retina and the same patch measured 100 milliseconds after the completion of a 300 millisecond bleach, which are labelled as curves A and B, respectively, indicates a loss of optical density near 500 nanometers, with a corresponding gain near 380 nanometers. Upon examination of the characteristic identifying wavelengths of rhodopsin and its photoproducts (see Figure 1, INTRODUCTION), it can be deduced that the process of bleaching caused a loss of rhodopsin (500 nanometers) and an increase in metarhodopsin II concentration (380 nanometers) over the 400 millisecond interval.

When curve B, an early post-bleach measurement, is compared to curve C, which was measured 650 seconds after the bleach, a decrease in optical density near 380 nanometers and an increase near 470 nanometers is noted. This observation suggests that metarhodopsin II has decreased in concentration during the 650 second interval, while the concentration of metarhodopsin III (470 nanometers) has simultaneously increased. In addition, the three measurements exhibit an approximate equality of optical density, which occurs near 420 nanometers. This wavelength, which is called an "isosbestic point," signifies that only two wavelengths are changing simultaneously to produce the observed spectra (Dartnall, 1962).

Figure B4(a) illustrates a difference spectrum which was obtained by subtracting curve C of Figure B3 from curve B of the same figure. Figure B4(a) thus represents a comparison between the early and late post-bleach measurements. A positive peak is seen at 380 nanometers in this figure, while a negative peak is observed at 470 nanometers*. A general characteristic of difference spectra plots is that a positive peak indicates that pigment was lost in the time interval between the two measurements. Thus, in the illustration in Figure B4(a), more 380 nanometer pigment was present early after the bleach than at the time of reference. Conversely, since a negative peak on a difference spectrum indicates a formation of pigment between the two measurements, it can be concluded that less 470 nanometer pigment was present early than at the time of reference. Furthermore, the crossing of the wavelength axis near 430 nanometers indicates that no change in pigment concentration occurred between the two measurements.

A single difference spectrum, such as the one illustrated in Figure B4(a), only yields information concerning the relative magnitudes of pigment concentration at two specific different times. It does not reveal the change that actually occurred during the interval. For this reason, difference spectra are calculated for every measurement in

---

*Wavelength resolution for a 34-waveband scan, as illustrated in figures of this Appendix, is approximately ±5 nanometers.

an experiment, utilizing the same reference curve (usually the final measurement) in each calculation. A superposition of these difference spectra thus offers one quantitative way of assessing the kinetics of formation and decay of photolabile species.

Figure B4(b) illustrates a superposition of three post-bleach difference spectra, which have been calculated from measurements on the same retinal patch. In this figure, the late post-bleach absorption spectrum (curve C of Figure B3) has been subtracted, as the reference, from three particular early and intermediate post-bleach measurements, which are numerically labelled in accordance with their sequential occurrence in time. Certain trends in the kinetics of the pigment species which are changing during these measurements can be observed by comparing the three curves.

For example, if the curves are examined at 380 nanometers, it can be seen that the optical density difference (ordinate value) is (a) greater than zero for curve 1; (b) less positive in curve 2; and (c) even less positive in curve 3. These observations are translated to a kinetic scheme in which the pigment (a) is present in greater concentration at the time of measurement of curve 1 than at the reference time; (b) decays during the time interval from curves 1 to 2; and (c) decays further during the time interval from curves 2 to 3. In addition, since the ordinate value of curve 3 is still positive, the pigment also decays during the interval between the curve 3 measurement and the

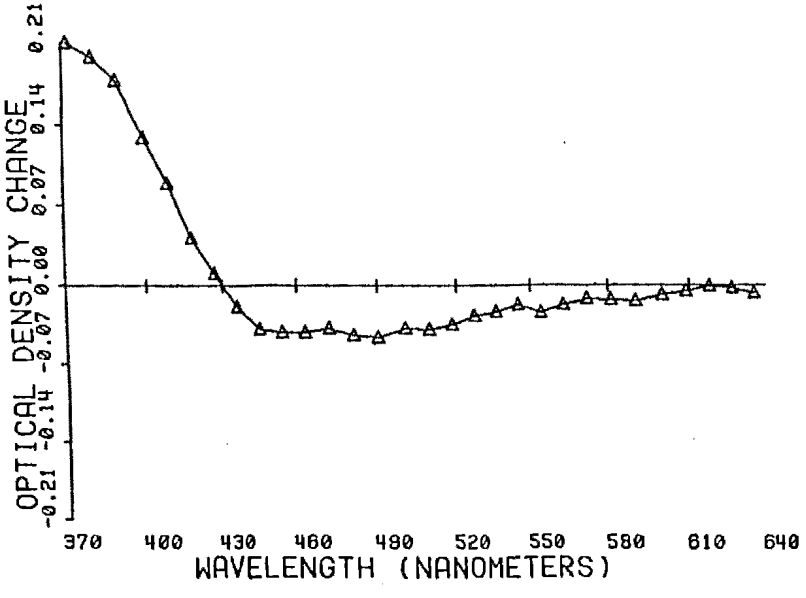
OPTICAL DENSITY CHANGE
0.21
0.14
0.07
0.00
-0.07
-0.14
-0.21
370
400
430
460
490
520
550
580
610
640
WAVELENGTH (NANOMETERS)

(a)

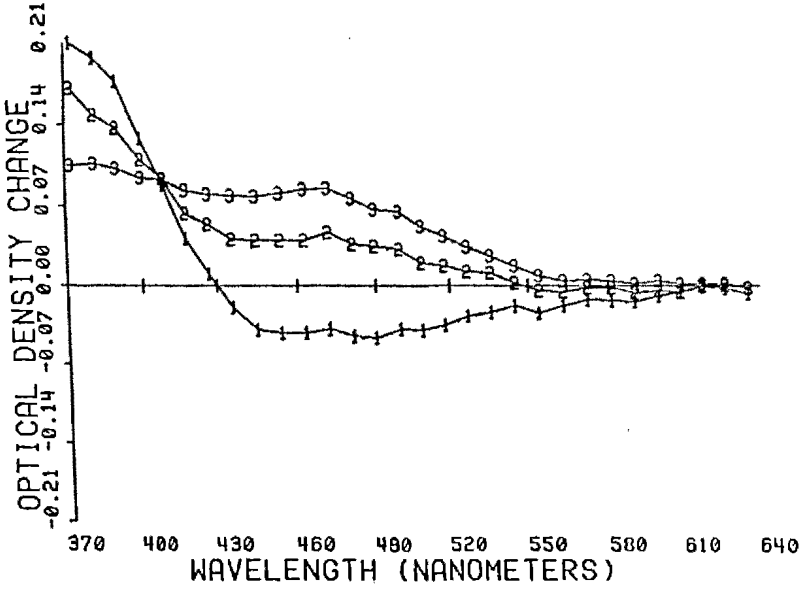
OPTICAL DENSITY CHANGE
0.21
0.14
0.07
0.00
-0.07
-0.14
-0.21
370
400
430
460
490
520
550
580
610
640
WAVELENGTH (NANOMETERS)

(b)

Figure B4

Figure B4. Record of typical difference spectra. (a) Difference in optical density resulting from subtraction of late post-bleach reference measurement (650 seconds; record C of Figure B3) from early post-bleach measurement (100 milliseconds; record B of Figure B3). All calculations were performed on PDP-11/40 computer by means of FORTRAN software programs. (b) Superimposed difference spectra. Record 1: same as (a). Record 2: same late post-bleach reference measurement, subtracted from measurement 60 seconds post-bleach. Record 3: same reference, subtracted from measurement 180 seconds post-bleach.

reference measurement.

In contrast, the 470 nanometer pigment initially (curve 1) has a concentration less than that of the reference, increases in concentration less than that of the reference, increases in concentration during the interval between curves 1 and 3, and decays between the time of curve 3 and the time of the reference. It can also be seen from Figure B4(b) that the three difference spectra intersect around the isosbestic point, near 430 nanometers, which indicates once again that only the two wavelengths are involved in producing the observed kinetics.

This information can be presented more clearly by isolating the wavelengths of maximum change as a function of post-bleach time. Figure B5 is an example of such a process, which consists of "looking up" in the data files the optical density magnitude differences, at the particular wavelengths, from each difference spectrum calculated (that is, for each scan of an experiment). Since the abscissa of the graph is now time, the kinetics are illustrated directly. Thus, the pattern of 380 nanometer pigment decay (assumed to be metarhodopsin II) and the formation and decay of the 470 nanometer pigment (presumably metarhodopsin III) can be displayed in an uncomplicated manner on a single graph. Figures such as Figure B5 thus summarize the total kinetic picture for a given bleaching experiment of a retinal patch.

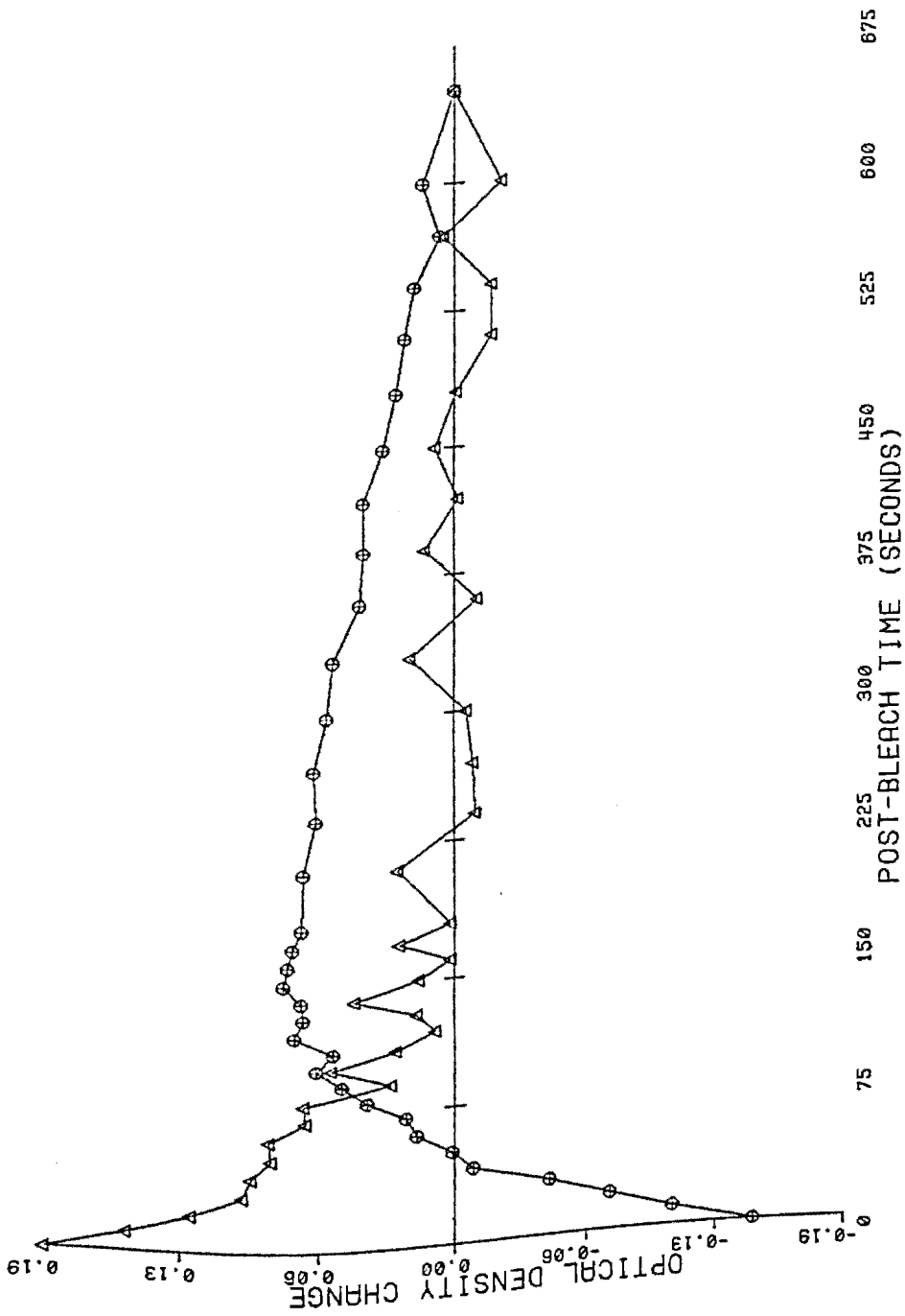
OPTICAL DENSITY CHANGE
0.19
0.13
0.06
0.00
-0.06
-0.13
-0.19
0
75
150
225
300
375
450
525
600
675
POST-BLEACH TIME (SECONDS)

Figure B5

Figure B5. Record of typical isolated-wavelength kinetics. All calculations were performed on PDP-11/40 computer via FORTRAN software programs. Wavelengths displayed were selected by locating maximum and minimum of difference spectra such as those illustrated in Figure B4, in which final late post-bleach measurement was utilized as reference curve for the subtraction. Optical density differences at these specific wavelengths were retrieved from each difference spectrum (calculated sequentially for each scan) and are displayed here as ordinate function. Abscissa represents time of measurement of particular scan following completion of bleach. Triangles: 380 nanometers. Circles: 470 nanometers.

DERIVATION OF MODELS

In order to provide a means by which quantitative comparisons could be made between many experiments, a mathematical model was employed. The model which has been utilized to describe metarhodopsin III kinetics involves unidirectional, linear, first-order processes, which are characterized by a single rate of formation, k_f, and decay, k_d. The differential equation which quantitates metarhodopsin III pigment concentration, C(t), normalized with respect to the amount of rhodopsin bleached, is thus given by

$$\frac{dC(t)}{dt} = k_f P(t) - k_d C(t) \quad . \quad (12)$$

P(t) represents the concentration of the last precursor of C(t), since all other photoproducts are assumed to have disappeared completely, due to the sequential, unidirectional nature of photoproduct transitions.

If P(t) is also described by exponential processes, and if its formation is assumed to be extremely rapid with respect to the kinetics of C(t), then P(t) can be approximated by a decay phase only,

$$P(t) \approx P' e^{-k_f t} \quad . \quad (13)$$

This allows Equation (12) to be rewritten as

$$\frac{dC(t)}{dt} = k_f P' e^{-k_f t} - k_d C(t) \quad . \quad (14)$$

This equation is of the form

$$\frac{dy}{dt} + ay = b(t) \quad ; \qquad (15)$$

with solution

$$y(t) = e^{-at} \int_{t_0}^{t} e^{a\theta} b(\theta) d\theta + k' e^{-at} \quad . \qquad (16)$$

Thus, the concentration, C(t), can be determined by substituting the parameters of Equation (14) into Equation (16), so that

$$C(t) = \frac{P'}{1-\frac{k_d}{k_f}} (e^{-k_d t} - e^{-k_f t}) + k' e^{-k_d t} \quad . \qquad (17)$$

If the boundary condition, C(0) = 0, is applied, then $k' = 0$, and Equation (17) reduces to

$$C(t) = \frac{P'}{1-\frac{k_d}{k_f}} (e^{-k_d t} - e^{-k_f t}) \quad . \qquad (18)$$

Two additional substitutions are made in order that the model can be characterized by half-times rather than rate constants (see INTRODUCTION), so that

$$C(t) = \frac{P'}{1-\frac{T_f}{T_d}} (e^{-t(\ln 2)/T_d} - e^{-t(\ln 2)/T_f}). \qquad (19)$$

As indicated previously, a particular retinal spot was only studied for 650 seconds, following the completion of a bleach. Because of the mathematics employed in calculating difference spectra, an ordinate value of zero in Figure B5

represents pigment absorption at 650 seconds, not at infinite time. Thus, the horizontal axis in Figure B5 is not an absolute level of zero optical density. This condition can be reflected by a modification in Equation (19) to include constant offset shift, C_{650}; thus,

$$C(t) = \frac{P'}{1-\frac{T_f}{T_d}} \left(e^{-t(\ln 2)/T_d} - e^{-t(\ln 2)/T_f}\right) - C_{650}; \quad (20)$$

or, substituting a single parameter, C', to represent the coefficient, $P'/(1-T_f/T_d)$,

$$C(t) = C' \left(e^{-t(\ln 2)/T_d} - e^{-t(\ln 2)/T_f}\right) - C_{650}. \quad (21)$$

CURVE-FITTING

Equation (21) describes a model for the metarhodopsin III kinetics as they are illustrated in Figure B5, for the purpose of curve-fitting the experimental data. The parameters, T_f and T_d, characterize the metarhodopsin III formation and decay processes directly. In addition, since the magnitude of P' is a measure of metarhodopsin II, the immediate precursor of metarhodopsin III, then additional information can be derived about the relative amount of metarhodopsin II which is involved in this photoproduct transition. The physiological interpretation of P' is described in greater detail in the RESULTS section.

Because of the nature of this model, which does not allow for any variation between the coefficients of the formation and decay phases, a less mathematically restrictive representation of Equation (21) was formulated. The formation

and decay processes were characterized by two separate coefficients, C_f and C_d, such that

$$C(t) = C_d e^{-t(\ln 2)/T_d'} - C_f e^{-t(\ln 2)/T_f'} - C_{650}'. \quad (22)$$

The purpose of this alternate model was to accommodate small fluctuations in the magnitudes of the optical density measurements, which might normally be expected to occur during the detection of biological phenomena.

Equations (21) and (22) were utilized separately to fit the experimental data on the PDP-10 computer of the NIH. The MLAB program (Knott and Reece, 1972) adjusted the parameters of the equation utilized by means of the Marguardt-Levenberg iterative curve-fitting algorithm (Smith, 1970), which minimizes the simultaneous sum of squares for the model with respect to the observation points.

A five-point, variable-interval, hyperbolic smoothing operation, which is a subroutine of the MLAB program, was utilized to smooth the data prior to curve fitting. This subroutine replaced each data value with a weighted average of itself and the two neighboring observations on each side of it. Weighting factors were determined to be the reciprocal of the distance to the neighboring values, with respect to the total interval of data observations.

The fit of metarhodopsin III data to Equation (22) is illustrated typically in Figure B6. The use of Equation (22) in the curve-fitting procedures resulted in a better fit of the experimental data, when compared with the fit to Equation (21). The improvement was noted both by the smaller standard deviation of the error, due to the additional adjustable

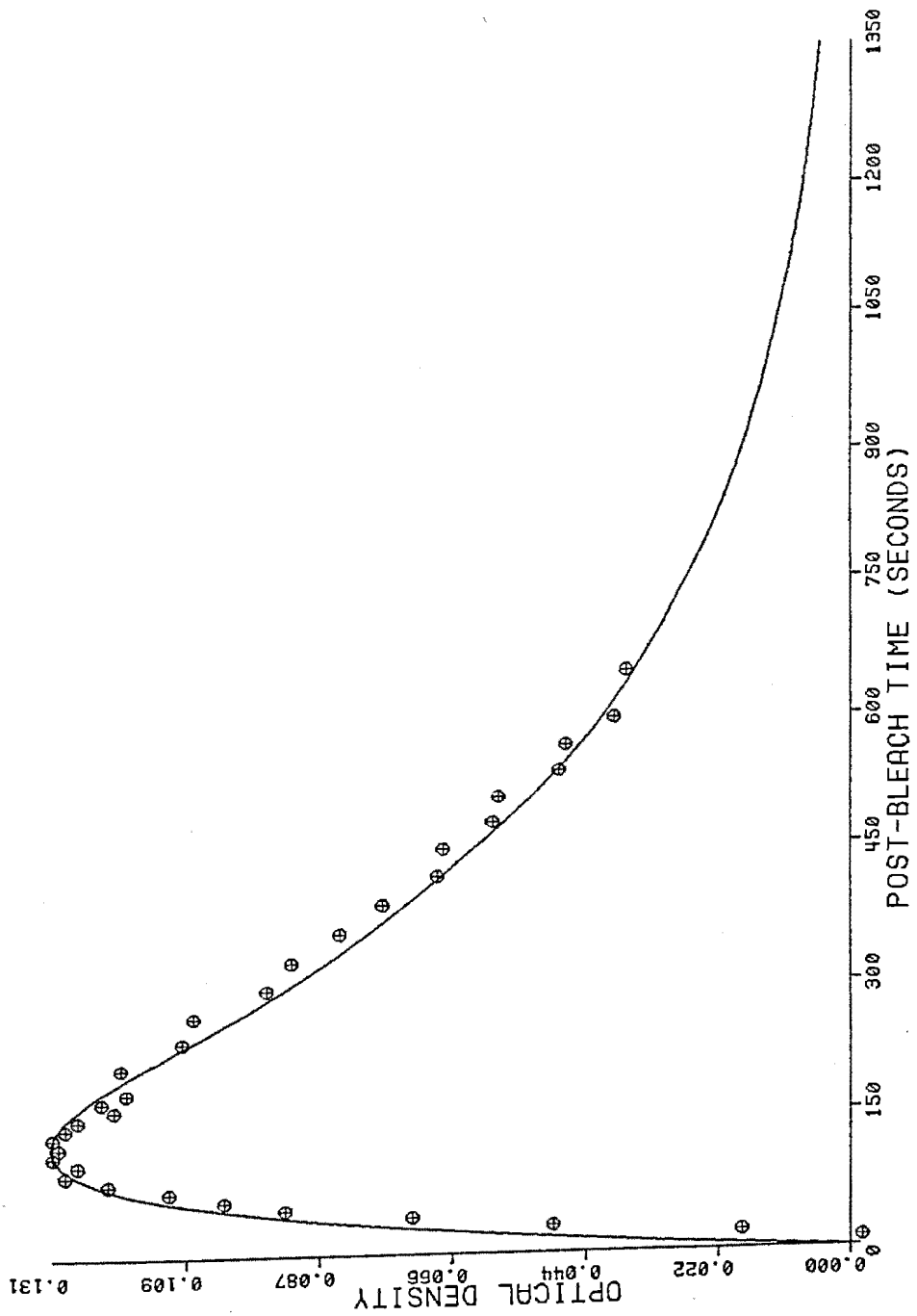
OPTICAL DENSITY
0.000
0.022
0.044
0.066
0.087
0.109
0.131
0
150
300
450
600
750
900
1050
1200
1350
POST-BLEACH TIME (SECONDS)

Figure B6

Figure B6. Graphical display of typical curve fitting. Circles represent optical density of actual data observations. Continuous line illustrates best fit of data to parameters of single, linear, first-order process described in Equation (14), as calculated by MLAB software curve-fitting technique on PDP-10 computer.

parameter, and by eye. As a consequence, the half-times, T_f' and T_d', which were calculated for the two-coefficient model, were assumed to be more reliable representations of the kinetics than T_f and T_d.

However, a single-coefficient model, to correspond with Equation (21), is more realistic physiologically than a two-coefficient model when independent processes are assumed (see RESULTS). For this reason, it was desired to convert the results obtained from curve-fitting to Equation (22) into the format of Equation (21). This operation was accomplished by calculating the average value, $\overline{C}$, of the two coefficients,

$$\overline{C} = \frac{1}{2} (C_d + C_f) \quad ; \quad (23)$$

for those experiments in which there was no statistically significant difference between the population means of C_f and C_d (see below). Although this compromise did not yield the best least-squares fit to the single-coefficient model, no statistically significant difference was observed between $\overline{C}$ and C'. The magnitude of $\overline{C}$ was thus utilized to approximate C' in Equation (21), for the purpose of calculating P'.

STATISTICAL COMPUTATIONS

Differences between well-defined populations of metarhodopsin III experiments were analyzed by the use of statistical methods on the parameters of the equations derived above. The mean value, $\overline{x}$, and standard deviation, σ_x, were computed for each parameter, x_i, based upon the standard formulas,

$$\bar{x} = \frac{1}{n} \sum_{i=1}^{n} x_i \quad ; \quad (24)$$

$$\sigma_x = \sqrt{\frac{1}{n} \sum_{i=1}^{n} (x_i - \bar{x})^2} \quad ; \quad (25)$$

for a population of n observations of magnitudes $x_1, x_2, \ldots, x_i, \ldots, x_n$.

Student's t-test was utilized to determine whether a statistically significant difference existed between the means, $\bar{x}$ and $\bar{y}$, of two sub-populations of a particular parameter. The statistic, t, was calculated from the formula,

$$t = \frac{\bar{x} - \bar{y}}{\sqrt{n_x \sigma_x^2 + n_y \sigma_y^2}} \sqrt{\frac{n_x + n_y - 2}{\frac{1}{n_x} + \frac{1}{n_y}}} \quad ; \quad (26)$$

where n_x and n_y represent the number of observations in the two sub-populations, respectively. The probability value associated with the magnitude of t, for $(n_x + n_y - 2)$ degrees of freedom, was located in a table of t-statistics (Meyer, 1975).

For all comparisons described in this dissertation, the probability level of P = 0.10 was selected as the acceptance criterion for a significant difference. Thus, if the probability associated with the magnitude of t was less than 0.10, a statistically significant difference between the mean values of the two sub-populations was inferred. All other comparisons, with probability values greater than 0.10, were concluded to exhibit statistically identical means.

REFERENCES

Abood, L. G., and Geiger, A. (1955). Breakdown of proteins and lipids during glucose-free perfusion of the cat's brain. Am. J. Physiol. 182: 557-560.

Abrahamson, E. W., and Ostroy, S. E. (1967). The photochemical and macromolecular aspects of vision. Progr. Biophys. molec. Biol. 17: 179-215.

Applebury, M. L., Zuckerman, D. M., Lamola, A. A., and Jovin, T. M. (1974). Rhodopsin. Purification and recombination with phospholipids assayed by the metarhodopsin I → metarhodopsin II transition. Biochemistry 13: 3448-3458.

Baumann, C. (1972). Kinetics of slow thermal reactions during the bleaching of rhodopsin in the perfused frog retina. J. Physiol. 222: 643-663.

Baumann, C. (1976). The formation of metarhodopsin 380 in the retinal rods of the frog. J. Physiol. 259: 357-366.

Baylor, D. A., and Fuortes, M. G. F. (1970). Electrical responses of single cones in the retina of the turtle. J. Physiol. 207: 77-92.

Boll, F. (1876). Zur anatomie und physiologie der retina. Mber. Berlin Akad. 41: 783-787.

Borgström, L., Norberg, K., and Siesjö, B. K. (1976). Glucose consumption in rat cerebral cortex in normoxia, hypoxia, and hypercapnia. Acta Physiol. Scand. 96: 569-574.

Bowmaker, J. K. (1973). The photoproducts of retinal-based visual pigments in situ: a contrast between Rana pipiens and Gekko gekko. Vision Res. 13: 1227-1240.

Bowmaker, J. K., and Loew, E. R. (1976). The action of hydroxylamine on visual pigments in the intact retina of the frog (Rana temporaria). Vision Res. 16: 811-818.

Bownds, D., Dawes, J., Miller, J., and Stahlman, M. (1972). Phosphorylation of frog photoreceptor membranes induced by light. Nature New Biol. 237: 125-127.

Bridges, C. D. B. (1962). Studies on the flash photolysis of visual pigments. IV. Dark reactions following the flash irradiation of frog rhodopsin in suspensions of isolated photoreceptors. Vision Res. 2: 215-232.

Broda, E. E., and Goodeve, C. F. (1941). The behavior of visual purple at low temperatures. Proc. roy. Soc. A. 179: 151-159.

Brown, J. E., and Pinto, L. H. (1974). Ionic mechanism for the photoreceptor potential of the retina of Bufo marinus. J. Physiol. 236: 575-591.

Brown, K. T., and Murakami, M. (1964). A new receptor potential of the monkey retina with no detectable latency. Nature 201: 626-628.

Brown, K. T., Watanabe, K., and Murakami, M. (1965). The early and late receptor potentials of monkey cones and rods. Cold Spr. Harb. Symp. on Quant. Biol. 30: 457-482.

Brown, P. K. (1961). A system for microspectrophotometry employing a commercial recording microspectrophotometer. J. Opt. Soc. Am. 51: 1000-1008.

Brown, P. K., and Wald, G. (1963). Visual pigments in human and monkey retinas. Nature 200: 37-43.

Busch, G. E., Applebury, M. L., Lamola, A. A., and Rentzepis, P. M. (1972). Formation and decay of prelumirhodopsin at room temperatures. Proc. Nat. Acad. Sci. U. S. 69: 2802-2806.

Carlson, S. D. (1972). Microspectrophotometry of visual pigments. Q. Rev. Biophys. 5: 349-393.

Caspersson, T. O. (1940). Methods for the determination of the absorption spectra of cell structures. J. Roy. Micr. Soc. 60: 8-25.

Chance, B. (1951). Rapid and sensitive spectrophotometry. I. The accelerated and stopped-flow methods for the measurement of the reaction kinetics and spectra of unstable compounds in the visible region of the spectrum. Rev. Sci. Instr. 22: 619-627.

Chance, B., Perry, R., Akerman, L., and Thorell, B. (1959). Highly sensitive recording microspectrophotometer. Rev. Sci. Instr. 30: 735-741.

Cohen, L. H., and Noell, W. K. (1960). Glucose catabolism of rabbit retina before and after development of visual function. J. Neurochem. 5: 253-276.

Collins, F. D., Love, R. M., and Morton, R. A. (1952). Studies in rhodopsin. 4: Preparation of rhodopsin. Biochem. J. 51: 292-298.

Cone, R. A. (1964). Early receptor potential of the vertebrate retina. Nature 204: 736-739.

Cone, R. A. (1972). Rotational diffusion of rhodopsin in the visual receptor membrane. Nature New Biol. 236: 39-43.

Cone, R. A., and Brown, P. K. (1969). Spontaneous regeneration of rhodopsin in the isolated rat retina. Nature 221: 818-820.

Cone, R. A., and Cobbs, W. H. (1969). Rhodopsin cycle in the living eye of the rat. Nature 221: 820-822.

Dartnall, H. J. A. (1957). The visual pigments. Methuen and Co., London.

Dartnall, H. J. A. (1962). The photobiology of visual processes. In The Eye, ed. by H. Davson, Academic Press, New York, Part II, 2: 321-533.

Dartnall, H. J. A., Goodeve, C. F., and Lythgoe, R. J. (1936). The quantitative analysis of the photochemical bleaching of visual purple solutions in monochromatic light. Proc. roy. Soc. A. 156: 158-170.

DePont, J. J. H. H. M., Daemen, F. J. M., and Bonting, S. L. (1970). Biochemical aspects of the visual process. VII. Equilibrium conditions in the formation of retinylidene imines. Archs. Biochem. Biophys. 140: 267-274.

Donner, K. O., and Hemila, S. (1975). Kinetics of long-lived rhodopsin photoproducts in the frog retina as a function of the amount bleached. Vision Res. 15: 985-995.

Donner, K. O., and Reuter, T. (1967). Dark-adaptation processes in the rhodopsin rods of the frog's retina. Vision Res. 7: 17-41.

Donner, K. O., and Reuter, T. (1969). The photoproducts of rhodopsin in the isolated retina of the frog. Vision Res. 9: 815-847.

Ebrey, T. G. (1968). The thermal decay of the intermediates of rhodopsin in situ. Vision Res. 8: 965-982.

Erhardt, F., Ostroy, S. E., and Abrahamson, E. W. (1966). Protein configuration changes in the photolysis of rhodopsin. 1. The thermal decay of cattle lumirhodopsin in vitro. Biochim. biophys. Acta 112: 256-264.

Ernst, W., and Kemp, C. M. (1972). The role of metarhodopsin III in the recovery of the PIII photoresponse of isolated rat retina after an intense light exposure. In The

Visual System, ed. by G. B. Arden, Plenum Press, New York, 24: 81-86.

Falk, G., and Fatt, P. (1966). Rapid hydrogen uptake of rod outer segments and rhodopsin solutions on illumination. J. Physiol. 183: 211-224.

Farnsworth, C. C., and Dratz, E. A. (1976). Oxidative damage of retinal rod outer segment membranes and the role of vitamin E. Biochim. biophys. Acta 443: 556-570.

Frank, R. N. (1969). Photoproducts of rhodopsin bleaching in the isolated, perfused frog retina. Vision Res. 9: 1415-1433.

Fuortes, M. G. F., and Hodgkin, A. L. (1964). Changes in time scale and sensitivity in the ommatidia of Limulus. J. Physiol. 172: 239-263.

Futterman, S. (1963). Metabolism of the retina. III. The role of reduced triphosphopyridine nucleotide in the visual cycle. J. biol. Chem. 238: 1145-1150.

Goldsmith, T. H., Dizon, A. E., and Fernandez, H. R. (1968). Microspectrophotometry of photoreceptor organelles from eyes of the prawn, Palaeomonetes. Science 161: 468-470.

Graymore, C. N. (1970). Metabolic survival of the isolated retina. Br. Med. Bull. 26: 130-133.

Grellman, K. H., Livingston, R., and Pratt, D. C. (1962). A flash-photolytic investigation of rhodopsin at low temperatures. Nature 193: 1258-1260.

Gyllenberg, G., Reuter, T., and Sippel, H. (1974). Long-lived photoproducts of rhodopsin in the retina of the frog. Vision Res. 14: 1349-1357.

Hagins, W. A. (1956). Flash photolysis of rhodopsin in the retina. Nature 177: 989-990.

Hagins, W. A. (1957). Rhodopsin in a mammalian retina. Ph.D. thesis. U. of Cambridge.

Hagins, W. A. (1972). The visual process: excitatory mechanisms in the primary receptor cells. Ann. Rev. Biophys. Bioeng. 1: 131-158.

Hagins, W. A., Penn, R. D., and Yoshikami, S. (1970). Dark current and photocurrent in retinal rods. Biophys. J. 10: 380-412.

Hanaoka, T., and Fujimoto, K. (1957). Absorption spectrum of a single cone in carp retina. Jap. J. Physiol. 7: 276-285.

Hárosi, F. I. (1972). Frog rhodopsin *in situ*: orientational and spectral changes in the chromophores of isolated retinal rod cells. Ph.D. thesis. Johns Hopkins U.

Hárosi, F. I., and MacNichol, E. F., Jr. (1974). Dichroic microspectrophotometer: a computer assisted, rapid wavelength scanning photometer for measuring linear dichroism in single cells. J. Opt. Soc. Am. 64: 903-918.

Hubbard, R., Bownds, D., and Yoshizawa, T. (1965). The chemistry of visual photoreception. Cold. Spr. Harb. Symp. quant. Biol. 30: 301-315.

Hubbard, R., Brown, P. K., and Kropf, A. (1959). Action of light on visual pigments. Vertebrate lumi- and meta-rhodopsins. Nature 183: 442-446.

Hubbard, R., and Kropf, A. (1958). The action of light on rhodopsin. Proc. nat. Acad. Sci. U. S. 44: 130-139.

Klethi, J., Urban, P. F., and Mandel, P. (1970). Free nucleotides in retina. FEBS Letters 8: 119-121.

Knott, G. D., and Reece, D. K. (1972). MLAB: a civilized curve-fitting system. Proc. ONLINE '72 Intl. Conf., Brunel Univ., Eng., 1: 497-526.

Koen, A. L., and Shaw, C. R. (1966). Retinol and alcohol dehydrogenase in retina and liver. Biochim. biophys. Acta 128: 48-54.

Korenbrot, J. I., and Cone, R. A. (1972). Dark ionic flux and the effects of light in isolated rod outer segments. J. gen. Physiol. 60: 20-45.

Koszewski, J., Jasny, J., and Grabowski, Z. R. (1968). Rapid scan flash spectrophotometer with a flying spot light source and magnetic storage. Applied Optics 7: 2178-2183.

Kühn, H., and Dreyer, W. J. (1972). Light dependent phosphorylation of rhodopsin by ATP. FEBS Letters 20: 1-6.

Kühne, W. (1878). On the photochemistry of the retina and on visual purple. Ed. by M. Foster, London, Macmillan.

Langer, H., and Thorell, B. (1966). Microspectrophotometry of single rhabdomeres in the insect eye. Exp. Cell. Res. 41: 673-677.

Lasansky, A., and Marchiafava, P. L. (1974). Light-induced resistance changes in retinal rods and cones of the tiger salamander. J. Physiol. 236: 171-191.

Lehninger, A. L. (1975). Biochemistry, Second Edition, Worth Publishers, Inc., New York, 417-542.

Liebman, P. A. (1962). In situ microspectrophotometric studies on the pigments of single retinal rods. Biophys. J. 2: 161-178.

Liebman, P. A., and Entine, G. (1964). Sensitive low-light-level microspectrophotometer: detection of photosensitive pigments of retinal cones. J. Opt. Soc. Am. 54: 1451-1459.

Liebman, P. A., and Entine, G. (1968). Visual pigments of frog and tadpole. Vision Res. 8: 761-775.

Liebman, P. A., Jagger, W. S., Kaplan, M. W., and Bargoot, F. G. (1974). Membrane structure changes in rod outer segments associated with rhodopsin bleaching. Nature 251: 31-36.

Lolley, R. N. (1972). Changes in glucose and energy metabolism in vivo in developing retinae from visually-competent (DBA/1J) and mutant (C3H/HeJ) mice. J. Neurochem. 19: 175-185.

Lolley, R. N., and Hess, H. H. (1969). The retinal rod outer segment of the frog: detachment, isolation, phosphorous fractions and enzyme activity. J. Cell. Physiol. 73: 9-24.

Lolley, R. N., and Schmidt, S. Y. (1974). Metabolism of the vertebrate retina. In The Eye, ed. by H. Davson and L. T. Graham, Jr., Academic Press, New York, 6: 343-378.

Lowry, O. H. (1974). In Morphological and Biochemical Correlates of Neural Activity, ed. by M. M. Cohen and R. S. Sneider, Harper and Row, New York, 178-191.

Lowry, O. H., Roberts, N. R., Schulz, D. W., Clow, J. E., and Clark, J. R. (1961). Quantitative histochemistry of the retina. II. Enzymes of glucose metabolism. J. biol. Chem. 236: 2813-2820.

Lythgoe, R. J. (1937). The absorption spectra of visual purple and of indicator yellow. J. Physiol. 89: 331-358.

Lythgoe, R. J., and Quilliam, J. P. (1938). The thermal decomposition of visual purple. J. Physiol. 93: 24-38.

Mahler, H. R. (1961). The use of amine buffers in studies with enzymes. Ann. N. Y. Acad. Sci. 92: 426-440.

Maker, H. S., and Lehrer, G. M. (1972). Carbohydrate chemistry of brain. In Basic Neurochemistry, ed. by R. W.

Albers, G. J. Siegel, R. Katzmann, and B. W. Agranoff, Little, Brown and Co., Boston, 169-190.

Marks, W. B. (1963). Difference spectra of the visual pigments in single goldfish cones. Ph.D. thesis. Johns Hopkins U.

Marks, W. B. (1965). Visual pigments of single goldfish cones. J. Physiol. 178: 14-32.

Matschinsky, F. M. (1970). Energy metabolism of the microscopic structure of the cochlea, the retina, and the cerebellum. In Advances in Biochemical Psychopharmacology, ed. by E. Costa and E. Giacobini, Raven Press, New York, 2: 217-243.

Matschinsky, F. M., Passonneau, J. V., and Lowry, O. H. (1968). Quantitative histochemical analysis of glycolytic intermediates and cofactors with an oil well technique. J. Histochem. Cytochem. 16: 29-39.

Matthews, R. G., Hubbard, R., Brown, P. K., and Wald, G. (1963). Tautomeric forms of metarhodopsin. J. gen. Physiol. 47: 215-240.

Meyer, S. L. (1975). Data Analysis for Scientists and Engineers. John Wiley and Sons, New York.

Miller, J. A., and Paulsen, R. (1975). Phosphorylation and dephosphorylation of frog rod outer segment membranes as part of the visual process. J. biol. Chem. 250: 4427-4432.

Morton, R. A., and Pitt, G. A. J. (1955). pH and the hydrolysis of indicator yellow. Biochem. J. 59: 128-134.

Norberg, K., Nillson, B., and Siesjö, B. K. (1975). Coupling between metabolism and blood flow in the brain in hypoxic hypoxia and hypoglycemia. Arzneim Forsch. 25: 1677-1678.

Norberg, K., and Siesjö, B. K. (1976). Oxidative metabolism of the cerebral cortex of the rat in severe insulin-induced hypoglycaemia. J. Neurochem. 26: 345-352.

Nordström, C. H., Rehncrona, S., and Siesjö, B. K. (1976). Restitution of cerebral energy state after complete and incomplete ischemia of 30 minutes duration. Acta Physiol. Scand. 97: 270-272.

Ostroy, S. E., Erhardt, F., and Abrahamson, E. W. (1966). Protein configuration changes in the photolysis of rhodopsin. II. The sequence of intermediates in thermal decay of cattle metarhodopsin in vitro. Biochim. biophys. Acta 112: 265-277.

Owen, A., Caplan, S. R., and Essig, A. (1975). The interaction of 2-deoxy-D-glucose and glucose: effects on the short-circuit current of frog skin. Biochim. biophys. Acta 389: 407-409.

Paulsen, R., Miller, J. A., Brodie, A. E., and Bownds, M. D. (1975). The decay of long-lived photoproducts in the isolated bullfrog rod outer segment: relationship to other dark reactions. Vision Res. 15: 1325-1332.

Pratt, D. C., Livingston, R., and Grellman, K. H. (1964). Flash photolysis of rod particle suspensions. Photochem. Photobiol. 3: 121-127.

Rapp, J. (1971). The kinetics of intermediate processes in the photolysis of bovine rhodopsin. Ph.D. thesis. Case-Western Reserve University.

Rapp, J., Wiesenfeld, J. R., and Abrahamson, E. W. (1970). The kinetics of intermediate processes in the photolysis of bovine rhodopsin. I. A re-examination of the decay of bovine lumirhodopsin-497. Biochim. biophys. Acta 201: 119-130.

Robinson, W. E., and Hagins, W. A. (1977). A light-activated GTPase in retinal rod outer segments. Biophys. J. 17: 196a.

Saibil, H., Chabre, M., and Worcester, D. (1976). Neutron diffraction studies of retinal rod outer segment membranes. Nature 262: 266-270.

Salford, L. G., Plum, F., and Siesjö, B. K. (1973). Graded hypoxia-oligemia in rat brain. I. Biochemical alterations and their implications. Arch. Neurol. (Chicago) 29: 227-233.

Shichi, H., Muellenberg, C. G., Hárosi, F. I., and Somers, R. L. (1977). Isolation of three isochromic forms of rhodopsin in digitonin. Vision Res., in press.

Smith, L. B. (1970). The use of interactive graphics to solve numerical problems. CACM 13: 625-634.

Smith, T. G., and Brown, J. E. (1966). A photoelectric potential in invertebrate cells. Nature 212: 1217-1219.

Thomas, R. C. (1976). The effect of carbon dioxide on the intracellular pH and buffering power of snail neurones. J. Physiol. 255: 715-735.

Tomita, T. (1970). Electrical activity of vertebrate photoreceptors. Q. Rev. Biophys. 3: 179-222.

Von Sengbusch, G., and Stieve, H. (1971). Flash photolysis of rhodopsin. I. Measurements on bovine rod outer segments. Zeitschr. Naturforsch 26b: 488-489.

Wald, G. (1933). Vitamin A in the retina. Nature 132: 316-317.

Wald, G. (1968). The molecular basis of visual excitation. Nature 219: 800-807.

Wald, G., Brown, P. K., and Smith, P. H. (1955). Iodopsin. J. gen. Physiol. 38: 623-681.

Wald, G., Durell, J. R., and St. George, R. C. C. (1950). The light reaction in the bleaching of rhodopsin. Science 111: 179-181.

Waterman, T. H., Fernandez, H. R., and Goldsmith, T. H. (1969). Dichroism of photosensitive pigment in rhabdomes of the crayfish, Orconcetes. J. gen. Physiol. 54: 415-432.

Weinstein, G. W., Hobson, R. R., and Dowling, J. E. (1967). Light and dark adaptation in the isolated rat retina. Nature 215: 134-138.

Wick, A. N., Dury, D. R., Nakada, M. I., and Wolfe, J. B. (1957). Localization of the primary metabolic block produced by 2-deoxyglucose. J. biol. Chem. 224: 963-969.

Williams, T. P., and Breil, S. J. (1968). Kinetic measurements on rhodopsin solutions during intense flashes. Vision Res. 8: 777-786.

Worthington, C. R. (1974). Structure of photoreceptor membranes. Ann. Rev. Biophys. Bioeng. 3: 53-80.

Wulff, V. J., Adams, R. G., Linschitz, H., and Abrahamson, E. W. (1958). Effect of flash illumination on rhodopsin in solution. Ann. N. Y. Acad. Sci. 74: 281-290.

Yang, C. C., and Legallais, V. (1954). A rapid and sensitive recording spectrophotometer for the visible and ultraviolet region. I. Description and performance. Rev. Sci. Instr. 25: 801-807.

Yoshizawa, T., and Horiuchi, S. (1973). Studies on intermediates of visual pigments by absorption spectra at liquid helium temperature and circular dichroism at low temperatures. In Biochemistry and Physiology of Visual Pigments, ed. by H. Langer, Springer-Verlag, 69-82.

Yoshizawa, T., and Kito, Y. (1958). Chemistry of the rhodopsin cycle. Nature 182: 1604-1605.

Yoshizawa, T., and Wald, G. (1963). Pre-lumirhodopsin and the bleaching of visual pigments. Nature 197: 1279-1286.